The objective of this research project, involving Arcelor Research, MEFOS, BFI, Aceralia, Saarstahl AG and Sidenor is to develop advanced methods and systems for online control of gas-stirred ladle treatment in order to improve refining reactions, removal of inclusions and homogenisation during alloying and to minimise slag entrapment and reoxidation.

Activities were driven in accordance with the planning. Developments led to a much clearer understanding of gas-stirred ladle treatments.

A correlation giving the open-eye area as a function of a slag Froude number fits well with all data obtained on water-scale models, in lab-scale hot metal experiments, with numerical simulations and with industrial data.

Image analysis procedures have been developed for automatic threshold and elimination of noised images. The implementation in plant of a video camera proved to be more difficult than expected.

The ladle vibration increases with the Froude number. This is true for a wide range of experiments driven on both pilot-scale steel ladle and water scale models and also for industrial plants. We can evidence resonance related to gravity mode. Finally a high vibration level corresponds to a risk of open-eye.

Contact and contact-less sensors give similar results. Their advantages and drawbacks are clarified.

The analysis of inclusion population during cleanliness bubbling in the plants made it possible to recommend:

- applying a soft bubbling, avoiding open-eye thanks to image analysis and/or based on low vibration;
- generating a minimum stirring to get effective inclusion removal, by aiming at a given vibration.

Price (excluding VAT) in Luxembourg: EUR 20

Publications Office
Publications.europa.eu

ISBN 978-92-79-07293-2

KI-NA-22988-EN-S

EC

Development of advanced methods for the control of ladle stirring process

EUR 22988

EUR 22988

PROJECT REPORT

Development of advanced methods for the control of ladle stirring process

STEEL RESEARCH

Interested in European research?

RTD info is our quarterly magazine keeping you in touch with main developments (results, programmes, events, etc.). It is available in English, French and German. A free sample copy or free subscription can be obtained from:

Directorate-General for Research
Information and Communication Unit
European Commission
B-1049 Brussels
Fax (32-2) 29-58220
E-mail: research@ec.europa.eu
Internet: http://ec.europa.eu/research/rtdinfo/index_en.html

How to obtain EU publications

Our priced publications are available from EU Bookshop (http://bookshop.europa.eu/), where you can place an order with the sales agent of your choice.

The Publications Office has a worldwide network of sales agents. You can obtain their contact details by sending a fax to (352) 29 29-42758.

EUROPEAN COMMISSION
Directorate-General for Research
Research Fund for Coal and Steel Unit

Contact: RFCS publications
Address: European Commission, CDMA 0/124, B-1049 Brussels
Fax (32-2) 29-65987; e-mail: rtd-steel@ec.europa.eu

European Commission

technical steel research

Development of advanced methods for the control of ladle stirring process

M. Burty, C. Pussé
Arcelor Research
Voie Romaine, BP 30320, F-57283 Maizières-lès-Metz

D.Y. Sheng
MEFOS
PO Box 812, S-971 25 Luleå

C. Dannert, H. Köchner
VDEH-BFI
Sohnstraße 65, Postfach 105145, D-40237 Düsseldorf

L.F. Sancho, J. Díaz
Aceralia
Apartado de correos 90, E-33480 Avilés (Asturia)

P. Valentin, C. Bruch
Saarstahl
Bismarkckstraße, 57-59 Postfach 101980, D-66330 Völklingen

A. Arteaga
Sidenor
Barrio Ugarte s/n Apt 152, E-48970 Basauri (Vizcaya)

Contract No 7210-PR/330
1 July 2002 to 30 June 2005

Final report

Directorate-General for Research

2007 EUR 22988 EN

LEGAL NOTICE

Europe Direct is a service to help you find answers
to your questions about the European Union

Freephone number (*):

00 800 6 7 8 9 10 11

(*) Certain mobile telephone operators do not allow access to 00 800 numbers or these calls may be billed.

A great deal of additional information on the European Union is available on the Internet. It can be accessed through the Europa server (http://europa.eu).

Cataloguing data can be found at the end of this publication.

Luxembourg: Office for Official Publications of the European Communities, 2007

ISBN 978-92-79-07293-2

ISSN 1018-5593

Printed in Luxembourg

PRINTED ON WHITE CHLORINE-FREE PAPER

FINAL SUMMARY

The theoretical and industrial aspects of gas stirring of steel in ladles have been considered over the last two decades. Numerical modeling (CFD simulation) and small-scale experiments have been used as tools for studying the process. Physical modeling (water as well as system with Wood metal) has been carried out to investigate the gas-stirred ladle system.

Three different groups of modeling studies are reported in the literature: Quasi single-phase, Lagrangian and Eulerian simulation. Simulation involving three phases or gas/steel/slag, has been applied for analyzing the fluid flow, heat transfer, mass transfer and associated phenomena such as chemical reaction and inclusion removal.

Development of transient mathematical models, which could simulate the vibrations or periodic oscillations in the ladle, is necessary. Recently, some effort on the dynamic simulation in other metallurgical reactors has been published, such as LES (Large Eddy Simulation) simulation of flows in moulds.

Hallberg et al. has described the profile of the free steel surface in the ladle. In this work, a method involving adaptive grid was used to describe the steady profile. Other methods such as scalar methods can also be used for simulations of steel/slag interface. However, simulations of a time dependent transient free surface including slag have not been found.

Minion et al. described the first application of measurements of vibrations applied on an electric arc ladle furnace. Two characteristic frequencies were found. Vibrations around 60 Hz were an indication of the stirring intensities while 120 Hz were found to be generated when arc heating was active.

Vibrations as an indicator of the onset of ladle slag carry-away into the ladle shroud have also been reported and used. Laser system has an advantage over the accelerometers since it could work without contact.

Therefore, the aim this multi-national multi-partner research project, involving ARCELOR Research (formerly IRSID) MEFOS, BFI, ACERALIA, SAARSTAHL AG and SIDENOR is to **develop advanced methods and systems for on-line control of gas stirred ladle treatment** processes in order to **improve refining reactions, removal of inclusions and homogenization during alloying and to minimize slag entrapment and re-oxidation**. The specific objectives of this research are to **determine the operational conditions when open-eye stirring occurs and to investigate and clarify the mechanisms, which contribute to measurable vibrations or oscillations in the ladle during the stirring process**.

Main activities and achievements may be summarized as following.

(1) Stirring phenomena and open-eye area

Similitude criteria (all partners)

The Froude number was defined as the parameter to compare the different gas stirring process at lab, pilot and industrial scales, on water and steel configurations and at reduced or full geometrical scales.

Gas injection and fluid flow (SAG)

SAG has analyzed the evolution with the gas flow rate of the gas plume feature generated by the real porous in a water model. A transition occur above a given gas flow rate.

Metal stirring (MEFOS - SAG)

For different gas flow rates, MEFOS has simulated the fluid flow in a 120-t ladle including the top slag layer, SAG a 170-t ladle without top slag.

Typical velocity over 0.5 m/s are generated even with a top slag layer: this is the driving force for open-eye generation.

Slag behavior (BFI – SAG – SIDENOR - MEFOS)

BFI has used the image analysis software to describe the open-eye area during water scale model experiments and hot pilot scale experiments. BFI has varied the gas flow rate and the thickness of slag.

SAG has implemented a video camera and used the BFI software to characterize the open-eye area. The gas flow rate was varied, the slag layer and property well controlled.

SIDENOR has used it image analysis software to check the effect of gas flow rate on the open-eye area, the slag thickness and composition being quite variable from one heat to another.

MEFOS has computed fluid flow and open-eye formation in a water model configuration and for a 120-t ladle, for different gas flow rate. The industrial configuration, MEFOS has varied the slag viscosity. MEFOS has analyzed the transient regime of gas-stirring and its impact on the slag behavior. In addition, MEFOS has used a water scale model, varying the gas flow rate, the slag thickness and position of the porous plug.

Conclusion over open-eye model (all partners)

The correlation between open-eye area and process parameters of has been evaluated according to several available formulas using the data from BFI, MEFOS, SAARSTAHL and SIDENOR.

The present set of data in the Yonezawa/Schwerdtfeger plot is conveniently positioned and shows that laboratory, pilot plant and steel plant data can be compared within this research project.

The effect of the slag viscosity, as evidenced by MEFOS numerical simulation is an open door to further model the open-eye area and possibly get a unique formulation that would be valid for water models and steel experiment.

Finally the measurement of the open-eye area represents a measurement of the true stirring in industrial conditions if the slag properties and thickness are controlled and/or well known. If not, the relationship is not evident as seen by SIDENOR

(2) Advanced methods and systems for on-line control of gas stirred ladle treatment processes, using image analysis and ladle vibration monitoring

The standard industrial practice of bubbling prior to this project was to aim at a given gas flow rate, and/or to avoid as much as possible the open-eye: the operator being allowed to modify the gas flow rate.

Two types of advanced techniques have been developed, based on either the monitoring of the open-eye area thanks to image analysis or on the ladle vibration monitoring.

On-line image analysis software (BFI & SIDENOR)

BFI has defined optimum image filtering. BFI and SIDENOR have explored different procedure to get a measurement of the open-eye. BFI has validated and used it on water scale model, on pilot steel furnace and then transferred the software to SAG industrial partner. SIDENOR has evaluated the software to specific plant trials consisting in varying the gas flow rate and simulating some pollution of the optics.

The approaches of SIDENOR and BFI were both able to solve the image processing problem using different main focuses. The basic steps of image analysis were obeyed by both partners in similar ways. The SIDENOR system was developed with strong emphasis on the image segmentation because of unfavorable conditions in the ladle furnace where the open-eye was observed. The BFI system was constructed with fast and accurate image segmentation in mind, as it is used as an on-line system at Saarstahl since first quarter of 2005. Both systems use adaptive algorithms for image segmentation. Open-eye classification is used by BFI to distinguish open-eyes from image anomalies.

Contact-less conoscopic holography (ACERALIA)

ACERALIA has developed the contact-less conoscopic holography applied to measure the ladle vibration. The evaluation was made at lab-scale prior to industrial plant tests. A positioning system was developed in order to ensure the 25-50 mm stand-off required for a precise measurement. The low frequency range, limited to 40 Hz is the optimum range for this method. Vibration increases logarithmically with the gas flow rate. Failed bubbling are detected using statistics.

Contact and contact-less sensors for vibration monitoring (ACERALIA and ARCELOR Research)

ACERALIA and ARCELOR Research **have used and compared different contact and contact-less sensors to monitor the ladle vibration, at lab and pilot scales on ARCELOR Research installation and in two plants.** Contact and contact-less sensors give similar results. Their advantages and drawbacks are clarified.

Conclusion on ladle vibration

ARCELOR Research has analyzed all data obtained for a wide range of experiments driven on both pilot-scale steel ladle and water scale models and also for industrial plants, for contact and contact less sensors. The ladle vibration increases with the Froude number, relating the gas flow rate and ladle diameter. A similar trend is found for the turbulent kinetic energy computed by MEFOS close to the ladle wall. ARCELOR Research has showed that vibration monitoring can also evidence possible resonance effect related to the development of gravity mode. Finally a high vibration level corresponds to a risk of open-eye.

(3) Impact of controlled gas-stirring on refining process and reactions, removal of inclusions and homogenization during alloying and to minimize slag entrapment and re-oxidation

Optimum stirring conditions for alloying (SAG)

SAG has analyzed the alloying time of different elements. It corresponds to figures given by correlations based on the stirring energy available in the literature. The needed time is somewhat smaller than the standard one used in the plant.

Open-eye, stirring and cleanliness (SAG)

SAG has analyzed the evolution of the inclusion population with time, in terms of total oxide content, inclusion composition and cleanliness index, together with assessing the open-eye area and for different gas stirring flow rates. During cleanliness stirring, some charges exhibited re-oxidation. The cleanliness index is lower for charges without open-eye formed during the stirring period.

Stirring effect over cleanliness (SIDENOR)

SIDENOR was faced with difficulty in using to use at large scale the open-eye monitoring by image analysis. SIDENOR has thus defined an index of risk of open-eye based on process parameters and evaluated it for 200 heats with respect to the metal cleanliness. As a matter of fact, no clear correlation could be evidenced.

Criteria for plug change (ACERALIA – ARCELOR Research)

ACERALIA and ARCELOR Research have analyzed on hundreds of charges the vibration response. Some treatments failed, with a lower vibration-level. Sometimes it corresponds to leak in the argon pipe connection,

Correlation vibration versus cleanliness (ARCELOR Research)

ARCELOR Research has analyzed the inclusion removal rate of charges elaborated with 100 or 200 l/min. The existence of an open-eye was also considered with respect to the vibration level. The vibration level is variable form one charge to another. Globally the inclusion removal rate is better with a low gas flow rate, but the spreading is high. A good correlation is obtained using the vibration level.

Conclusion over cleanliness (all partners)

The analysis of inclusion population during cleanliness bubbling in the plants made it possible to recommend to

- apply a soft bubbling, avoiding open-eye thanks to image analysis and/or based on a low vibration-level,
- generate a minimum stirring to get an effective inclusion removal, by aiming at a given defined range of ladle vibration.

At the end of the common research, main outcomes and possible applications on European steel plants are underlined:

- The concept of soft bubbling procedure,
- The similarity criteria and the advanced methods to monitor to bubbling favors the transferability.

Future developments are proposed in order to take into consideration the slag physical property and especially its viscosity.

TABLE OF CONTENTS

1 LIST OF TABLES 10
2 LIST OF FIGURES 11
3 NOTATIONS 15
4 GENERAL CONTEXT AND MAIN OBJECTIVES OF THE PROJECT 17
5 WORK UNDERTAKEN – RESULTS AND DISCUSSION 19
5.1 Comparison of initially planned activities and work accomplished 19
5.2 Description of activities and discussions 20
5.2.1 Our concern: inputs & outputs 20
5.2.2 Several approaches to clarify what happens during gas-stirred ladle treatment 21
5.2.3 Activities and new results 21
5.2.3.1 Stirring and stirring phenomena 22
5.2.3.1.1 Similarity 22
5.2.3.1.2 Gas injection (plug, pressure versus gas flow rate …) 23
5.2.3.1.3 Metal stirring (including calculation, model ….) 26
5.2.3.1.4 Slag behavior (calculation, evaluation) 29
5.2.3.2 Advanced on-line methods to control ladle stirring 59
5.2.3.2.1 Open-eye analysis 61
5.2.3.2.2 Ladle vibration monitoring by contact and contact-less sensors 75
5.2.3.3 Transient phenomena 95
5.2.3.4 Towards improved ladle treatment process 96
5.2.3.4.1 Response time 96
5.2.3.4.2 Optimum stirring: index of true stirring 96
5.3 Conclusions 108
5.4 Exploitation and impact of the research results 109
6 REFERENCES 111
7 TECHNICAL ANNEX 115
8 ANNEX OF DETAILS 121
8.1 SAG theoretical calculations - Flow pattern in the ladle 121
8.2 Installation of a video camera at SIDNEOR for open-eye observation 135

1 LIST OF TABLES

Table 1- Progress versus planning..19
Table 2- List of inputs and outputs of the modeling considered in the present project 20
Table 3- Various complementary approaches used in the project 21
Table 4- Characteristics of ladles referenced in the project 23
Table 5- ANOVA analysis results of open-eye area for 300, 400 and 500 l/min data populations..43
Table 6- Open-eye and production data to be correlated...44
Table 7- Regression coefficients t values, almost all are clearly significant...........................45
Table 8- Simulation process parameters for a 120-t gas stirred ladle...................................48
Table 9- Physical properties of water and AK50 oil at 20°C...52
Table 10- Experimental parameters for the water model tests..52
Table 11- Main features of treatment at CAS station in ACERALIA LDA..............................60
Table 12- Evaluation of optical filters for image processing system (BFI).............................64
Table 13- Measurement campaigns at gas stirred ladle treatment processes (BFI).............66

2 LIST OF FIGURES

Figure 1 - Influence of the gas flow rate on the formation of bubble plume and gas jet water model and literature [21] 25

Figure 2 - Gas pressure and gas flow rate in 170-t ladles (159 industrial heats) 26

Figure 3 - Predicted flow pattern and contour plot of steel/slag mixing at the central plane of a eccentric gas stirring ladle (gas flow rate: 200 l/min, slag height: 10 cm) 28

Figure 4 - Influence of gas flow rate on the computed velocity of the steel....28

Figure 5 - Physical model for extensive testing, validation and improvement of the image processing unit at BFI 29

Figure 6 - Area of the open-eye relative to the bath surface area plotted against the stirring gas flow rate for the physical model experiments (variation of liquid level, constant thickness of layer on liquid)....30

Figure 7 - Laboratory set-up for gas-stirred melt treatment....31

Figure 8 - Image captured from the slag/steel surface in the gas-stirred induction furnace (slag thickness 0.003 m, stirring gas flow rate 2.3 l/min) 31

Figure 9 - Area of the open-eye relative to the bath surface area plotted against the stirring gas flow rate for the gas-stirred induction furnace 32

Figure 10 - Influence of gas flow rate and slag density on slag velocity and emulsification...33

Figure 11 - Formation of gas bubbles and open-eye continuously measured by the on-line digital image processing system at lower gas flow rates in a 170-t ladle....35

Figure 12 - Generation of an open-eye - gas flow rate : 8 STP m³/h, 170-t ladle....37

Figure 13 - Generation of an open-eye - gas flow rate : 15 STP m³/h, 170-t ladle....38

Figure 14 - Generation and disappearance of the open-eye gas flow rate 20 STP m³/h, 170-t ladle....39

Figure 15 - Circulating waves on the surface of the steel melt at elevated gas flow rates gas flow rate 35 STP m³/h, 170-t ladle....40

Figure 16 - Time of the development of the open-eye 170-t ladle....41

Figure 17 - Geometry of the open-eye versus gas flow rate 170-t ladle 41

Figure 18 - Area measured with different threshold methods and after applying moving average for three consequent flow rates....42

Figure 19 - Correlation between measured open-eye area and standard deviation in this measurement 45

Figure 20 -Correlation between measured and corrected average flow rate and average counter pressure 46

Figure 21 - Contour plot of steel/slag mixing at top surface of a centric gas stirring ladle with different gas flow rate (slag height: 10 cm) 47

Figure 22 - Contour plot of steel/slag mixing at top surface of a eccentric gas stirring ladle with different gas flow rate (slag height: 10 cm)....49

Figure 23 - Comparison of the open eye size by different process parameters (centric gas stirring) 50

Figure 24 – Computed influence of the slag viscosity on the open-eye area (120-t ladle).....50

Figure 25 - Photo of the experimental water model 51
Figure 26 - Comparison of the open-eye between the water model and numerical simulation (centric gas stirring, gas flow rate: 7 l/min, oil height: 6cm) 53
Figure 27 - Comparison of numerical simulation and water model by the variation of A/hH as a function of parameter, Q^2/gH^5 (centric stirring, gas flow rate: 7~20.2 l/min, oil height: 2~7cm) 54
Figure 28 - Contour plot of mixing density of steel/slag at central plane of 55
Figure 29 - Transient simulation of the mixing of steel/slag in a gas stirring ladle 56
Figure 30 - Relation between A/(h H) and Q^2/gH^5 for water modeling, lab and plant trials and calculations 57
Figure 31 - Relation between A/h^2 and $HQ^{-0.66}$ for water modeling, lab and plant trials and calculations 58
Figure 32 - Simplified scheme of the gas bubbling system at ACERALIA (Avilés LD plant)..59
Figure 33 - BFI image processing system..61
Figure 34 - BFI image processing software..62
Figure 35 - Schematic view of a steelmaking ladle and the camera setup 63
Figure 36 - Sample image taken at measurement campaign 669 at gas stirred ladle treatment process 67
Figure 37 - Geometric transformations to achieve measurable figures.................................69
Figure 38 - Histogram of the image in the figure 70
Figure 39 - Area measured with different fixed thresholds and after applying moving average for three consequent flow rates..72
Figure 40 - Area measured with maximum entropy, fixed threshold and k-means clustering for images captured from the same heat, slag condition, plug state and flow rate (300 l/min) but different image acquisition parameters 73
Figure 41 - Principle of the vibration-based analysis of gas stirring in ladle...........................75
Figure 42 - Configuration of a Conoscope (left) and of a Conoprobe (right) 76
Figure 43 - Comparison of results for different lenses and the accelerometer.......................77
Figure 44 - Vibration diagrams of a complete CAS treatment at ACERALIA: (a) signal and (b) spectrogram..78
Figure 45 - The final version of CH based sensor (ACERALIA): External view (left) and internal detail showing the 25 mm Conoprobe, the linear translation stage, and proximity sensor (right)...79
Figure 46 - Spectrogram obtained with the final prototype of ACERALIA vibration sensor based in 25 mm Conoprobe...79
Figure 47 - Evolution of the measured vibration and the relevant stirring variables as can be seen in the standard report. The upper part contains general data: Heat number, date, ladle number, ladle life, plug life, steel level, slag thickness, time of events, bubbling pattern, gas consumption and mean pressures. The curves represent the evolution of the processed vibration, the gas flow rate, pressure and control valve aperture 80
Figure 48 - Static relation between the vibration measured and the gas flow rate.................81
Figure 49 - Effect of slag layer thickness and porous plug life on the ratio stirring / gas flow rate 82

Figure 50 - Full-scale water model of ARCELOR Research centre 83

Figure 51 – ARCELOR Research induction furnace (300-kg) used for pilot trials with the laser vibrometer 83

Figure 52 - 6-t metal capacity ladle used at ARCELOR Research.......................................83

Figure 53 - Accelerometer compares to laser vibrometer 84

Figure 54 - Accelerometer compares to laser vibrometer and to a reference gauge 84

Figure 55 - Schematics of the study of vibration propagation between the argon circuit and ladle support...85

Figure 56 - The coherence between the signal of the porous plug ladle wall is close to 1, meaning a good vibration transmission..85

Figure 57 - The coherence between the signal of the argon circuit and ladle support is close to 1, meaning a major direct way of vibration transmission 85

Figure 58 – Principle of comparison of ladle vibration and of liquid pressure fluctuation. Good agreement between ladle vibration and pressure fluctuation in the liquid bath. Same evolution with gas flow rate 86

Figure 59 - Energy spectra are similar but shifted for different gas flow rates on IRSID water model. Several frequencies are evidenced which may correspond to gas plume or surface instability...87

Figure 60 - Gravity mode appears predominant in the first industrial trials, due to ladle transfer procedure 88

Figure 61 - Solid movement of the liquid pool as observed from the top surface of the ladle ([35])...88

Figure 62 - Industrial spectra revealing energetic frequency range up to 100 Hz or more, depending on the case 88

Figure 63 - A logarithmic increase with injected gas flow rate of vibrations is measured on both water model and steel pilot steel ladles. A good agreement is observed between water model and steel ladles...89

Figure 64 - Measured increase with the argon flow rate of the ladle vibration index in ARCELOR plant. Some scattering is observed...90

Figure 65 - Increase of the open-eye area as seen during first feasibility trials 90

Figure 66 - Comparison of frequency sensitivity of accelerometer and conoscopic sensor with two different lenses. The reduction of sensitivity at higher frequencies is clear for the 100 Hz component of the vibration 91

Figure 67 - Spectral distribution variation for a test with a scale ladle, using a conoprobe with 75 mm lens; gas flow rate varies from 20 to 50 l/min. For this configuration the interesting frequencies appear around 100 Hz 92

Figure 68 - Results after the processing of the interesting frequencies in the previous trial; sensitivity is low due to the involved frequencies around 100 Hz and the 75 mm lens used 92

Figure 69 - Transient simulation results of the turbulent energy close to the ladle wall 93

Figure 70 – Increase of ladle vibration with the Froude number – Water scale models, pilot scale steel ladles, industrial plant data and numerical simulation...................................94

Figure 71 – Time evolution of the gas flow rate and of the ladle vibration (ARCELOR Research)– Response time of 1 to 2 min...96

Figure 72 - Analyses of Al, C, Mn and Si 97
Figure 73 - Influence of the alloying time on the C content (dC = Ct – Cstart) 97
Figure 74 - Alloying time until “steady state” for Al, C, Mn and Si 98
Figure 75 - Influence of stirring energy on complete alloying time 99
Figure 76 - Comparison between normal and testing sampling 99
Figure 77 - Relationship between time required for complete mixing and energy density 99
Figure 78 - Oxygen content of Al deoxidized heats...100
Figure 79 - Oxygen activity, solved and oxidic oxygen content...101
Figure 80 - Position of 170-t heats in the system Fe – a(O) – Al 102
Figure 81 - Oxygen removal during ladle treatment of RH treated heats.............................103
Figure 82 - Typical inclusions at the end of ladle treatment in the pseudo-ternary system CaO´- Al_2O_3´- MgO´ 104
Figure 83 - Correlation between cleanness and open-eye...104
Figure 84 - Inclusion cleanness versus stirring energy [*) blue brittle method] 105
Figure 85 – Optimum rate of inclusion removal for a given ladle vibration range (ARCELOR Research)...107
Figure 86 – Optimum ladle vibration range regarding quality control of the metal (ARCELOR Research)...107

3 NOTATIONS

A area of the open-eye

H height of top (slag) layer

h height of bulk fluid (with slag layer)

Q stirring gas flow rate

λ scaling factor

U_p plume rise velocity

g gravitational constant

D inner diameter of ladle

Fr Froude number

d_B size of the bubbles

ρ_s, ρ_M density of slag and metal

σ interfacial tension between slag and metal

α angle of inclination

U_M velocity of the metal

ν_s, ν_M kinematic viscosity of slag and metal

CP counter pressure, the pressure measured just after flow meter

CQ corrected flow rate in SIDENOR, Min((CP-2.58)/0.0055;Q)

CCP corrected counter pressure in SIDENOR, Min(0.0055 Q + 2.58; CP)

stdA standard deviation of open-eye area

SC slag condition in Sidenor, comes from visual observation: Fluid or Cold

We Weber number $We = \dfrac{u_l^2 \rho_l}{\sqrt{\sigma_{sl} g(\rho_l - \rho_s)}}$

$\dot{\varepsilon}$ rate of energy dissipation

T temperature

W weight of the melt

4 GENERAL CONTEXT AND MAIN OBJECTIVES OF THE PROJECT

The theoretical and industrial aspects of gas stirring of steel in ladles have been considered over the last two decades. Numerical modeling (CFD simulation) and small-scale experiments have been used as tools for studying the process [1,2]. Physical modeling (water as well as system with Wood metal) has been carried out to investigate the gas-stirred ladle system [3-6].

Three different groups of modeling studies are reported in the literature: Quasi single-phase [7], Lagrangian [8] and Eulerian simulation [9,10]. Simulation involving three phases or gas/steel/slag has been applied for analyzing the fluid flow, heat transfer, mass transfer and associated phenomena such as chemical reaction and inclusion removal [11].

Development of transient mathematical models, which could simulate the vibrations or periodic oscillations in the ladle, is necessary. Recently, some effort on the dynamic simulation in other metallurgical reactors has been published, such as LES (Large Eddy Simulation) simulation of flows in moulds [12, 13].

Hallberg et al. has described the profile of the free steel surface in the ladle [14]. In this work, a method involving adaptive grid was used to describe the steady profile. Other methods such as scalar methods can also be used for simulations of steel/slag interface. However, simulations of a time dependent transient free surface including slag have not been found.

Minion et al. described the first application of measurements of vibrations applied on an electric arc ladle furnace [15]. Two characteristic frequencies were found. Vibrations around 60 Hz were an indication of the stirring intensities while 120 Hz were found to be generated when arc heating was active.

Vibrations as an indicator of the onset of ladle slag carry-away into the ladle shroud have also been reported and used by Krajcik and Kiss Technology [16, 17]. Krajcik used accelerometers attached to ladle shroud manipulator arm while the technology used by Kiss Technology is based on laser interferometry. Due to the vibration of the object, the object beam is subjected to a small frequency shift, which is described as the Doppler frequency. The laser system has an advantage over the accelerometers since it could work without contact.

Therefore, the aim this multi-national multi-partner research project, involving ARCELOR Research (formerly IRSID), MEFOS, BFI, ACERALIA, SAARSTAHL AG and SIDENOR is to develop advanced methods and systems for on-line control of gas stirred ladle treatment processes in order to improve refining reactions, removal of inclusions and homogenization during alloying and to minimize slag entrapment and re-oxidation. The specific objectives of this research are to determine the operational conditions when open-eye stirring occurs and to investigate and clarify the mechanisms, which contribute to measurable vibrations or oscillations in the ladle during the stirring process.

5 WORK UNDERTAKEN – RESULTS AND DISCUSSION

5.1 Comparison of initially planned activities and work accomplished

No major deviation is to be reported between planned activities and work accomplished. The initial planning was revised (second horizontal bar in the task-planning) in the course of the project so as to really take profits from the interaction between the partners (**Table 1**). In such a way, we agreed on changing the activity #4.2 of MEFOS from in-plant vibration measurement, very similar to the ones driven by ACERALIA and ARCELOR Research (previously IRSID) into numerical simulation of flow in the ladle as function of gas flow rate of and of effect of the slag viscosity on the open-eye area.

Meeting and reporting were organized every 6 months. Exchange of experience and information and interaction between the partners proved to be useful to converge towards the expected deliverables of the project.

Table 1- Progress versus planning

N°	Themes	Partners
1	**Interaction between steel and slag**	
1.1	Design and construction of a small ladle	MEFOS
1.2	Gas stirring experiments measuring open-eye and surface oscillations	MEFOS
1.3	Numerical simulation of open-eye stirring, small scale experiments	MEFOS
1.4	Numerical simulation of open-eye stirring, plant conditions	MEFOS
1.5	Initial situation assessment - Recording and classifying of suitable parameters describing efficiency of gas stirring	SAG
1.6	Physical modeling for extensive testing, validation and improvement of the image processing unit	BFI
1.7	Laboratory trials in hot melts with well defined gas stirring intensities and slag layer properties	BFI
1.8	Analysis of stirring condition in full scale water model and pilot scale ladles	IRSID
1.9	Definition of the stirring standards	SIDENOR
1.10	Installation of a camera for open-eye observation	SIDENOR
1.11	Analysis of the image by digital processing	SIDENOR
1.12	Determination of the "real" stirring based on bath open-eye and its surface movement, inlet gas pressure and slag	SIDENOR
1.13	Global analysis of metal-slag interaction during bubbling pr	All partner
2	**Development of sensors**	
2.1	Comparison of vibration based sensors	IRSID
2.2	Stirring and vibration in lab scale and pilot scale ladles	IRSID
2.3	Comparison of vibration based sensor and image processi	IRSID
2.4	Development of prototype image processing system for on-line control and analysis of melt surface during ladle	BFI
2.5	Operational trials at different gas stirred ladle treatment processes and under varying operating conditions for improvement of image processing system	BFI
2.6	Functional Specifications of the sensors	ACERALI/
2.7	Technical Specifications of the sensors	ACERALI/
2.8	Detailed Requirements	ACERALI/
2.9	Performing individual trials and tests	ACERALI/
2.10	Comparison of sensors and of signal treatment	All partner
3	**Transient stirring phenomena**	
3.1	Analysis of surface oscillations with and without slag using fluid mechanics	MEFOS
3.2	Development of models describing time depending behavior of the flow pattern in the ladle	MEFOS
3.3	Verification and validation of transient numerical model	MEFOS
3.4	Analysis of stirring and interface deformation according to the bubbling conditions	IRSID
4	**Industrial trials**	
4.1	Industrial test of sensors and evaluation of impact on metal cleanliness	IRSID
4.2	Plant measurements of vibrations, oscillations: --> modified into numerical simulation of slag viscosity and transient flow to be compared to vibration measurement	MEFOS
4.3	Adaptation and installation of the digital image processing system - Verification and validation of defined efficiency	SAG
4.4	Development and implementation of a theoretical model foi on-line evaluation of stirring efficiency by observing surface patterns at different stages of gas stirred ladle treatment	BFI
4.5	Extensive testing during measurement campaigns at gas stirred ladle treatment processes	BFI / SAG
4.6	Long term operational experiments to verify classified characteristic surface pattern and defined efficiency parameters and final adjustment of the on-line digital	SAG
4.7	Test of sensor in inclusion flotation period at industrial scal	ACERALI/
4.8	Test of sensor in strong stirring for metal-slag	ACERALI/
4.9	Definition of best sensor location and best signal treatmen	ACERALI/
4.10	Interpreting results	ACERALI/
4.11	Check of values with those from real conditions of the proc	ACERALI/
4.12	Integration of the measurements	ACERALI/
4.13	Integration in the steel plant application	ACERALI/
4.14	Development and installation of an on-line model to implement automatic stirring programs at LFV	SIDENOR
4.15	Evaluation of the stirring programs reliability	SIDENOR
4.16	Exchange of results between the partners and common analysis and interpretation	All partners
4.17	**Evaluation, documentation and reporting**	

5.2 Description of activities and discussions

5.2.1 Our concern: inputs & outputs

Table 2 summarizes our concern. The analysis starts with variable and uncontrolled gas stirring process and conditions:

- Different ladle sizes,
- Variable gas flow rate and stirring duration,
- Stirring adjusted by operator eye,
- Variable slag layer,
- Unknown porous plug state.

Table 2- List of inputs and outputs of the modeling considered in the present project

Inputs	Industrial assessment Water modeling Numerical simulation Mathematical model	Outputs
Different ladle sizes and liquid Variable gas flow rate and stirring duration Stirring adjusted by operator eye Variable slag layer Unknown porous plug state Metal sampling	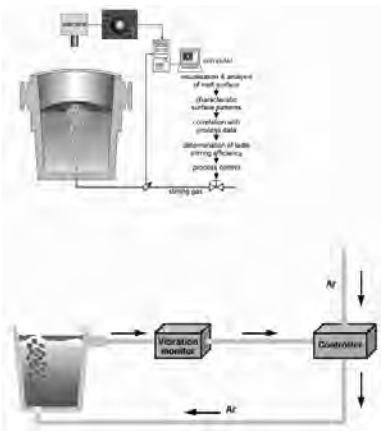	Open-eye area influencing parameters Similarity criteria Image analysis software Vibration monitoring tools Optimum stirring conditions

Experimental approaches at lab, pilot and industrial scales based on open-eye or on ladle vibration monitoring have been used to evaluate the influence of process parameters on the true gas stirring. Numerical and mathematical modelings are used in parallel, also to interpret the measurements and extend the conclusions.

As an output, we get:

- A better understanding of the phenomena occurring in the ladle during gas-stirring,
- Some critical process parameters,
- Similarity criteria,
- Image analysis software and vibration monitoring tools,
- Optimum stirring conditions.

5.2.2 Several approaches to clarify what happens during gas-stirred ladle treatment

We have used complementary approaches with several simulating tools according to three axes of work in order to identify the critical process parameters (**Table 3**):

- get parameters to be able to have a general application of the results,
- develop advanced methods to assess the true stirring,
  - o image analysis of open-eye and ladle vibration,
- evaluate the impact on the metal cleanliness of the use of these methods,
  - o optimum stirring conditions?

Table 3- Various complementary approaches used in the project

Parameters	Tools	Partner	Specifications	Variations / remarks
Similarity	Evaluation of existing correlations of open eye	BFI, MEFOS, SIDENOR, SAG		
Similarity	Analysis of parameters governing ladle vibration	ARCELOR Research		Include all data
Open-eye	Image analysis	BFI	Development of software	Test on water scale model, on pilot steel furnace and implementation at SAG steel plant
Open-eye	Image analysis	SIDENOR	Development of software	Test on video from plant
Open-eye	Numerical model and image analysis	MEFOS		Water scale model and plant configuration Effect of slag viscosity
Vibration	Contact-less sensor	ACERALIA	Conoscopy	Test at lab-scale and in plant
Vibration	Contact and contact-less sensor	ARCELOR Research	Laser vibrometer and accelerometer	Test on water scale models, on pilot scale steel furnaces and in plant
Impact on metal	Evaluate controlled gas stirring conditions	SAG	Analysis of metal alloying time Analysis of metal cleanliness	
Impact on metal	Evaluate controlled gas stirring conditions	SIDENOR		
Impact on metal	Evaluate controlled gas stirring conditions	ARCELOR Research	Optimum stirring	Focus on inclusion removal rate

5.2.3 Activities and new results

The main deliverable results of the project are successively presented hereafter in terms of:

- Stirring phenomena and conclusions on open-eye area,
- Advanced methods and systems for on-line control of gas stirred ladle treatment processes, using image analysis and ladle vibration monitoring,
- Impact of controlled gas-stirring on refining process and reactions, removal of inclusions and homogenization during alloying and to minimize slag entrapment and re-oxidation.

Some details are included in the Annex.

5.2.3.1 Stirring and stirring phenomena

5.2.3.1.1 SIMILARITY

Ladle water models were used to model fluid flow. At first, relevant parameters were defined and identified to ensure the transferability of the industrial ladle stirring process to the laboratory scale. Most important ones are the stirring gas flow rate, the depth of liquid in the ladle and the radius of the ladle. Concerning the model similarity, the ladle Froude number similarity must be met for ruling out any influence of the geometry of the gas injection nozzle [18]. The ladle Froude number is defined as

$$Fr = \frac{U_P^2}{gH} \quad \text{or} \quad Fr = \frac{U_P}{\sqrt{gH}} \qquad (1)$$

The ladle Froude number similarity

$$Fr_{physical\ model} = Fr_{ladle} \qquad (2)$$

is fulfilled when the gas flow rate Q used in the physical model is adjusted to

$$Q_{physical\ model} = Q_{ladle} * \lambda^{2.5} \qquad (3)$$

with λ as scale factor ($\lambda = L_{physical\ model}/L_{ladle}$).

Other slightly different correlations are also proposed [19].

The gas flow rates to be used in the physical model were calculated from the industrial gas flow rates according to the formula above, additionally taking into account the Ferro static or hydrostatic pressure and the temperatures of liquid steel or water. Further similarity calculations showed that with a geometric scale factor between about 1/3 and 1/5, both natural convection phenomena similarity and the ladle Froude number similarity can be met [20].

Comparability of the laboratory set-up with industrial-scale ladle stirring processes was also ensured by using the same similarity calculations. Similarity criteria that had been developed for water modeling experiments were adapted to the steel experiment on laboratory set-ups. A scaling factor $\lambda = D_{furnace}/D_{steelmaking\ ladle}$ was calculated from the inner diameters D of an industrial steelmaking ladle and the laboratory furnace. Parameters of the laboratory trials were defined and/or converted according to this scaling factor. The gas flow rates to be used at the laboratory were calculated from the gas flow rates used in steelmaking according to $Q_{laboratory\ trials} = Q_{ladle} * \lambda^{2.5}$, additionally taking into account the different Ferro static pressures and temperatures of the liquid steel in both cases.

Relevant parameters of the different ladle considered in the project are gathered in **Table 4**.

Table 4- Characteristics of ladles referenced in the project

Name	liquid	Slag	Inner diameter (m)	Liquid height (m)	Gas flow rate (l/min STP)
1- water model BFI	Water	Colored oil, thickness 0.003 to 0.018	0.44 to 0.51	ca 0.5	3 to 30
2- induction furnace BFI	steel	Steelmaking slag, Thickness 0.003 to 0.006	0.3	0.23	2 to 30
3- industrial ladle SAG	Steel 170 t	thickness: 0.05 m Viscosity: 0.8 Pa s (1550°C) (*)	3.3	3.2	0 to 666
4- industrial ladle SIDENOR	Steel 130 t		3	2.5	
5- industrial ladle ACERALIA	Steel 300 t	Thickness 0.06 to 0.12 m	3.9	3.7	Up to 800
6- water model ARCELOR Research	water		0.5 1.0	0.45 0.8	Up to 150
7- induction furnace ARCELOR Research	Steel 300 kg		0.35	0.4	0-10
8- induction furnace ARCELOR Research	Steel 6 t		1	1.1	0-40
9- industrial ladle ARCELOR	Steel 90 t	0.1-0.3	2.5	2.5	0-500
10- industrial ladle MEFOS	Steel 120 t	0.1	2.8	2.8	100-600
11- water model MEFOS	water	Oil AK50	0.6	0.65	3.7-36.7

(*) Slag atlas, Verlag Stahleisen GmbH, Düsseldorf, page 364

5.2.3.1.2 GAS INJECTION (PLUG, PRESSURE VERSUS GAS FLOW RATE …)

<u>Water model experiment to evaluate porous plug at SAG</u>

For the evaluation of the properties of the technical porous plug used in the steel plant of Saarstahl AG, experiments were carried out with a water model using the lower part of an industrial 170-t ladle. Aim of the trials with the water model was the examination of the gas bubble formation at varying gas flow rates from 0 to 40 m^3/h. Two typical screenshots are shown in **Figure 1**. It shows the shape of gas bubbles arising from a gas flow rate of 1 STP m^3/h (a). Single discrete gas bubbles with diameters of about 4 mm can be seen, which start from the porous plug as spheres, change their shape during arising to spherical calottes and form a so called gas plume. With increasing gas flow rates, the sizes of the gas bubbles arise and the distances between two consecutive bubbles leaving the porous plug decrease leading to a higher amount of colliding and combining bubbles. Approximately at a gas flow rate of 7 STP m^3/h a change in the gas bubble formation occurs (b). Single discrete gas bubbles almost cannot be seen anymore. The gas bubbles do not release as single discrete ones from the porous plug but stretch upwards at the slits of it. The change from a two phase gas plume into a continuous gas jet starts.

A summary of the measured gas bubble diameters as a function of the gas flow rate (c) is compared with a curve that Zhang and Taniguchi [21] obtained by interpolating different equations describing the size of the gas bubbles as a function of the gas flow rate:

$$d_B = 0.624 \quad Q^{0.406} \tag{4}$$

According to this, the bubble size increases only slightly with increasing gas flow rate and diverges from the observations made at the water model where a strong increase of the bubble sizes at gas flow rates above 7 STP m^3/h occurred. This can be explained easily by the fact that the existence of a gas plume even for higher gas flow rates has been supposed whereas in the water model at gas flow rates above 7 STP m^3/h, a change to a gas jet has been observed.

The conclusion of the water model experiment is that the porous plug used generates small bubbles at lower gas flow rates favoring the regime of a floating of the inclusions during the rinsing period. On the other hand there is a disadvantage of this porous plug since the generated huge bubbles will probably lead to an intensive gas jet and consequently this will be the reason of the generation of large open-eyes in the breakthrough zone in the surface of steel melt.

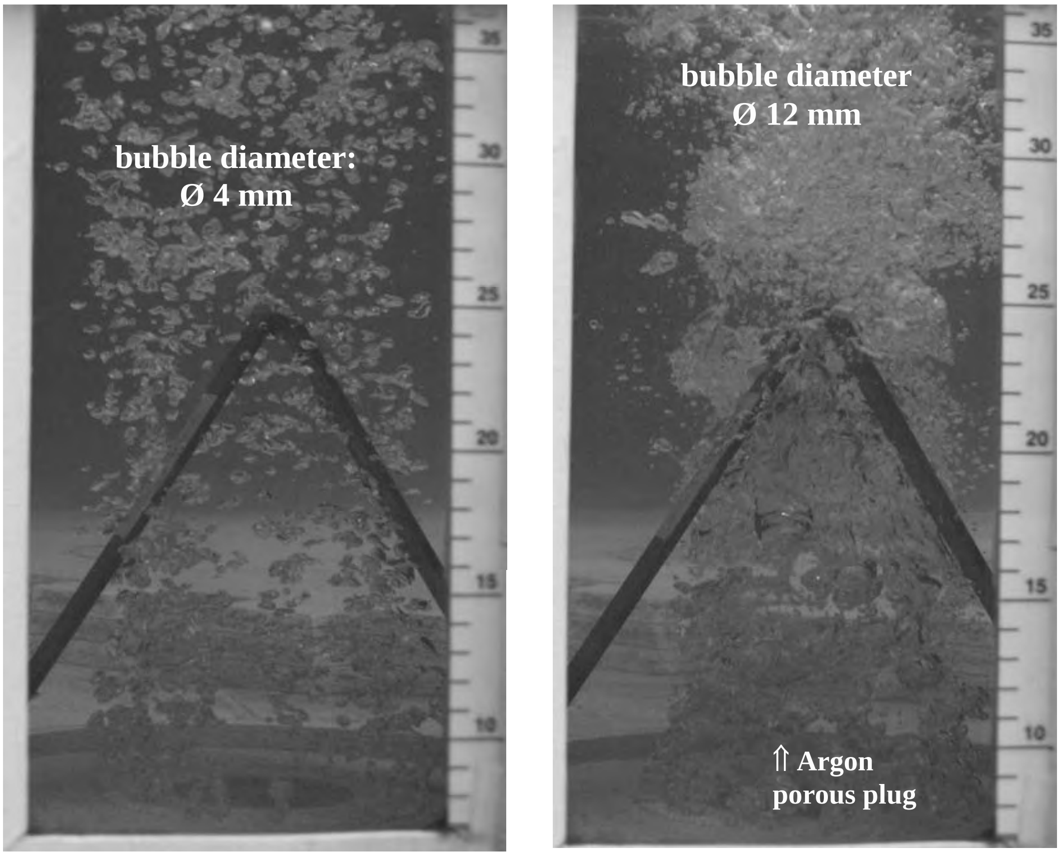

a) gas bubble plume

flow rate: 1 STP m³/h,

b) gas jet

flow rate: 7 STP m³/h

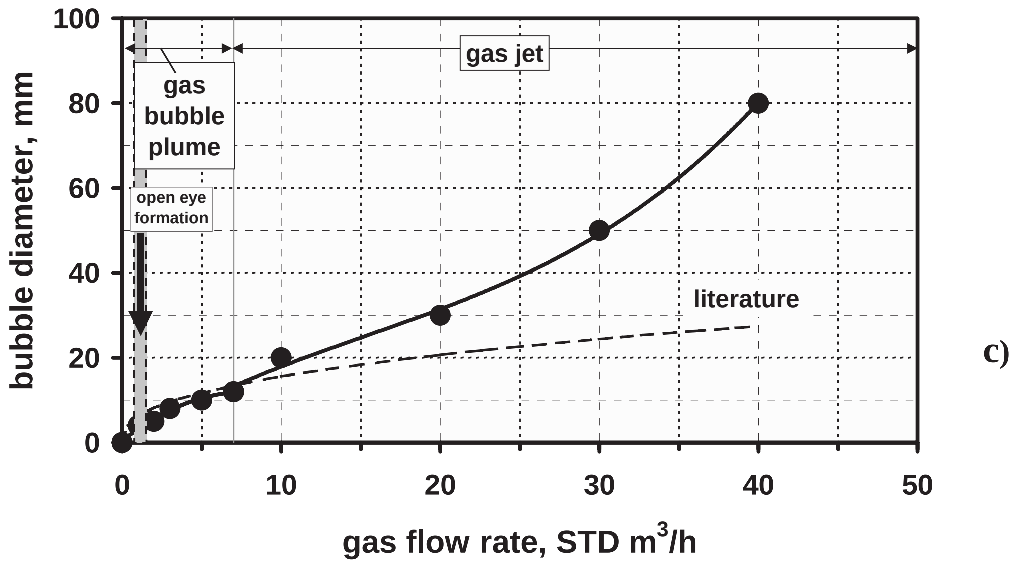

Figure 1 - Influence of the gas flow rate on the formation of bubble plume and gas jet water model and literature [21]

Efficiency of the gas stirring process in SAG plant - Gas flow rate and gas pressure

To evaluate the efficiency of the gas stirring process, relevant process data have to be identified first. Therefore gas flow rates and gas pressures of 159 industrial 170-t heats had been recorded by SAG, the results are shown in **Figure 2**. There is no clear correlation between gas pressure and gas flow rate. This fact is also confirmed by SIDENOR and ACERALIA industrial partners.

Moreover it can be concluded that a blockage of the porous plugs is coming into existence. With regard to the results of the water model, the porous plug seems to operate mostly in the jetting instead of the bubbling regime. From this point of view, -most of the technical 170-t heats are operating with a gas jet. The emulsification of the top slag - particularly in the presence of huge bubbles forming a gas jet - has to be considered when the flow rate exceeds the critical value of 15 STP m³/h indicating an open-eye formation during alloying after tapping. On the other hand, using low gas flow rates <= 2 STP m³/h for example during the rinsing period, the bubble plume will support the flotation of inclusions from the steel melt up to the surface and their separation into the top slag. This situation is characterized by small bubbles coming through the top slag avoiding the generation of open-eyes according to the theoretical 3D calculations of the steel flow pattern in paragraph 5.2.3.1.3.

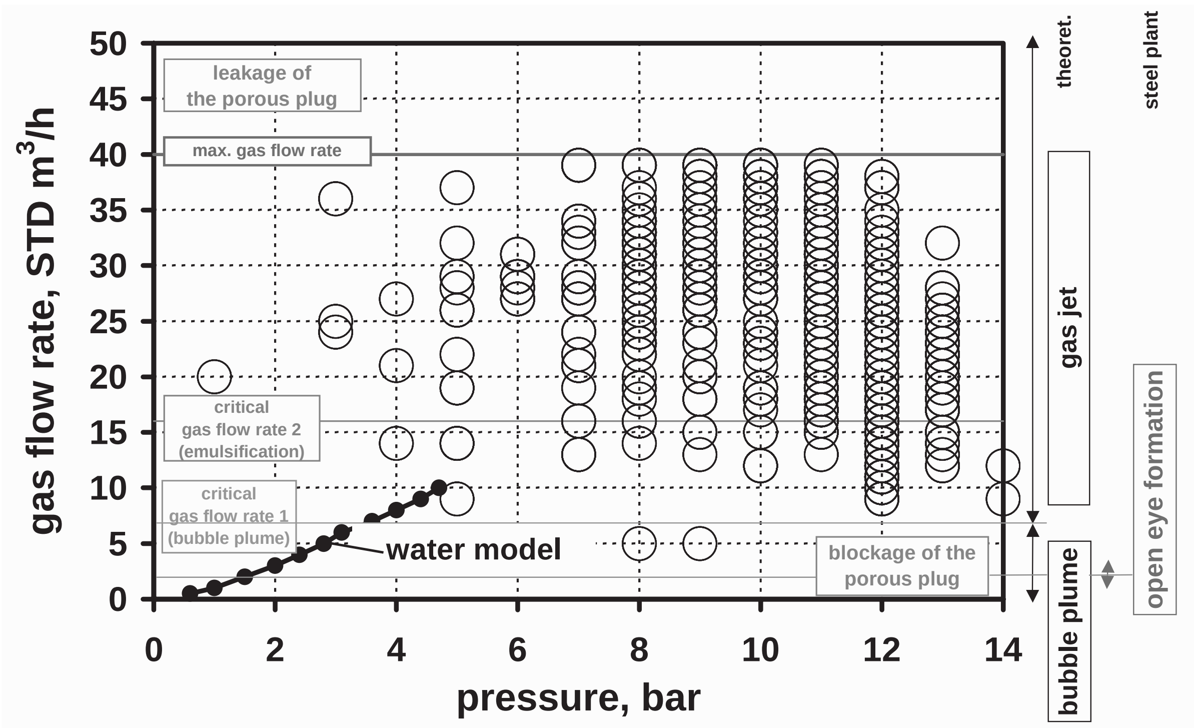

Figure 2 - Gas pressure and gas flow rate in 170-t ladles (159 industrial heats)

5.2.3.1.3 METAL STIRRING (INCLUDING CALCULATION, MODEL ….)

The theoretical model developed and used by MEFOS covers argon injection into liquid steel with top slag during the ladle treatment period. Solutions for three phases; argon, steel and slag are included. The calculations are performed using the transient solution mode based on well-established Eulerian two-fluid model (gas/liquid).

The following general governing transport equations need to be solved:

$$\frac{\partial(\alpha_i \rho_i \varphi_i)}{\partial t} + div(\alpha_i \rho_i v_i \varphi_i - \alpha_i \Gamma_{\varphi i} grad \varphi_i) = \alpha_i S_{\varphi i} \quad (5)$$

Eq. (5) is used to represent all conservation equations by setting $\Gamma_{\varphi i}$ and $S_{\varphi i}$ to appropriate values according to the dependent variable φ_i . The continuity, momentum equations for liquid phases and gas, together with the equations of the turbulent model, form the total set of differential equations that describe the fluid flow in the system.

A two-phase k-ε model has been used [22]. Incorporation of the slag phase into the three-phase model of the argon-stirred steel bath has been done using two additional scalar equations [23]. Gas is injected into the liquid system through nozzles located at the bottom of the ladle. A non-slip boundary condition is imposed for the momentum boundary conditions at walls. In the grids closest to the ladle wall, logarithmic wall functions are used [24]. The top free surface of the liquid is assumed frictionless. Gas is allowed to leave the system, but not liquid. The shape of the surface is assumed to be flat. The buoyancy and gravity force are set up in the momentum equation at the gas-stirring periods. The interfacial momentum transports between gas/liquid consist of several forces, like the drag, lateral lift and virtual mass forces. The details of these source terms can be referred from reference [25].

The solution of the governing equations, including boundary conditions and source terms, is obtained by using the CFD software package Phoenics 3.4. The algorithm IPSA is used to solve the gas-fluid problem. The gas stirring cases are simulated using 3D body-fitted grid system and both centric and eccentric gas stirring are simulated. The calculations are done in a one-step transient-solution mode. The stable solutions are reached after about 20000 iterations and require roughly 80 hours (31*31*41 meshes) on a Sun Enterprise 4000 with six 350 MH_z CPU's.

The flow pattern of eccentric gas-stirring in the cross section of the 120-t ladle is shown in **Figure 3**. The gas flow rate is set to 200 l/min. The buoyancy forces, caused by the injected gas, give rise to high vertical velocities in the plume region. After the liquid steel reaches the surface, downward convection currents force the steel to return from the open eye back to the steel bath. Outside the open eye, the steel flow is almost parallel to the slag/steel interface and directed towards the ladle wall, then downwards along the side wall. A big recirculation loop region develops in the bulk of the ladle. Steel movement drags the slag with it causing radial velocities in the slag. Two asymmetric recirculations are formed in the bulk of the steel. The velocities in the plume zone and near the free surface are relatively high compared with the centric stirring. A clearly counter clockwise recirculation loop is found in the up-right slag region. This is due to the gas plume quite closed to the right side wall and the high horizontal velocities near the steel/slag interface drags the slag moves to the right side wall, then separates to up and down. The refractory erosion is expected close to that region.

3D calculations with Computational Fluid Dynamics, CFD, were also carried out by SAG partner to evaluate the flow pattern under real conditions with different gas flow rates at the steel plant of Saarstahl AG. Details are given in Annex. However the result of the 3D calculation is that the steel velocity increases very strongly with the gas flow rate.

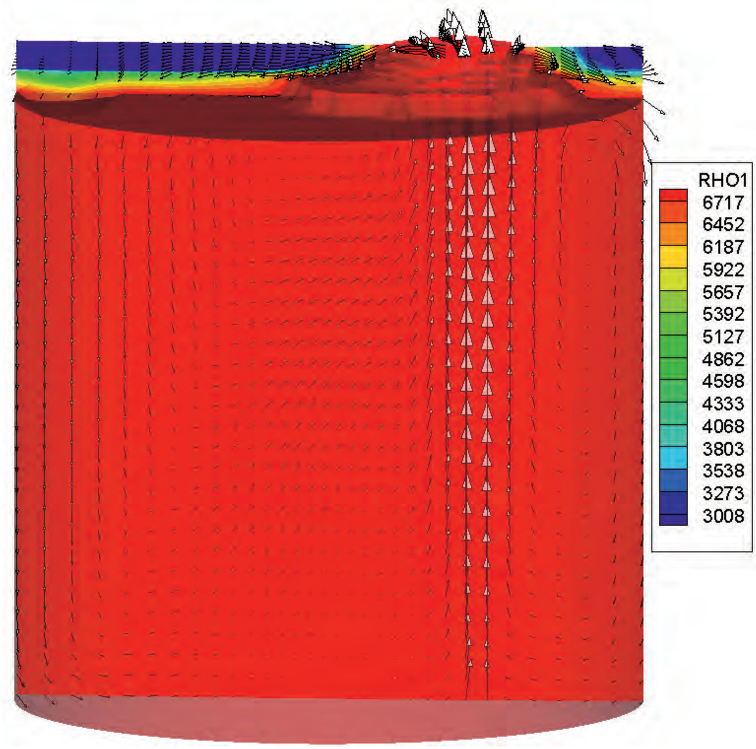

Figure 3 - Predicted flow pattern and contour plot of steel/slag mixing at the central plane of a eccentric gas stirring ladle (gas flow rate: 200 l/min, slag height: 10 cm)

As a conclusion, for both configurations of 120 and 170 tons capacity, the typical metal velocity at the top surface can exceed 0.5 m/s for a gas flow rate over 100 l/min even with a slag layer, which tends to damp the fluid flow (Figure 4). This is the driving force for the metal stirring and the opening of the slag layer leading to an open-eye.

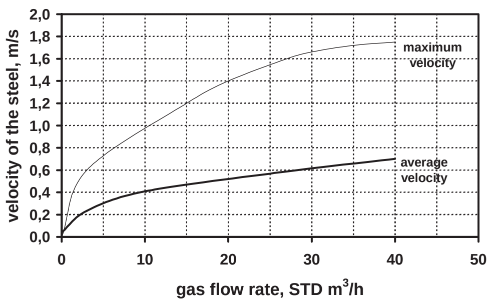

(a) 170-t ladle (SAG)

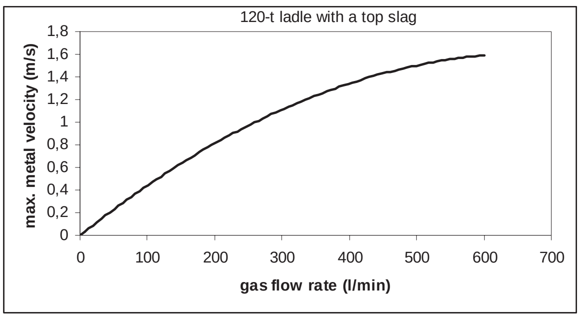

(b) 120-t ladle (MEFOS)

Figure 4 - Influence of gas flow rate on the computed velocity of the steel

5.2.3.1.4 *SLAG BEHAVIOR (CALCULATION, EVALUATION)*

This paragraph summarizes all the results obtained in this project regarding the open-eye versus process parameters. Critical process parameters are emphasized.

5.2.3.1.4.1 Open-eye versus process parameters (BFI)

Activity on water model

A cylindrical physical model with a scale factor of 0.18 was set up (**Figure 5**).

Ladle stirring was modeled by pressurized air injected vertically through the bottom of the acrylic glass cylinder model. A CCD camera was mounted perpendicular to the surface to monitor the surface fluctuation of the modeling fluid during experiments. It was coupled to a computer with the software for ladle surface image analysis. Water was used as model fluid for liquid steel and colored oil as model fluid for slag. The gas was injected eccentrically at about ½ of the ladle radius.

An image sequence of up to 100 images was acquired for each set of parameters. The images were evaluated with the image processing software. As a result, the size of the open-eye relative to the area of the ladle surface was calculated for each image and then averaged for each image sequence. The influence of the parameters on the size of the open-eye is discussed in the following.

Figure 5 - Physical model for extensive testing, validation and improvement of the image processing unit at BFI

To examine the effect of stirring gas flow rate on the size of the open-eye, gas flow rates were changed from 2.8 to 27.8 l/min. **Figure 6** shows the variation of the size of the open-eye with respect to gas flow rate. The size of the open-eye increases with the gas flow rate. As the case of eccentric stirring was modeled, the open-eye always interfered with the edge of the physical model. It might therefore expand in a different way compared to the case of centric stirring. *Since a threshold flow level is needed to form a plume at the surface, the curves are not going through the origin. This threshold flow level for the generation of open-eye increases with the thickness of the layer on the liquid.*

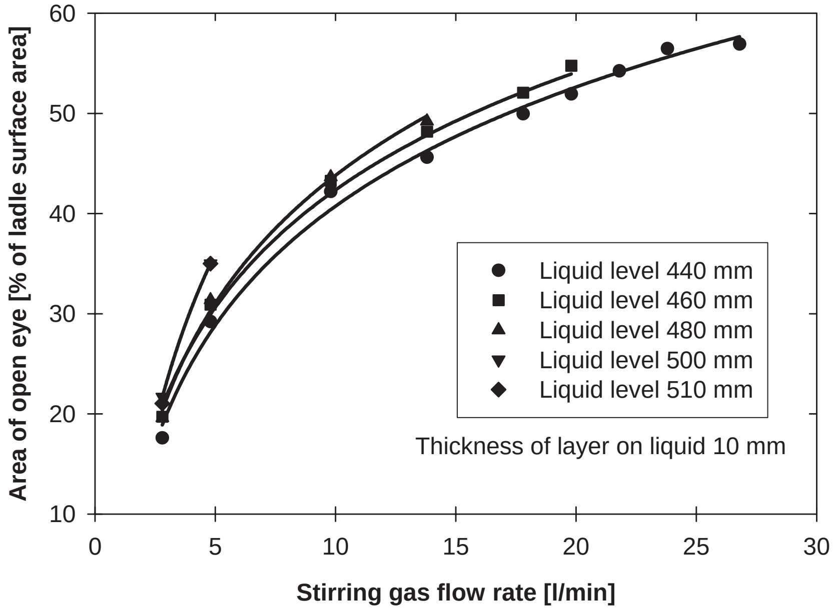

Figure 6 - Area of the open-eye relative to the bath surface area plotted against the stirring gas flow rate for the physical model experiments (variation of liquid level, constant thickness of layer on liquid)

Activity on pilot steel induction furnace

For the laboratory trials in the induction furnace for 150 kg of steel, standard carbon steel was heated up to an average temperature of 1610 °C and a synthetic slag was added. To ensure defined slag layer properties, a typical secondary steelmaking slag was prepared from the oxides and granulated in the laboratory beforehand. Ladle stirring was carried out by pressurized argon injected through a centrically located stirring plug in the bottom of the induction furnace. A CCD camera was mounted perpendicular to the surface of the liquid steel bath to monitor surface fluctuations during the experiments. It was connected to a computer where the software for ladle surface image analysis was running (**Figure 7**).

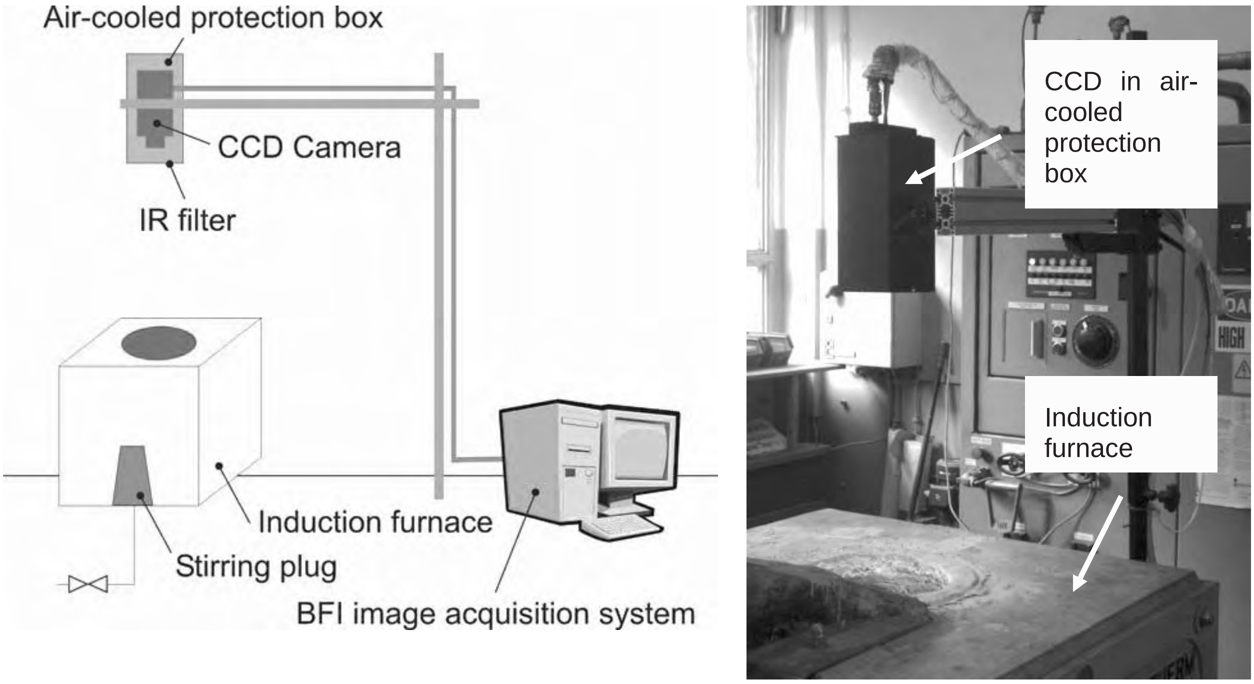

Figure 7 - Laboratory set-up for gas-stirred melt treatment

Thirty images were captured from the slag/steel surface in the gas-stirred induction furnace for each set of parameters. **Figure 8** shows a typical image as example. Ten different stirring gas flow rates were set and two slag thicknesses were used during the trials.

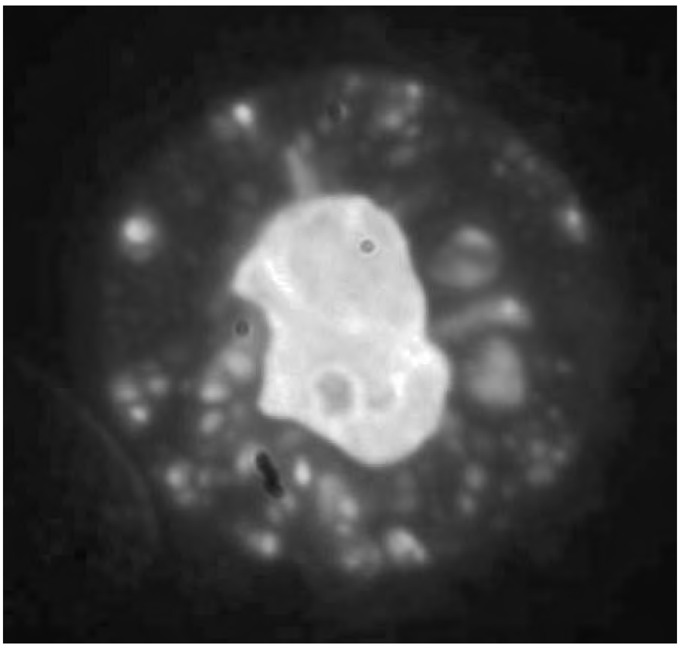

Figure 8 - Image captured from the slag/steel surface in the gas-stirred induction furnace (slag thickness 0.003 m, stirring gas flow rate 2.3 l/min)

A stirring gas flow rate of 1 l/min in the laboratory trials corresponds to a flow rate of approximately 40 m^3/h in the industrial ladle. This is calculated from the scaling factor λ =

$D_{induction\ furnace}/D_{steelmaking\ ladle}$ of 0.092, also taking into account the mean height and temperature of the liquid.

With a slag thickness of 0.003 m, stable open-eyes were observed at all stirring gas flow rates. With a slag thickness of 0.006 m, the stirring gas flow rate had to be increased beyond the specification of the stirring plug in the laboratory set-up to obtain an open-eye. Therefore, the stirring gas flow and, consequently, the open-eye became unstable.

The images captured for each set of parameters were evaluated using the BFI image processing software (§5.2.3.2.1) to determine the average area of the open-eye for each gas flow rate.

As a result of the trials, the area of the open-eye is plotted against the stirring gas flow rate in **Figure 9**. It increases with stirring gas flow rate. Again, since a threshold flow level is needed to form a plume at the surface, the curve is not going through the origin. Deviations from the increase of the relative area of the open-eye result from circumstances of the laboratory trials. The induction heating had to be switched off temporarily during the measurements because it caused strong bath movements that disturbed the bath surface. Turning off the induction heating then resulted in rapid cooling of the liquid steel with a concurrent increase of steel viscosity that influenced the formation of the open-eye. This effect was minimized by reheating of the liquid steel after each measurement.

The error bars in **Figure 9** indicate the standard deviations of the relative area of the open-eye over the thirty images that were captured for each stirring gas flow rate. The standard deviations are very small at low stirring gas flow rates and increase slightly at high stirring gas flow rates. The stirring plug is working more reproducible at low stirring gas flow rates.

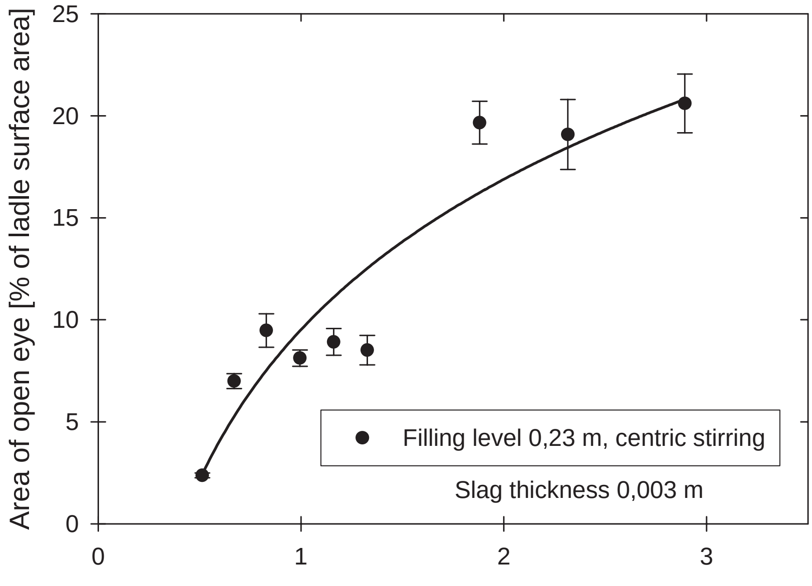

Figure 9 - Area of the open-eye relative to the bath surface area plotted against the stirring gas flow rate for the gas-stirred induction furnace

Model of open-eye area

The objective of this task was to develop a theoretical model to predict the open-eye area from operational parameters like stirring gas flow rate or bath height.

For the development of a theoretical model, an equation was set up that allows the prediction of open-eye area A from process parameters like bath height h, slag thickness H and stirring gas flow rate Q. **Several models for estimation of the open-eye have been described in the literature recently** [26, 27-29]. For example, a macroscopic model has been developed by Mazumdar and Evans [26] that correlates the dimensionless open-eye plume area A/h^2 with two dimensionless variables (H/h and Froude number Fr) and two system specific constants. Plant and laboratory data could be fitted well and the system specific constants could be evaluated for each system, so that a mathematical prediction of open-eye area A was possible.

Data from the BFI physical modeling and laboratory trials was arranged according to the theoretical model in **Figure 30** and **Figure 31**. The data fitted well with the theoretical correlations, showing only very small deviations that are comparable to those found in the literature. This is further discussed in the intermediate conclusion paragraph 5.2.3.1.4.5.

5.2.3.1.4.2 Open-eye versus process parameters in industrial condition (SAG)

Regarding slag emulsification, theoretical calculations [30, 31], in combination with the previously mentioned 3D numerical simulations patterns (Figure 4) are indicating that the velocity of the top slag depends on the gas flow rate following:

$$u_{\mathrm{i,\,krit}} = \left(\frac{8}{\rho_{\mathrm{S}}}\right)^{1/2} \cdot \left\{\frac{2}{3}\sigma \cdot g \cdot \left(\rho_{\mathrm{M}} - \rho_{\mathrm{S}}\right) \cdot \cos\alpha\right\}^{1/4} \qquad (6)$$

The velocity of the slag is in the range of the maximum velocity U_{M} according to [30,32]:

$$U = 0.1367 \cdot \left(\frac{\rho_{\mathrm{M}}}{\rho_{\mathrm{S}}}\right)^{2/3} \cdot \left(\frac{u_{\mathrm{M}} \cdot l}{\upsilon_{\mathrm{S}}}\right)^{1/3} \cdot \left(\frac{u_{\mathrm{M}} \cdot l}{\upsilon_{\mathrm{M}}}\right)^{-2/15} \cdot \left[(1-U)(0.1108 - 0.0693U)\right]^{2/15} \qquad (7)$$

It is possible to calculate the velocity of the slag depending on the slag density. The result is the higher the gas flow rate the higher the velocity of the top slag (**Figure 10**). The calculations are showing in addition, that the slag velocity is higher in presence of top slags with a lower density.

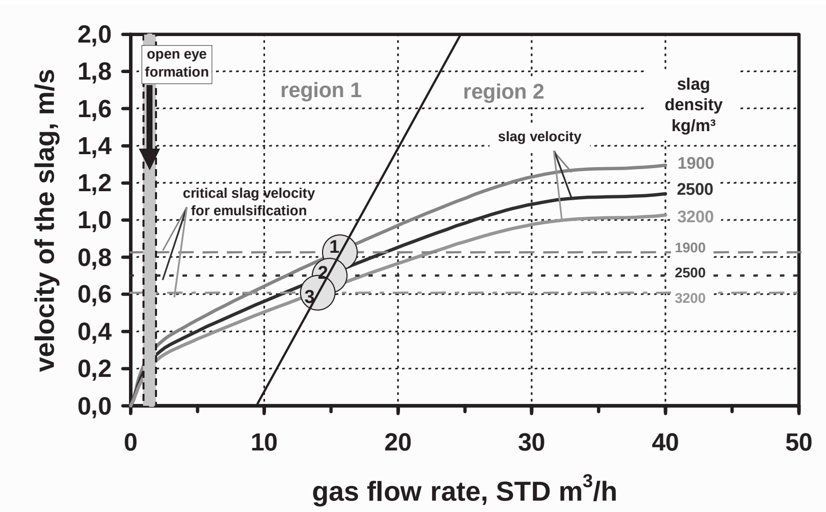

Figure 10 - Influence of gas flow rate and slag density on slag velocity and emulsification

Long term operational experiments to verify classified characteristic surface pattern and defined efficiency parameters and final adjustment of the on-line digital image processing system

Within the framework of this project, a camera system had to be installed in the steel plant of Saarstahl AG which is going to deliver the data for BFI's image processing system for on-line control and analysis of melt surface during ladle stirring. Having checked up the necessary boundary conditions between the departments involved of Saarstahl AG, BFI and the supplier, the camera system could be and was finally installed. It was decided to perform the investigations with the ladle stirring process in the turret of the continuous caster no. 4 of the Saarstahl AG so that the camera was mounted oblique above the corresponding ladle position. In detail the camera system contains the following components: A CCD color video camera which is installed in a compressed air cooled housing. To get a glare-free image of the melt surface, the lens of the camera is equipped with a 780 nm infrared filter, after recommendation from BFI partner (see §5.2.3.2.1.1). Additionally the wide-range automatic electronic shutter of the camera allows to get an appropriate exposure under the respective lighting conditions. The video signals of the camera are transmitted by wire to the control room of the continuous caster where they can be observed on a monitor. A personal computer equipped with a frame grabber card allows processing the video signals with the help of BFI's image processing system. **After a lot of testing and overcoming severe problems, this system was installed successfully**. It allows storing video sequences as well as single images of the melt surface in the ladle during the stirring process. This system is able to catch the breaking off of the slag surface on the melt at the beginning of the stirring process.

To support the successful implementation of the on-line digital image processing system of the BFI at the end of 2004 and in 2005, long term experiments were initiated with regard to open-eye formation and cleanness as determined by the schedule of the research project. The formation of gas bubbles and open-eyes was investigated at the end of the ladle treatment.

A more detailed on-line consideration of the stirring process could be established using the on-line digital image processing system of BFI as shown exemplarily in **Figure 11** taking into consideration the gas flow and the size of the open-eye. Within these trials, a long stirring time was applied to study very intensively the phenomena coming into existence in the top slag during the rinsing period.

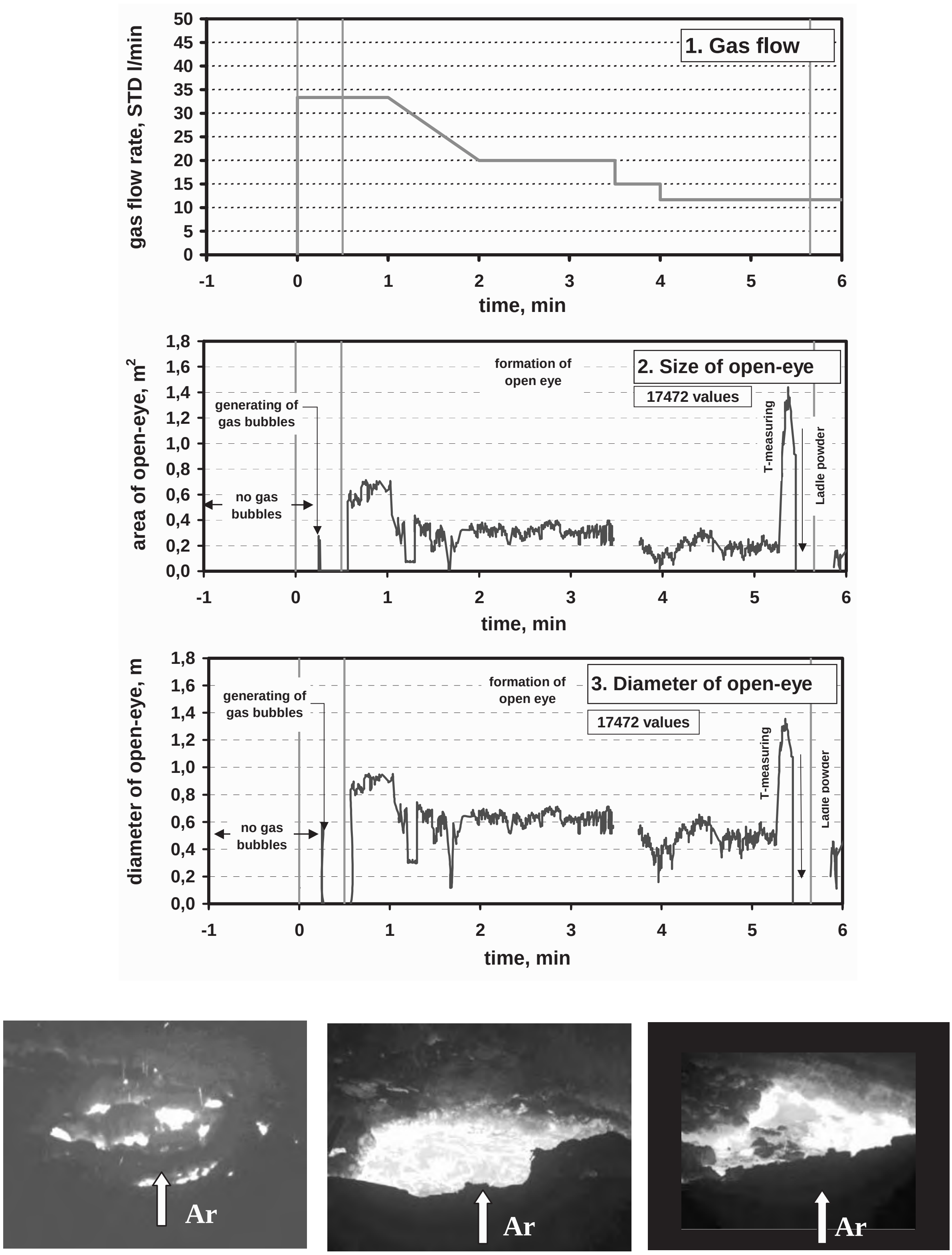

Figure 11 - Formation of gas bubbles and open-eye continuously measured by the on-line digital image processing system at lower gas flow rates in a 170-t ladle

Characteristic images of gas bubbles, open-eye and pseudo-open-eye is shown in lower part of Figure 11 determined and influenced by the rate of gas flow with low intensities. After introduction of the stirring gas individual gas, bubbles break through the top slag, so one may call this part the "break-through-period". Shortly after this typical behavior, an open-eye is formed in the surface of the top slag, this time is defined within the framework of this project the "open-eye-period". Now and then it occurs that the open-eye is replaced by of a liquid top slag consequently appearing as region with bright radiation on the dark surface of top slag, it might by called as the "pseudo open-eye-period".

Applying high gas flow rates, such as 8 STP m³/h on **Figure 12** or 15 STP m³/h on **Figure 13**, shows very clearly the typical generation of open-eyes during the ladle treatment, characterized by:

- Start of the injection of the stirring gas,
- Opening of the top slag,
- Generation of an open eye,
- Completion of the open-eye.

In addition to that formation and disappearance of the open-eye can be originated easily as stated on **Figure 14**. Even circulating waves were detected in the surface during stirring at higher gas flow rates as outlined on **Figure 15**.

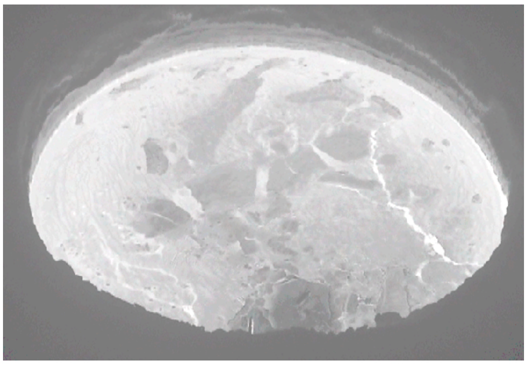

1. Start of the introduction of stirring gas in the presence of
a closed top slag

t = 0 s
top slag: liquid, without movements
solid at interphase slag/atmosphere
with a crack in solid slag layer

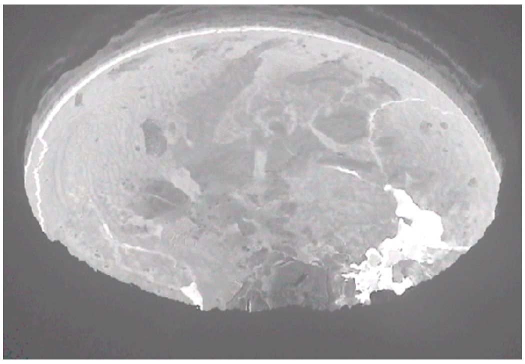

2. Opening of the top slag
t = 2 s

top slag: liquid, without movements
solid at interphase slag/atmosphere
liquid slag spread over solid part

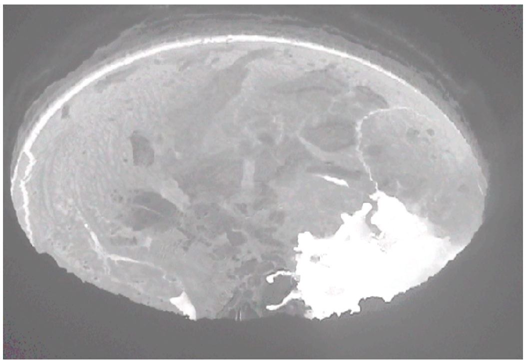

3. Generation of the open-eye

t = 4 s
geometry of the open-eye:
length: 0.39 m, width: 0.33 m
area : 0.11m^2
top slag: liquid, without movements
solid at interphase slag/atmosphere
liquid slag spread over the solid part

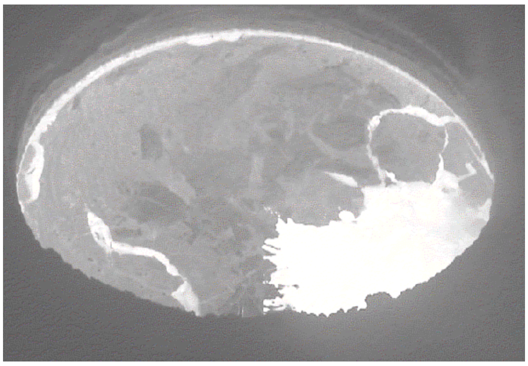

4. Completion of the open-eye

t = 8 s
geometry of the open-eye:
length: 0.58 m, width: 0.41 m
area : 0.19 m^2
top slag: liquid, without movements
solid at interphase slag/atmosphere
liquid slag spread over the solid part
to a large extent

Figure 12 - Generation of an open-eye - gas flow rate : 8 STP m³/h, 170-t ladle

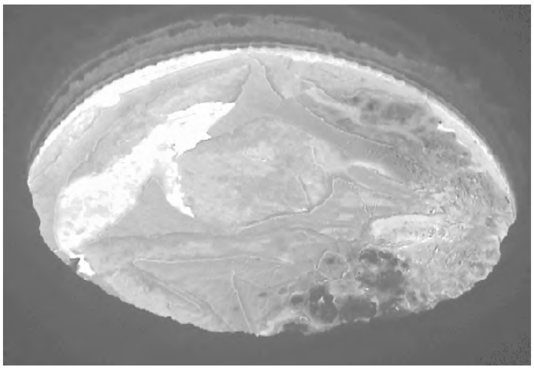

1. Start of the introduction of stirring gas in the presence of a closed top slag

t = 0 s
top slag: liquid, without movements
solid at interphase slag/atmosphere

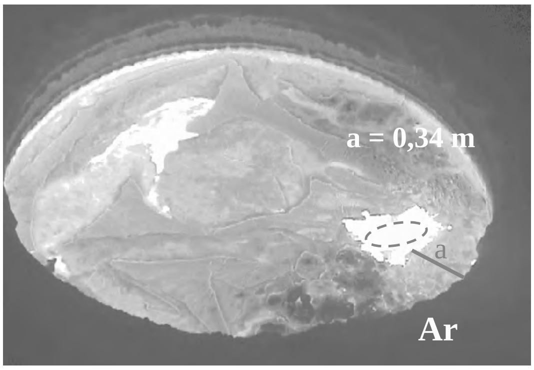

2. Opening of the top slag

t = 2 s
length: 0.42 m
width: 0.13 m
area : 0.043 m^2
top slag: liquid, without movements
solid at interphase slag/atmosphere
liquid slag spread over solid one

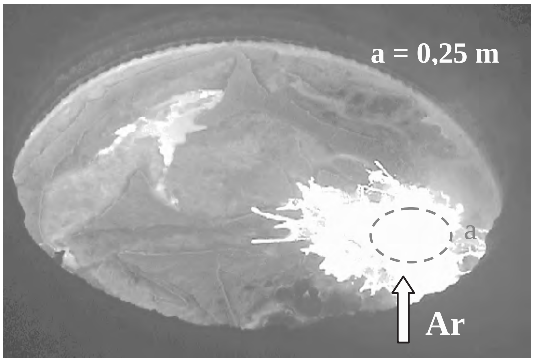

3. Generation of a open-eye

t = 4 s
length: 0.51 m
width: 0.34 m
area : 0.13 m^2
top slag: liquid, without movements
solid at interphase slag/atmosphere
liquid slag spread over the solid part to a large extent

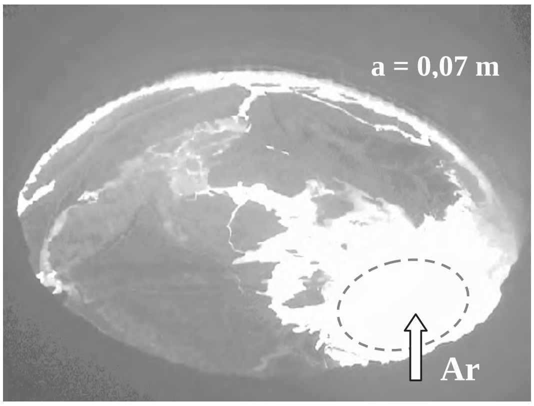

4. Completion of the open-eye

t = 8 s
length: 0.79 m
width: 0.50 m
area : 0.31 m^2
top slag: liquid, without movements
solid at interphase slag/atmosphere
liquid slag spread over the solid part to a larger extent

Figure 13 - Generation of an open-eye - gas flow rate : 15 STP m³/h, 170-t ladle

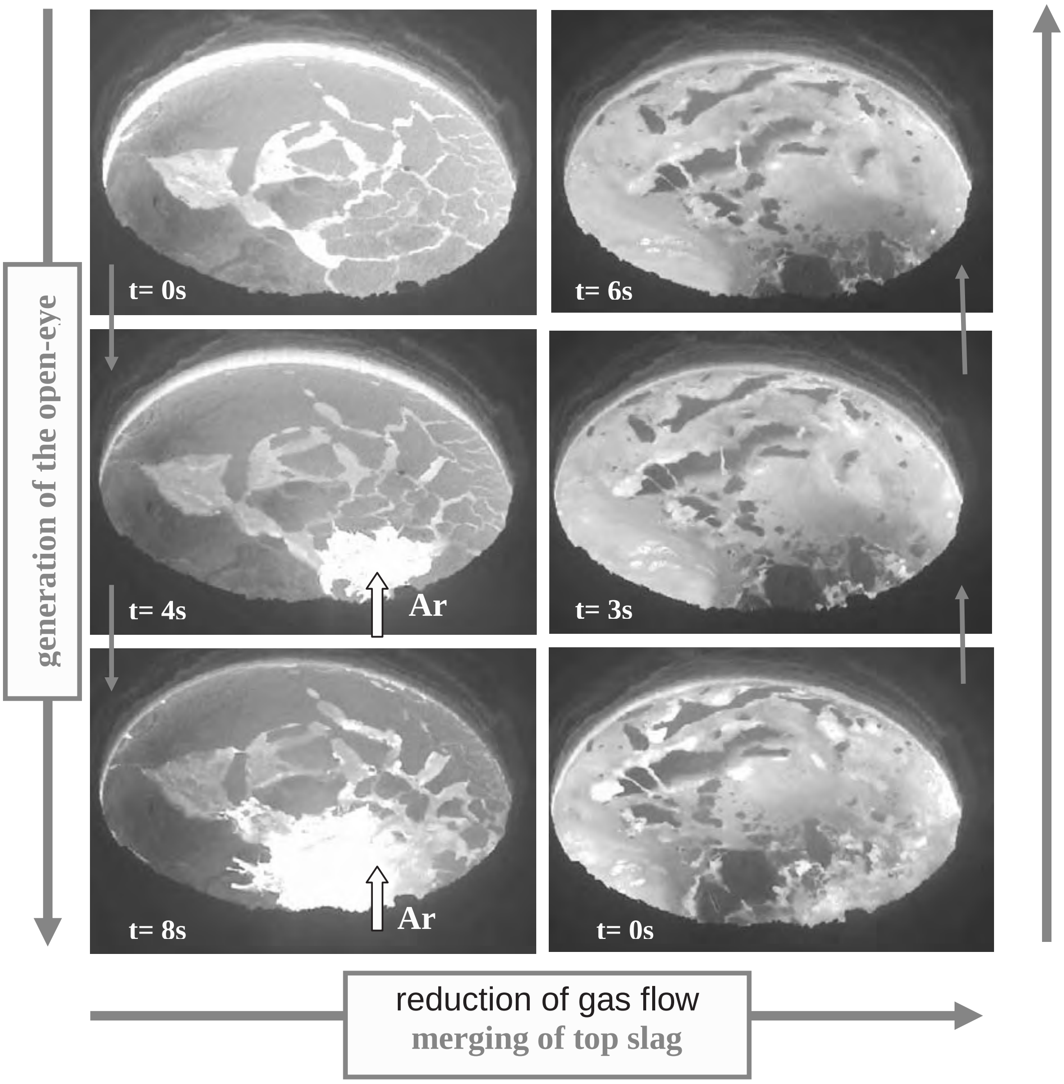

Figure 14 - Generation and disappearance of the open-eye gas flow rate 20 STP m³/h, 170-t ladle

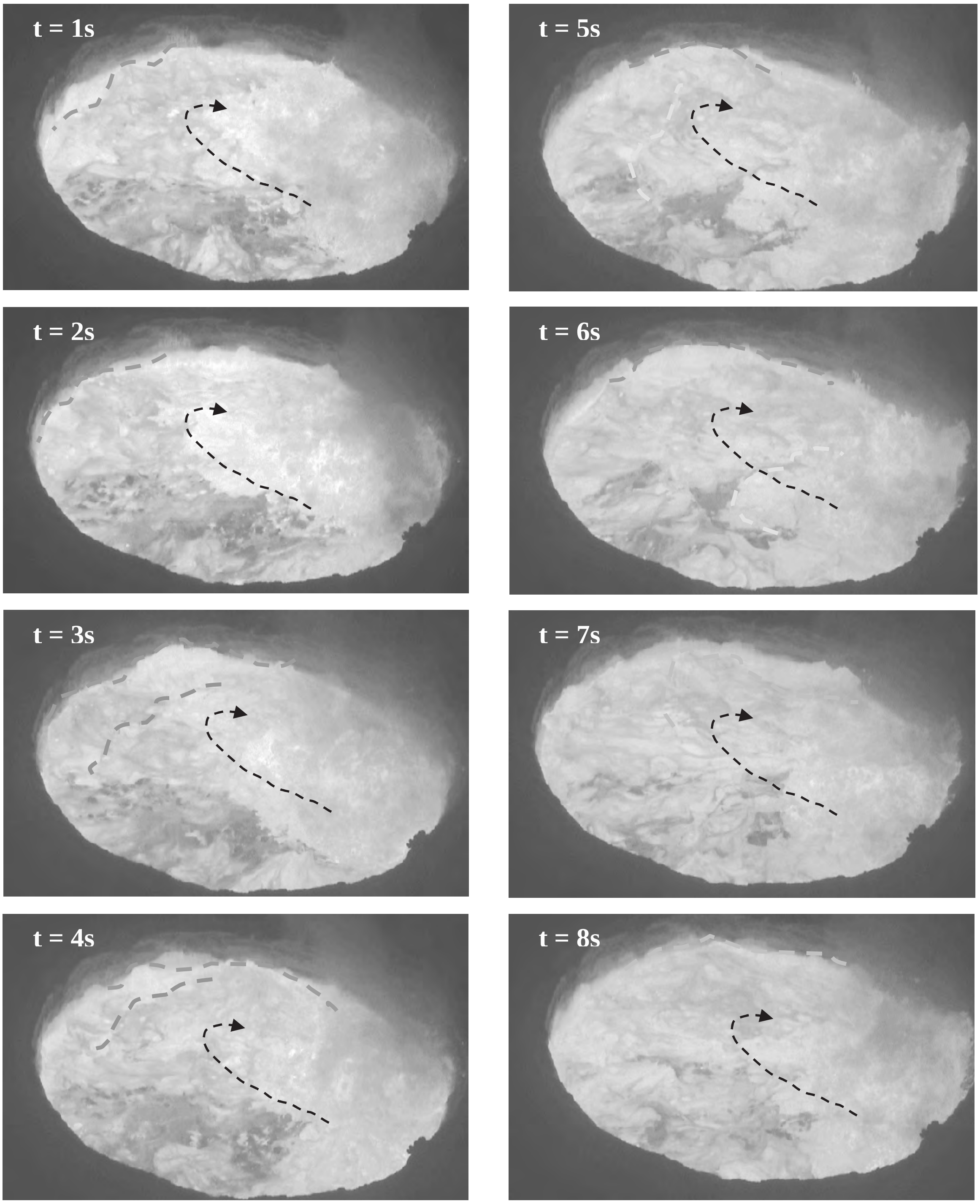

Figure 15 - Circulating waves on the surface of the steel melt at elevated gas flow rates gas flow rate 35 STP m³/h, 170-t ladle

The conclusion of these intensive experiments is that open-eyes are formed within a very short period of a few seconds after the breakthrough of the first liquid slag (**Figure 16**) and that shape and size are influenced very strongly by the gas flow rate (**Figure 17**).

All the results are summarized in the intermediate conclusion paragraph #5.2.3.1.4.5.

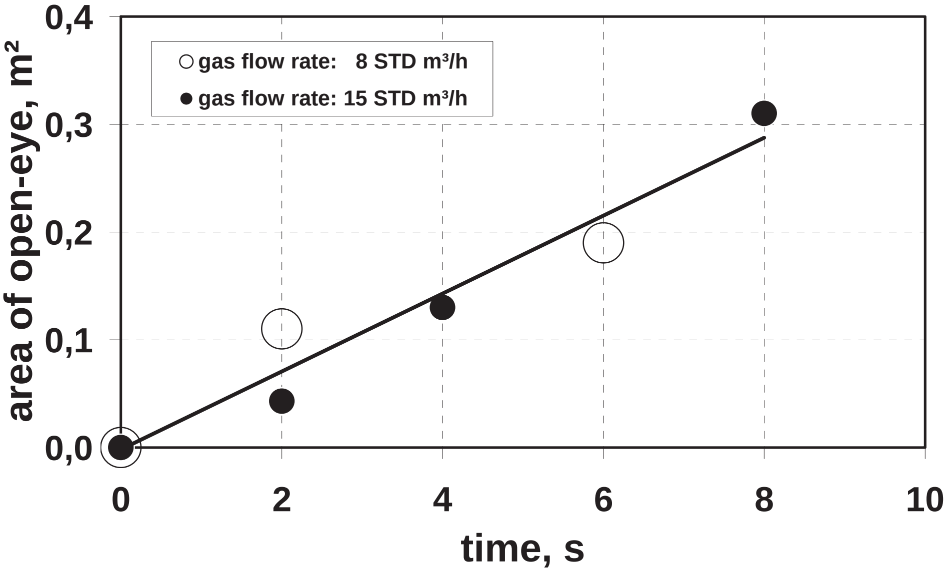

Figure 16 - Time of the development of the open-eye 170-t ladle

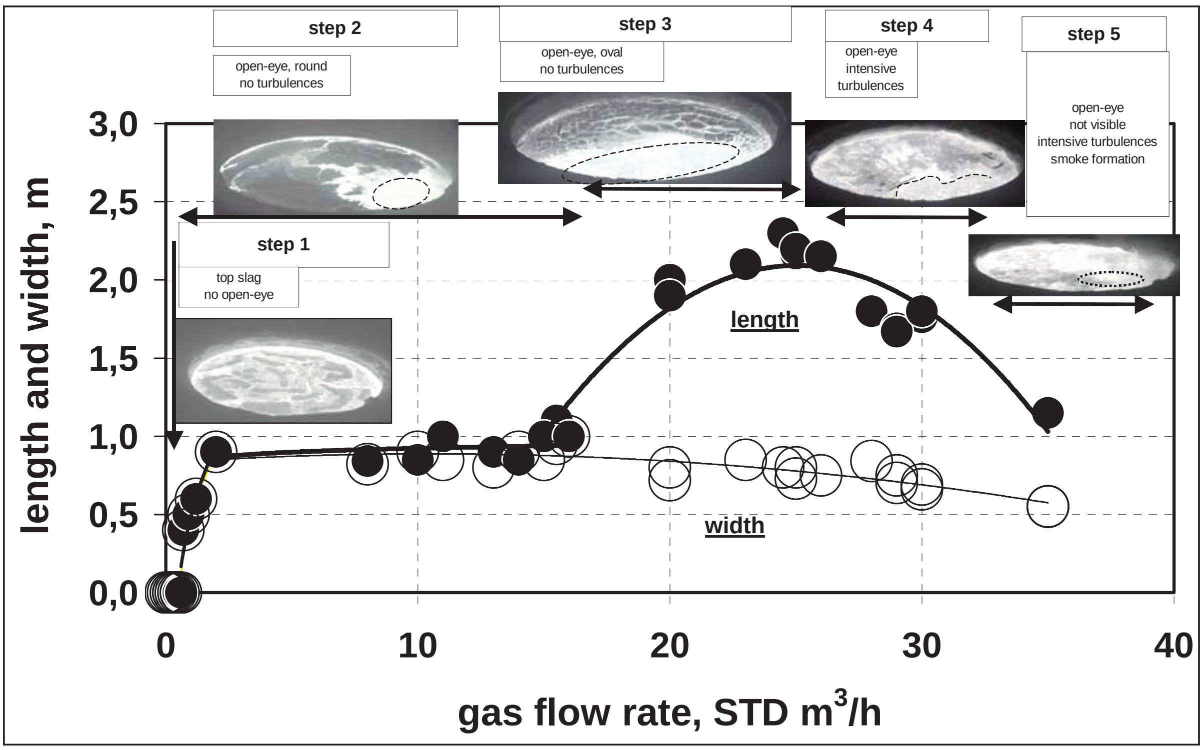

Figure 17 - Geometry of the open-eye versus gas flow rate 170-t ladle

5.2.3.1.4.3 Open-eye versus process parameters in SIDENOR industrial plant

Using image processing described in the next part (§5.3.2.1.2) "open-eye" areas have been calculated in industrial trials at SIDENOR and they have been related to several process parameters: Argon flow rate (Q), argon counter-pressure (CP), slag thickness (H), bath height (h), slag apparent temperature…

Before a general study, an industrial trial was performed by changing the gas flow rate in the same heat without adding any new alloy that could affect slag or heating, without slag or plug state effect. Three data sets were defined for gas flow rate of 300, 400 and 500 l/min. The open-eye area averages grow significantly with the flow rate (**Figure 18**) but the open-eye area also shows important variability.

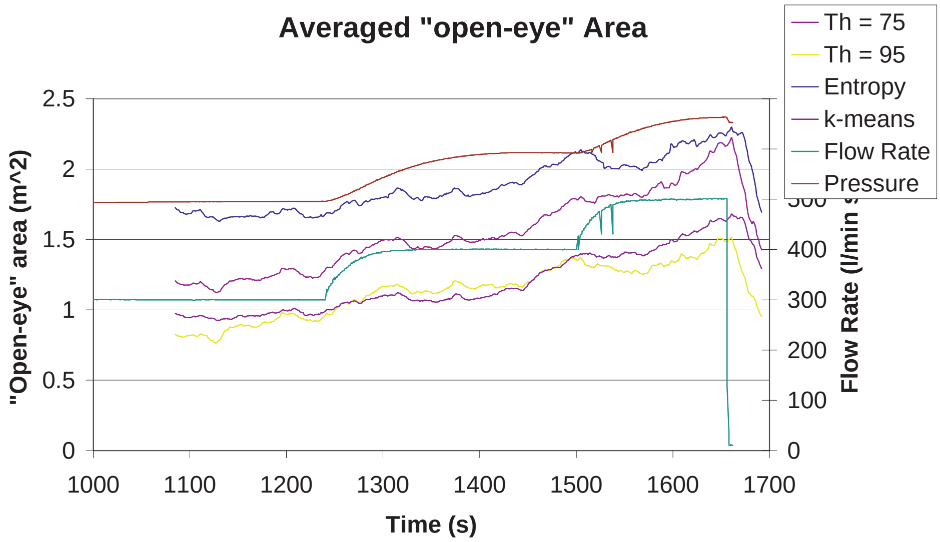

Figure 18 - Area measured with different threshold methods and after applying moving average for three consequent flow rates

Formal statistical study was performed to confirm that they were representing distinguishable data populations. The first study was Analysis of Variance with respect to one factor, the flow rate. The analysis of variance compares variability inside the groups (each of the three data sets) and variability between groups to determine if there is any significant difference. As described in **Table 5** in this case there is a significant difference because the statistic F is very high, 86. This result does not mean that the three groups are statistically distinguishable among each other; it means they are globally distinguishable.

Table 5- ANOVA analysis results of open-eye area for 300, 400 and 500 l/min data populations

SUMMARY				
Groups	*Samples*	*Sum*	*Average*	*Variance*
500	71	105.71	1.49	0.15
400	131	164.35	1.25	0.06
300	88	79.82	0.91	0.05

ANALYSIS OF VARIANCE						
Variation Origin	*Sum of Squares*	*Degrees of Freedom*	*Average of squares*	*F*	*Probability*	*F critical value*
Among groups	13.85	2	6.926	86.49	4.0 E-30	3.03
Inside the groups	22.98	287	0.080			
Total	36.83	289				

Another statistical analysis was performed, the two-sample Kolmogorov-Smirnov test. This test can tell us if two set of data belong to different distributions or not. The sets of data have been compared by pairs, the results are the following:

- 500 l/min data and 400 l/min data

D = 0.3367, p-value = 5.835e-05, alternative hypothesis: two.sided

- 400 l/min data and 300 l/min data

D = 0.5822, p-value = 6.661e-16, alternative hypothesis: two.sided

- 500 l/min data and 300 l/min data

D = 0.7342, p-value = < 2.2e-16, alternative hypothesis: two.sided

As p-values are very low in all the cases, the alternative hypothesis is discarded, so the graphical result is confirmed statistically. Those data sets present different averages as explained before but standard deviation is different too, and grows with flow rate. Kurtosis and skewness are between -2 and 2, indicating that those data are not far from normal distribution.

One interesting conclusion from this study was that growing flow rates caused greater average open-eye areas but also higher standard deviations in those areas. This is not surprising as the higher the stirring more important is slag surface movement and therefore greater standard deviation should be expected.

After this test, more image data were recorded and measured. Thousands of images were recorded and treated and heavy computational work was employed. In this case, it is not possible to get a simple and direct relationship between open-eye area and flow rate. Three main reasons explain this lack of success:

1. Slag influence in open-eye formation, both slag width and fluidity/temperature ought to be important as several theoretical and laboratory works show,
2. Overall brightness and even images histogram are sensitive to slag state and stirring regime, in our analysis measured average open-eye area tends to be overestimated in soft stirring and to be underestimated in high stirring bright/fluid slag conditions,
3. Flow rate from one heat is not necessarily comparable with another one even if the plug is the same because real flow rate in the ladle is always a fraction of measured flow rate due to leaks (always present in industrial practice), and those leaks depend on several factors that change from heat to heat.

For this reasons many other variables were collected, to get better correlations. The summary of the results is shown in **Table 6**. With modified parameters, an alternative relationship was sought between open-eye and stirring parameters available at SIDENOR:

$$StdA = 0.02645\ CCP + 0.02576\ SC_{FLUID} - 113.5\ H + 1042\ H^2 - 3114\ H^3 \qquad (8)$$

Overall results from the regression are:

- Multiple R-Squared: 0.6429
- F-statistic: 11.52 on 5 and 32 DF, p-value: 2.037e-06

Table 6- Open-eye and production data to be correlated

(SC: cold slag = 0; fluid slag = 1)

Image Set	FR	CP	CFR	CCP	A	staA	H	SC	h	Comments
1	300	4,96	300	4,23	0,907	0,227	0,070	0	2,71	
2	400	5,93	400	4,78	1,255	0,252	0,072	0	2,71	
3	500	6,63	500	5,33	1,489	0,290	0,073	0	2,71	
4	300	3,29	129	3,29	2,100	0,315	0,090	0	2,60	Poor Image
5	800	3,34	138	3,34	1,116	0,078	0,084	0	2,55	
6	400		400	4,78	2,135	0,203	0,092	0	2,54	
7	250	3,43	155	3,43	1,173	0,104	0,081	0	2,63	
8	600	3,45	158	3,45	1,451	0,080	0,112	0	2,53	
9	200	3,1	95	3,1	0,805	0,118	0,105	0	2,88	
10	300	3,8	222	3,8	1,120	0,111	0,075	0	2,58	
11	400	4,7	385	4,7	0,623	0,062	0,103	0	2,68	
12	30	0,1	0	0,1	0,093	0,008	0,103	0	2,68	
13	350	4,4	331	4,4	0,998	0,050	0,096	0	2,59	
14	80	2,2	0	2,2	0,762	0,035	0,096	0	2,59	
15	300	4,67	300	4,23	0,891	0,048	0,094	0	2,91	
16	60	2,2	0	2,2	0,491	0,029	0,094	0	2,91	
17	800	3,5	167	3,5	0,723	0,094	0,144	0	2,59	
18	0	0,3	0	0,3	0,688	0,034	0,144	0	2,59	
19	0	0,4	0	0,4	0,196	0,055	0,139	0	2,61	
20	250	3,5	167	3,5	2,711	0,350	0,110	0	2,72	Poor Image
21	230	3,9	230	3,845	2,456	0,190	0,110	0	2,72	
22	700	4,2	295	4,2	0,844	0,119	0,112	1	2,53	
23	200	3,4	149	3,4	1,197	0,102	0,105	1	2,88	
24	80	2,3	0	2,3	0,620	0,075	0,102	1	2,58	
25	240	3,1	95	3,1	1,520	0,173	0,102	1	2,58	
26	500	5,8	500	5,33	0,924	0,114	0,103	1	2,68	
27	300	4,1	276	4,1	0,928	0,193	0,100	1	2,59	
28	80	1,6	0	1,6	0,667	0,023	0,100	1	2,59	
29	250	3,2	113	3,2	0,538	0,098	0,100	1	2,59	
30	150	2,8	40	2,8	0,594	0,141	0,096	1	2,59	
31	300	6,3	300	4,23	0,557	0,115	0,094	1	2,91	
32	500	4,15	285	4,15	2,973	0,356	0,108	1	2,60	Poor Image
33	700	4,12	280	4,12	1,589	0,062	0,097	1	2,55	
34	350		250	4,505	1,645	0,247	0,109	1	2,54	
35	250	3,04	84	3,04	1,356	0,112	0,117	1	2,47	
36	300	4,62	300	4,23	1,609	0,145	0,097	1	2,63	
37	600	5,2	476	5,2	1,892	0,184	0,115	1	2,69	
38	800	7,1	800	6,98	1,230	0,105	0,115	1	2,69	Poor Image
39	1000	12,2	1000	8,08	1,531	0,257	0,098	1	2,60	
40	800	9,2	800	6,98	1,464	0,177	0,098	1	2,60	
41	840	4,3	313	4,3	1,115	0,151	0,144	1	2,59	
42	1000	3,8	222	3,8	0,707	0,096	0,139	1	2,61	

All the coefficients are significant (t values greater in absolute value than 2), except SC_{FLUID} but it has been included because t value is not less than 1, helps to improve the rest of the values and the result is meaningful (**Table 7**).

Table 7- Regression coefficients t values, almost all are clearly significant

	Estimate	Std. Error	t value	Pr(>|t|)
(Intercept)	4,04E+03	1,23E+03	3.277	0.00253
CCP	2,65E+01	5,50E+00	4.808	3.46e-05
SC_{Fluid}	2,58E+01	1,85E+01	1.395	0.17274
H	-1,14E+05	3,67E+04	-3.097	0.00405
H^2	1,04E+06	3,54E+05	2.941	0.00604
H^3	-3,11E+06	1,11E+06	-2.808	0.00843

In expression (8), stdA is considered as the parameter measuring open-eye size, as it is related to the average open-eye area (**Figure 19**) and seems to lead to better overall multiple R^2 than average area. Similar procedure has been followed with corrected counter-pressure (CCP), both flow rate and counter pressure being correlated, corrected values are more correlated even (**Figure 20**). Corrected values for both CP and Q offer better results, anyway they can not be regarded as 100% reliable indicators of real stirring power.

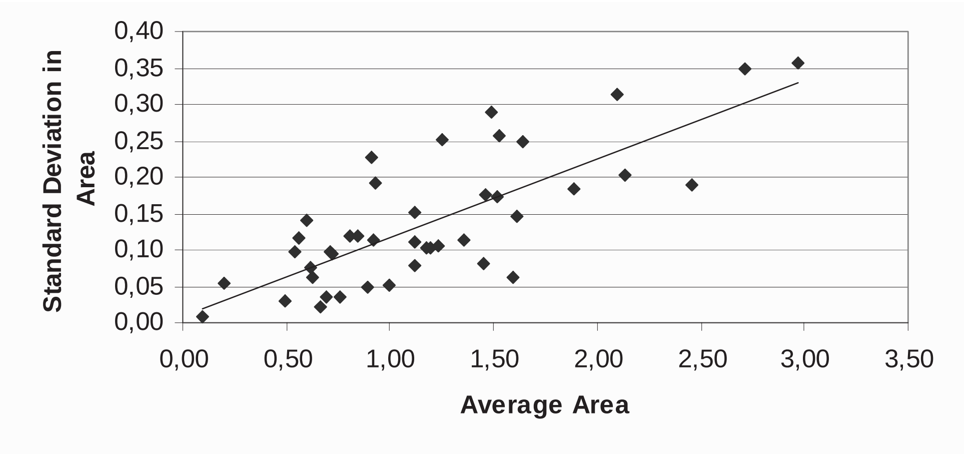

Figure 19 - Correlation between measured open-eye area and standard deviation in this measurement

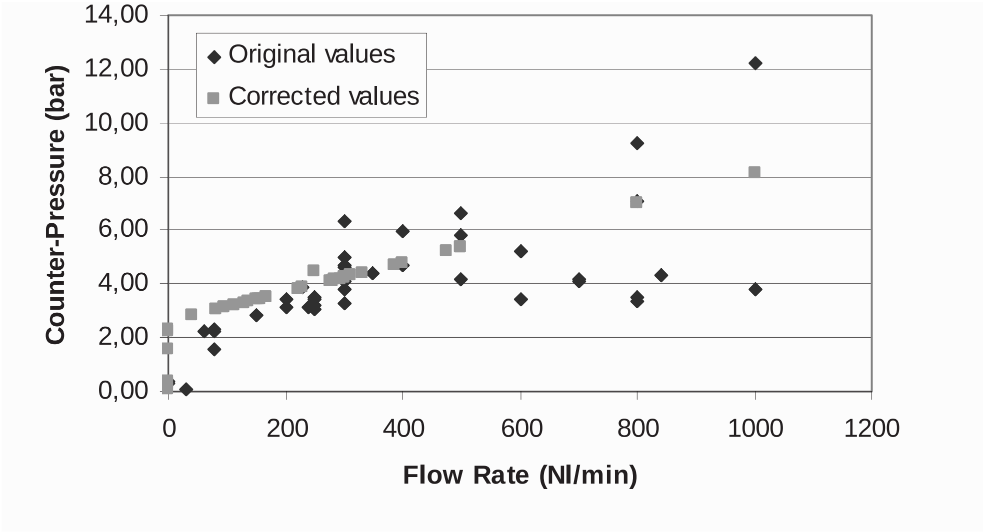

Figure 20 -Correlation between measured and corrected average flow rate and average counter pressure

The main conclusion from expression (8) is the confirmation that in industrial conditions open-eye size is related to stirring power but also to slag condition and thickness. Therefore to obtain real stirring flow rate from open-eye measurements, slag effect should be always taken into account.

Eq (8) differs from the linear relationship between A/h^2 and $HQ^{-0,66}$ that works for laboratory trials. The latter relationship exhibits a low R^2, less than 0.40, if all raw data from SIDENOR are considered. Mainly the slag condition, which can be maintained constant at laboratory scale, can vary a lot in industrial practice, due to metallurgical processes and temperature changes. This is further discussed in the intermediate conclusion paragraph 5.2.3.1.4.5.

5.2.3.1.4.4 Computed and observed slag behavior (MEFOS)

Numerical calculations

Figure 21 shows a series of the surface contours of the mixing of steel/slag under the conditions of **centric** stirring of different gas flow rates. **Table 8** shows the simulation process parameters for a gas stirring ladle. The red color stands for the steel and the blue color stands for the slag: the higher the gas flow rate, the larger the open eye. The quite **low gas flow rate (soft stirring) can lead to no open eye at all**. These phenomena can be easily understood for the velocity field. Higher gas flow rates leads the higher velocities of steel near the top surface, which gives higher energy to push the slag away from the plume region. From the recirculation loop in the slag layer, it can be found that the slag near the top surface has a velocity toward the centre of plume. The steel is likely to push away slag from the centre, however, the slag tends to flow back to cover the centre. The final force balance decides how large the open-eye is. As shown on Figure 21f, when the gas flow rate is 600 l/min, there is a quite big open area formed at the top surface. This is a re-oxidation site. If the ladle is not covered with a lid, the argon stream enters directly into the surrounding air. Air is sucked from the sides into the rising argon stream. Hence, there will be an argon-air mixture above the open eye region with oxygen concentration increasing.

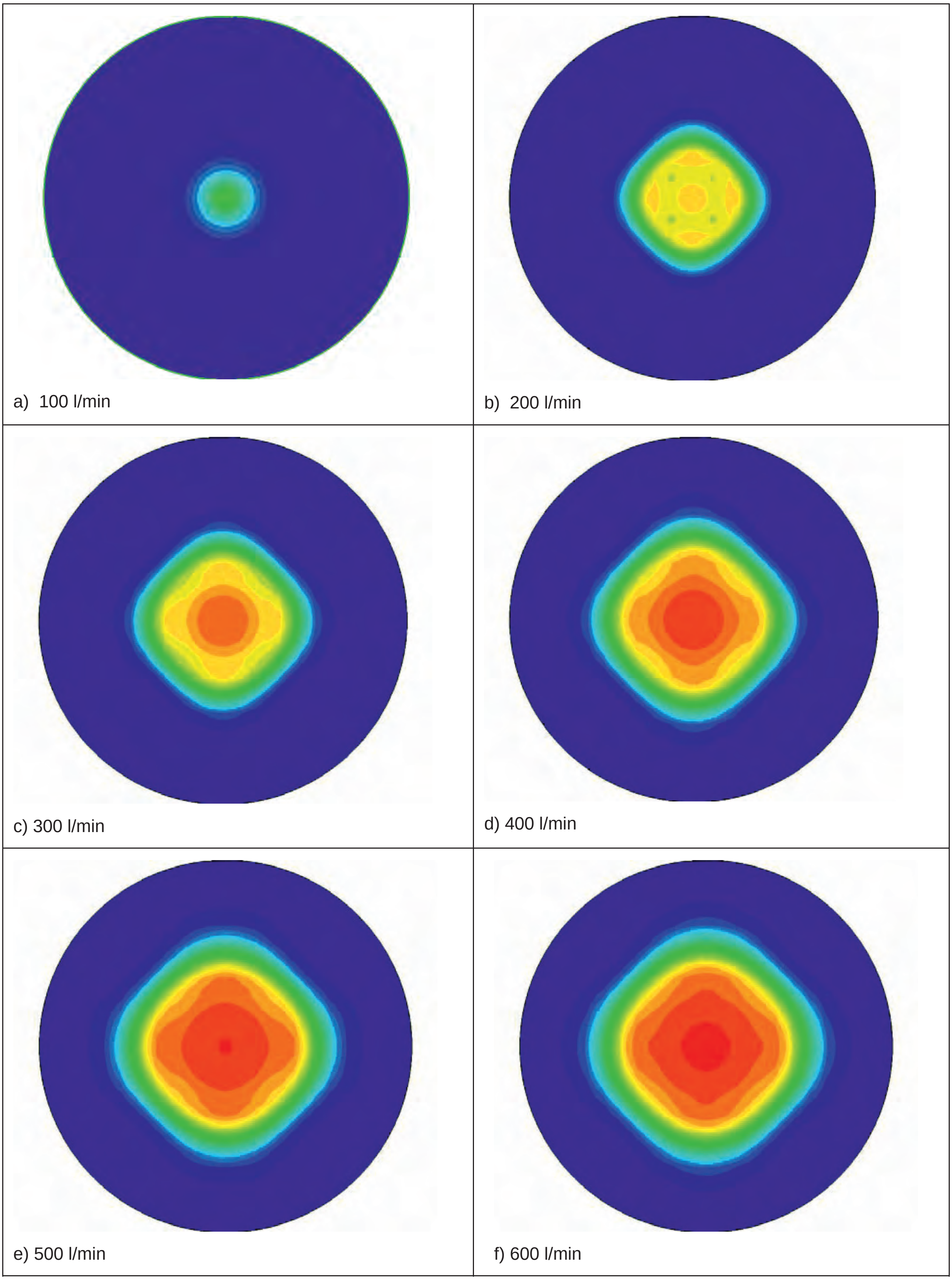

Figure 21 - Contour plot of steel/slag mixing at top surface of a centric gas stirring ladle with different gas flow rate (slag height: 10 cm)

Table 8- Simulation process parameters for a 120-t gas stirred ladle

Gas stirring position	Centric, Eccentric
Gas flow rate	100 – 600 l/min
Slag composition	53% CaO, 32% Al_2O_3, 7.5% MgO and 7.5% SiO_2
Slag thickness	10 cm
Porous plug number	1
Gas stirring	Bottom injection

Figure 22 shows a series of the surface contours of the mixing of steel/slag under the conditions of **eccentric** stirring of different gas flow rates. Similarly the open eye size increases with the increase of the gas flow rate. Compared to the centric stirring, the open eyes size is relative smaller especially at the high gas flow rate conditions (Figure 22e,f). The gas plume close to the right side wall gives resistance to the expending of open eye. The shape of open eye becomes irregular also.

Influence of slag viscosity: Slag viscosity is a thermo physical property that affects the kinetic conditions during ladle treatment. The slag viscosity is a function of the slag composition and temperature. In this study, a series numerical investigation has been made to study the influence of slag viscosity on the open-eye formation and steel-slag interaction.

Six different cases are calculated and the results are shown on **Figure 23** (a~f):

1. Case A: gas flow **200 l/min**, slag thick. = 10 cm, slag kinematic viscosity = **4.6e-5** m^2s^{-1}
2. Case B: gas flow 200 l/min, slag thick. = 10 cm, slag kinematic viscosity = 4.6e-4 m^2s^{-1}
3. Case C: gas flow 200 l/min, slag thick. = 10 cm, slag kinematic viscosity = 4.6e-3 m^2s^{-1}
4. Case D: gas flow 200 l/min, slag thick. = 10 cm, slag kinematic viscosity = 4.6e-2 m^2s^{-1}
5. Case E: gas flow 200 l/min, slag thick. = 10 cm, slag kinematic viscosity = **4.6e-1** m^2s^{-1}
6. Case F: gas flow **50 l/min**, slag thick. = 10 cm, slag kinematic viscosity = 4.6e-1 m^2s^{-1}

The slag viscosity has a significant influence on the open eye formation. The flow resistance increases with the slag viscosity. On the Figure 23a, a part of steel can flow over the top of the slag layer due to the lower viscosity of slag. This part of steel will come back to the steel bath due to the gravity, which tends to break up the slag layer (Figure 23b). This might lead to a strong slag emulsification in the ladle. The slag velocity decreases with the increase of slag viscosity (Figure 23c~f). On Figure 23f, **the open-eye disappears when the gas flow rate is quite low**, due to lack of stirring energy to push away the slag layer from plume region.

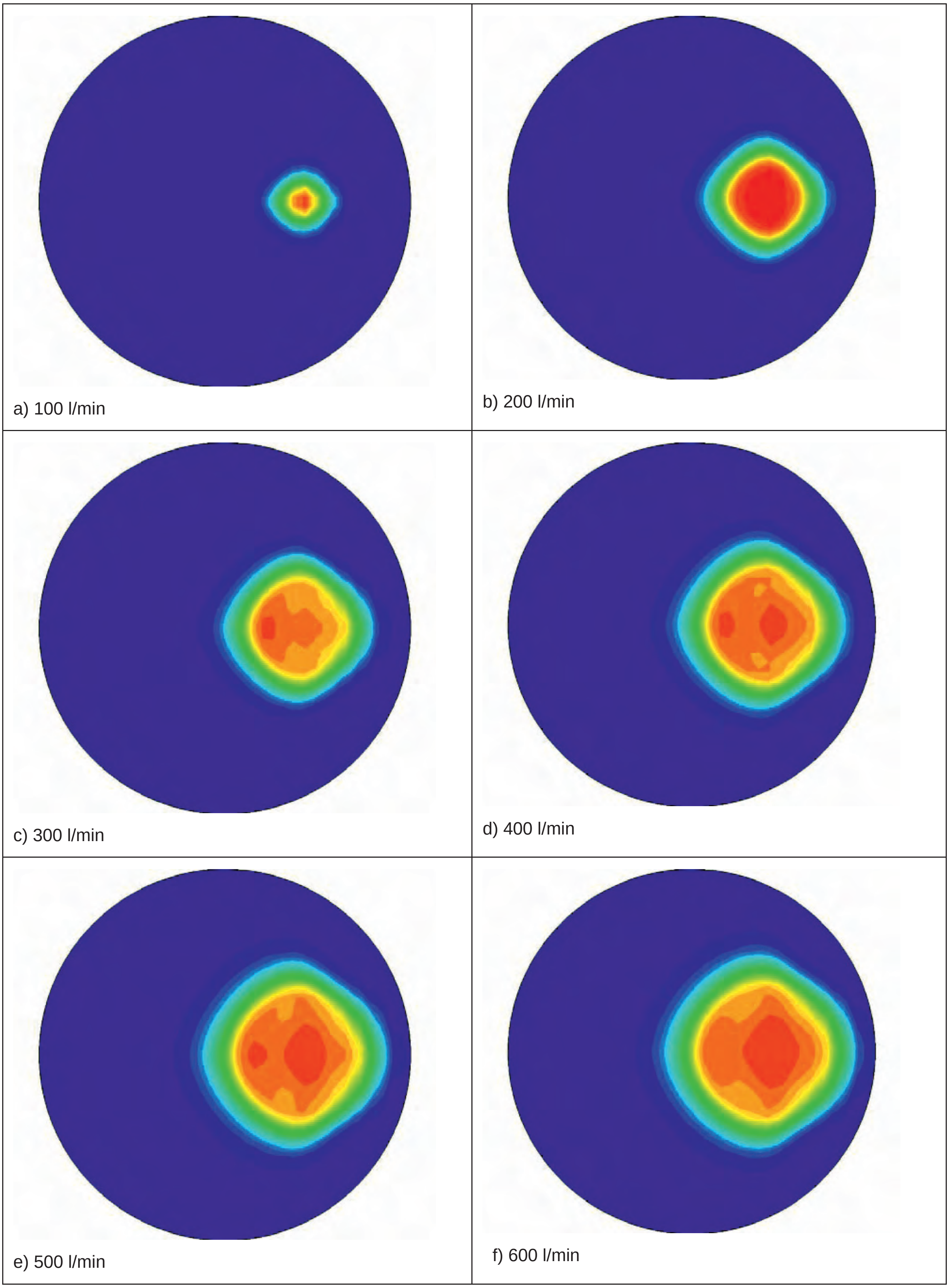

Figure 22 - Contour plot of steel/slag mixing at top surface of a eccentric gas stirring ladle with different gas flow rate (slag height: 10 cm)

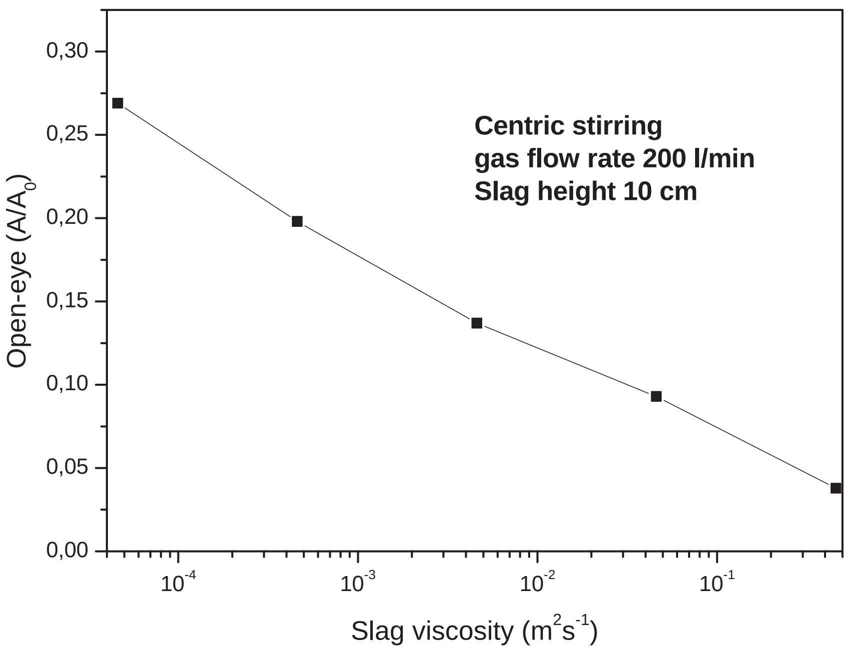

Figure 23 - Comparison of the open eye size by different process parameters (centric gas stirring)

Figure 24 plots the relation between the ratio of open-eye area and ladle surface (A/A_0) and slag viscosity: **a logarithmic decreasing relationship is obtained**.

Figure 24 – Computed influence of the slag viscosity on the open-eye area (120-t ladle)

Water model

A water model has been built up to simulate the gas/water/oil flow in the ladle (**Figure 25**). The physical simulation is three-dimension (3D) and three phases: argon, steel and slag are included. Open-eyes and slag entrapment could be simultaneous observed and measured by the water modeling work. The process parameters including gas flow rate, slag height, positions of porous plug and number of porous plug are investigated.

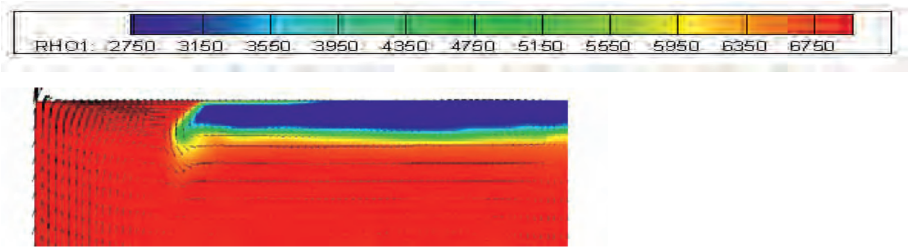

a gas flow rate 200 l/min, slag thickness = 10 cm, slag kinematic viscosity = 4.6e-5 m^2s^{-1}

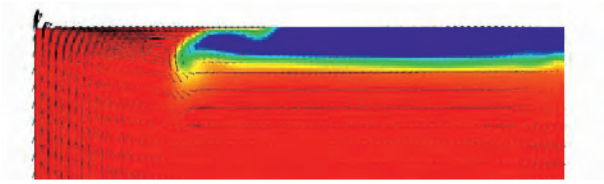

b gas flow rate 200 l/min, slag thickness = 10 cm, slag kinematic viscosity = 4.6e-4 m^2s^{-1}

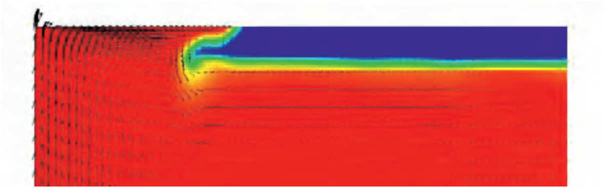

c gas flow rate 200 l/min, slag thickness = 10 cm, slag kinematic viscosity = 4.6e-3 m^2s^{-1}

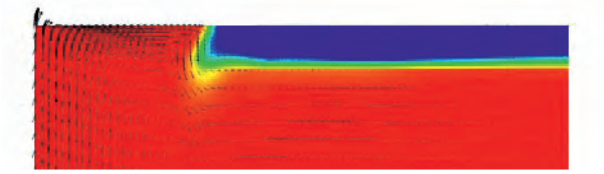

d gas flow rate 200 l/min, slag thickness = 10 cm, slag kinematic viscosity = 4.6e-2 m^2s^{-1}

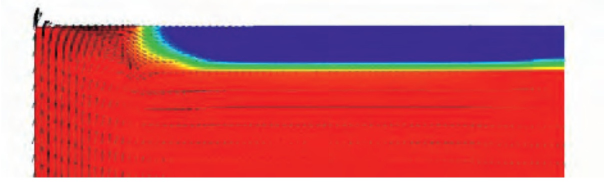

e gas flow rate 200 l/min, slag thickness = 10 cm, slag kinematic viscosity = 4.6e-1 m^2s^{-1}

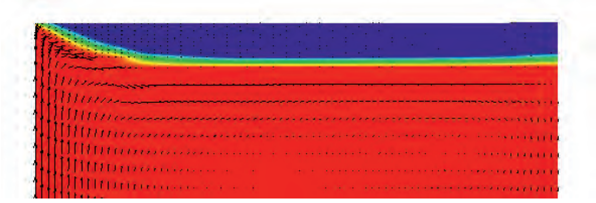

f gas flow rate 50 l/min, slag thickness = 10 cm, slag kinematic viscosity = 4.6e-1 m^2s^{-1}

Figure 25 - Photo of the experimental water model

The experiments have been performed at room temperature. Water simulates the steel phase and silicon oil, AK50, simulates the top slag. Physical properties of the water and oil are listed in **Table 9**. In order to visualize the open eye, trace amount of color, called Sudan Red, was added in the oil phase. The addition of Sudan Red would not change the physical properties of the AK50 oil according to the supplier.

Table 9- Physical properties of water and AK50 oil at 20°C

Physical properties	**Water**	**AK50 oil**
Density (kg/m^3)	998.2	964.6
Dynamic viscosity (Pa·s)	$1005 \cdot 10^{-6}$	$54.0 \cdot 10^{-3}$
Kinematic viscosity (m^2/s)	$1.004 \cdot 10^{-6}$	$56.0 \cdot 10^{-6}$
Surface tension (mN/m)	72.8	20.8

Gas was injected through the ladle bottom by three different nozzles, A, B and C. The nozzle diameter is 3 mm. Different gas flow rates has been used, 3.6-36.7 l/min. The size and the variation of the open eye were recorded by a digital video camera during 3 minutes and the video camera is place above the slag phase. The size of the open eye was obtained by image analysis of the video film. Investigation of slag entrapment has been done via the side window by taking photo with a digital camera. The water level has been constant, 650 mm and the oil level has been varied between 20-70 mm. The **Table 10** shows the test parameters.

Table 10- Experimental parameters for the water model tests

Series	**Gas flow rate (Nl/min)**	**Slag level (mm)**	**Nozzle position** [1]
1 – 9	3.7, 5,7, 9.2,14.7, 20.2, 25.7, 31.2, 36.7	20	B
10 – 18	— | | —	30	B
19 – 27	— | | —	40	B
28 – 36	— | | —	50	B
37 – 45	— | | —	60	B
46 – 54	— | | —	70	B
55 – 63	3.7,5,7, 9.2,14.7, 20.2, 25.7, 31.2, 36.7	20	A
64 – 72	— | | —	30	A
73 – 81	— | | —	40	A
82 – 90	— | | —	50	A
91 – 99	— | | —	60	A
100 –108	— | | —	70	A
109 –117	3.7,5,7, 9.2,14.7, 20.2, 25.7, 31.2, 36.7	20	A, C
118 –126	— | | —	30	A, C
127 –135	— | | —	40	A, C
136 – 144	— | | —	50	A, C
144 – 153	— | | —	60	A, C
154 – 162	— | | —	70	A, C

The open-eye size increases with the gas flow rate and the open-eye size decreases with the increased slag height. However, it should be pointed out that it is not a clear linear relationship between the slag height and open-eye size especially for the thick slag (larger than 40 mm). **Figure 26** compares water model and numerical simulation. The computed open-eye image shows reasonable agreement with the water model experiment. **Figure 27** shows the comparison of numerical simulation and water model results by the variation of A/hH as a function of parameter, Q^2/gH^5. The experiment results are from the centric gas stirring with gas flow rate: 7~20.2 l/min and oil height: 2~7 cm. The correlation is presented below and it is quite similar with previous published works. **Numerical simulation results keep good agreement the water model experiments**.

$$\log\left(\frac{A}{hH}\right) = (1.12 \pm 0.04) + (0.37 \pm 0.02)\log\left(\frac{Q^2}{gH^5}\right) \qquad (9)$$

This is further discussed in the intermediate conclusion paragraph 5.2.3.1.4.5.

a) water model experiment b) numerical simulation

Figure 26 - Comparison of the open-eye between the water model and numerical simulation (centric gas stirring, gas flow rate: 7 l/min, oil height: 6cm)

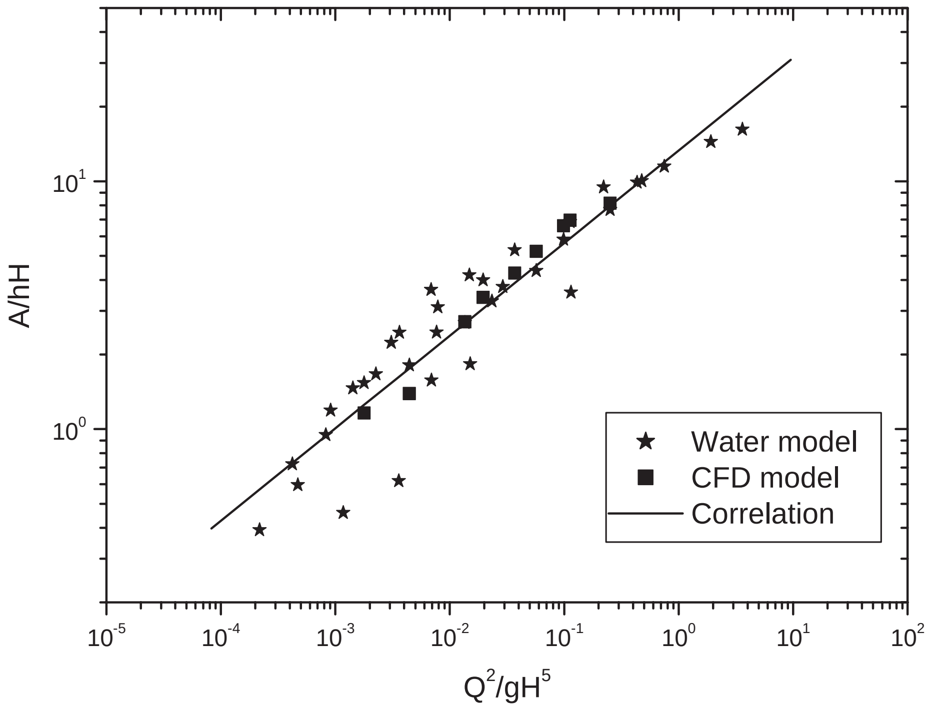

Figure 27 - Comparison of numerical simulation and water model by the variation of A/hH as a function of parameter, Q^2/gH^5 (centric stirring, gas flow rate: 7~20.2 l/min, oil height: 2~7cm)

Slag entrapment: In considering the wave formation at the steel/slag interface, it is of great interest to find out if it would be possible to predict the occurrence of dispersion of slag into metal. Xiao et al. [33] used both physical modeling with oil and water and mathematical modeling to show that entrapment of a lighter phase into a heavier occurs at an oil head wave. Moreover, the authors claimed that entrapment initiates in a steel ladle when the **Weber** number equals 12.3.

In the CFD simulation the local Weber number can be evaluated by using the calculated velocity in this grid. The surface tension is set to 0.12 N/m. The contour plot of the density in the ladle is shown in **Figure 28**. The marked point with the calculated Weber number of 11.9 is located at the gas/slag/steel mixed region. Most of the slag entrapments occur closed to this region. These results indicate that the Weber number close to the interface may be useful in determining the tendency for slag dispersion into steel. If taking the properties of slag and steel, ρ_{slag}=2743 kg/m^3 and ρ_{steel}=6981 kg/m^3, when the interfacial tension of the slag and steel in the gas stirred ladle are chosen to 0.012 N/m, 0.12 N/m and 1.2 N/m, the horizontal critical steel velocity is about 0.19 m/s, 0.35 m/s and 0.62 m/s. At equilibrium the interfacial tension of slag/steel is about 1.2 N/m, but this value decreases significantly when the interface is unstable and chemical reaction occurs. From early published measurements [34], a gas flow rate over 100 l/min corresponds to a horizontal velocity near the surface larger than 0.2 m/s. Hence, **it is recommended that the soft stirring gas flow rate is lower than 100 l/min in order to avoid the slag entrapment.**

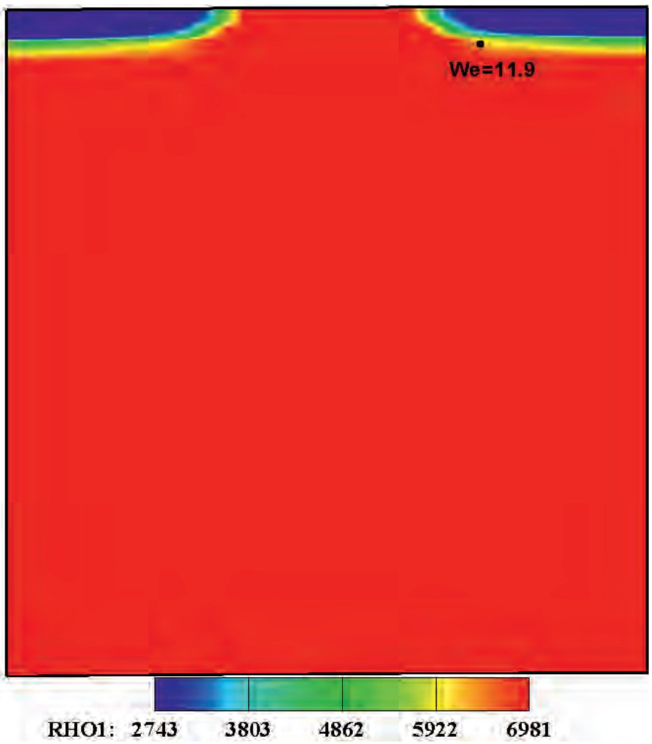

Figure 28 - Contour plot of mixing density of steel/slag at central plane of a centric gas stirring ladle (gas flow rate: 200 l/min, slag height: 10 cm)

Transient simulation of open eye formation: A transient two-dimensional simulation has been done to study the open-eye formation. **Figure 29** shows a series of simulation results. Steel surface velocities increase after 6s gas stirring and the slag begins to be pushed away from the gas plume area. Due to the high slag viscosity, the slag layer is a kind of flow resistance to the steel stream. A part of steel will flow downward after meeting the front of slag layer. The downward velocities give the possibility to drag the slag into the steel bath and form the slag entrapment. At the same time, it is observed that another part of steel tries to flow through the slag surface with high horizontal velocities. The horizontal velocities of steel decreases rapidly above the slag layer, then, the steel tends to flow down to penetrate into the slag layer. This leads to steel droplets mixing into the slag layer (splash phenomena) and create a large steel/slag mixing area. **When increasing the gas flow rate, the open-eye size will increase and a strong slag entrapment occurs. Slag droplets were entrapped into the steel bath, which is a kind of source of the big inclusions.**

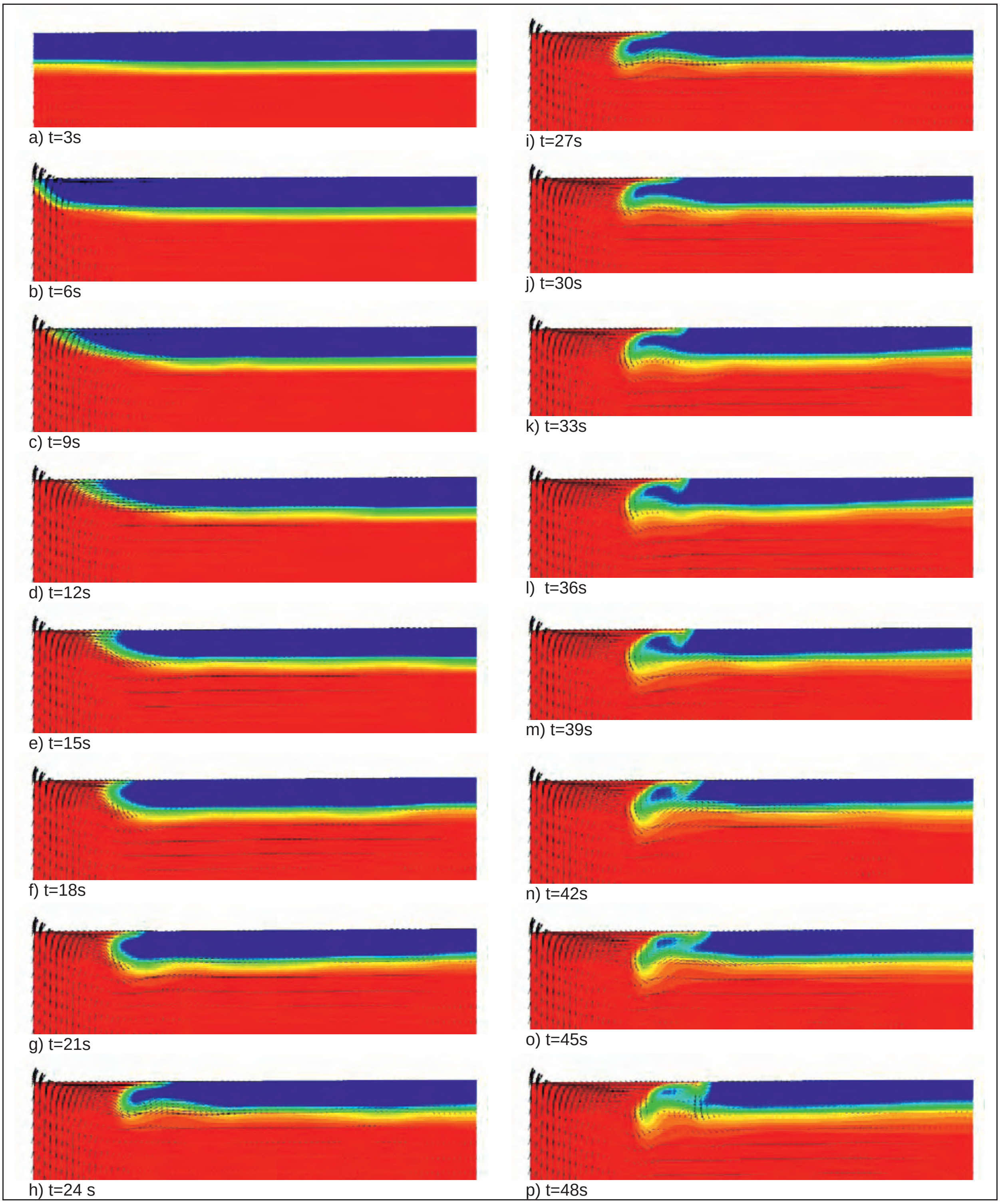

Figure 29 - Transient simulation of the mixing of steel/slag in a gas stirring ladle

5.2.3.1.4.5 Conclusion over open-eye model

As already mentioned in this report, mainly two approaches exist in the recent development regarding correlations between open-eye area and process parameters. These are evaluated using the data from BFI, MEFOS, SAARSTAHL and SIDENOR:

- Yonezawa/Schwerdtfeger (**Figure 30**). The present set of data in this plot is conveniently positioned and shows that laboratory, pilot plant and steel plant data can be compared within this research project,
- Mazumdar/Evans (**Figure 31**). This plot does not intend to unify all data like the previous one. The positioning of the best-fit straight lines is determined by two dimensionless constants according to $A/h^2=K1-K2*(QH^{-0.66})$. K1 and K2 depend on the characteristics of the gas-liquid system; K2 additionally depends on the vessel dimensions. Therefore, data of each different system (water model, pilot plant, steel plant) should and does display best-fit straight lines with different slopes and intercepts.

The effect of the slag viscosity, as evidenced by MEFOS numerical simulation (**Figure 24**) is an open door to further model the open-eye area and possibly get a unique formulation that would be valid for water models and steel experiment.

Finally the measurement of the open-eye area represents a measurement of the true stirring in industrial conditions if the slag properties and thickness are controlled and/or well known.

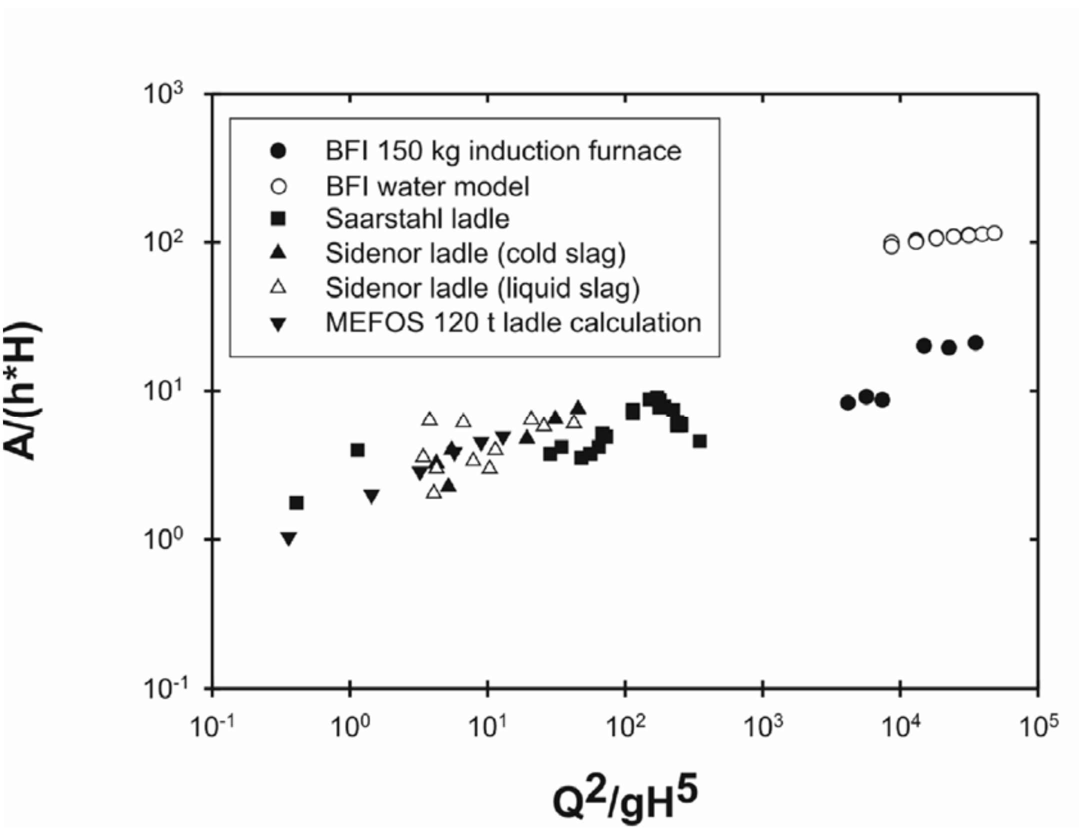

Figure 30 - Relation between A/(h H) and Q^2/gH^5 for water modeling, lab and plant trials and calculations

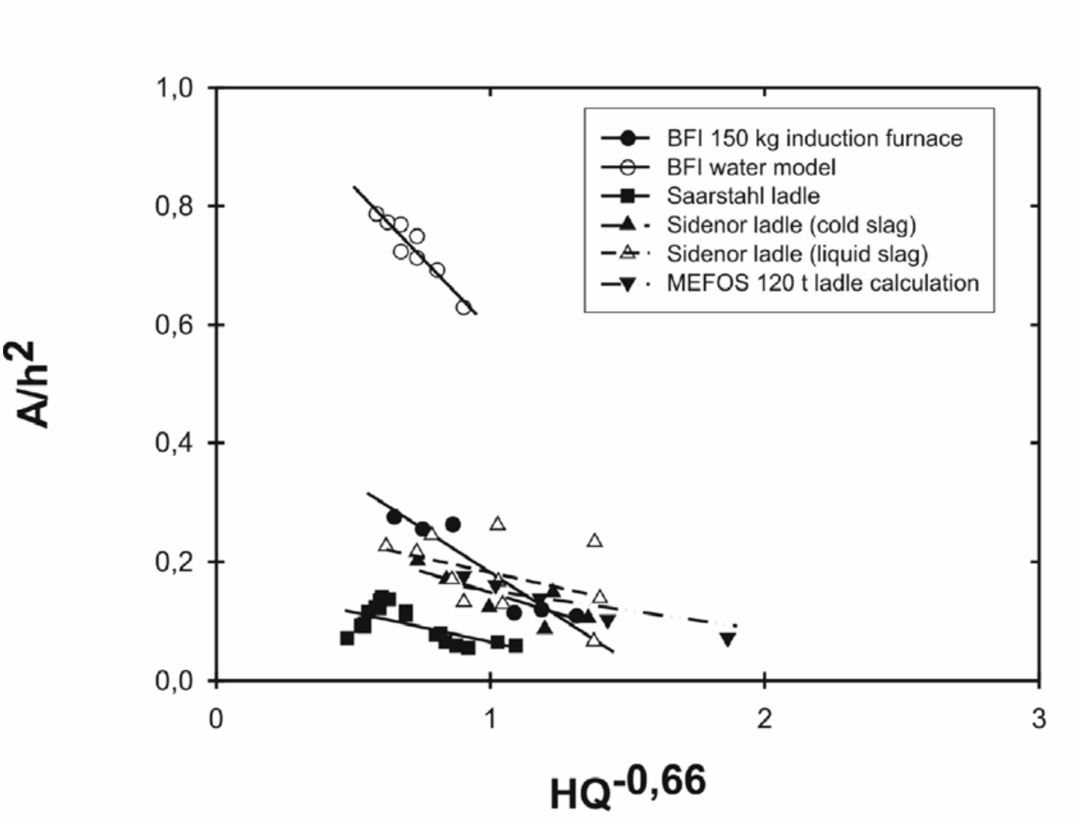

Figure 31 - Relation between A/h^2 and $HQ^{-0.66}$ for water modeling, lab and plant trials and calculations

5.2.3.2 Advanced on-line methods to control ladle stirring

The **standard industrial practice in SIDENOR** before the help of any image analysis was a regulated control of the inert gas flow rate from the ladle furnaces LF1 and LF2 control room. Although quantitative criteria for flow rates have been established according to the different metallurgical operations (ferroalloys or slag makers additions, vacuum, strong desulphurization, etc.), the refining bay operator visual criterion prevails. The latter has proved to be the most practical in terms of "real stirring", as there are important differences between the stirring effect on the bath surface and the injected flow rates used. So, the bubbling and the diameter of the "red eye" formed on the vertical of the plug are the indicators of the "stirring strength". In the vacuum station, a TV camera helps to regulate the flow rate so that a stable level can be maintained in the ladle.

The stirring system installed at LF1 and LF2 has the following configuration:

- a stream for regulation of argon or nitrogen flow by means of a mass flow meter, accurate for the overall range of normal use (50 to 1000 l/min),
- a stream, controlled by % valve opening, habitually used with 100% valve opening when strong stirring needed (to open plugs, , ferroalloy mixing,…),
- an emergency by-pass to be actuated when a mechanical device failure occurs.

A flow rate set point can be selected and validated to keep an accurate and stable flow rate. Pressure measurement after flow meter is available (we call it back-pressure or counter-pressure), so flow rates and plug pressure relationship studies are possible. The PLC data are transferred to plant data base and stored there with a frequency of 0.5 Hz.

ACERALIA has two LD steelplants in Asturias, the one in which the research and the trials of this project have been performed is placed in Avilés (LDA). Bubbling processes are present along the production route from converter to continuous casting. The most important stirring processes in the ladle take place during Secondary Steelmaking operations. In Avilés plant, the major part of the production is treated in the CAS station. In addition, CAS bubbling pattern has the most varying gas flow rate and the plant is better accessible with better features for the safety of the trials.

A scheme of the circuit for bubbling gas feeding /adjustment is depicted in **Figure 32**. Argon or Nitrogen from the general supply of the plant can be chosen as bubbling gas by means of valves V1, V2 and V3. The flow rate is regulated through V4 which is controlled by software taking into account the flow rate and the pressure values from FT and PT3 transducers. This stream is conducted to the ladle car by a flexible tube and, finally, supplied to the ladle through an automatic connection between the car and the ladle. The ladle has one bottom off-centered porous plug at 700 mm from the ladle axis.

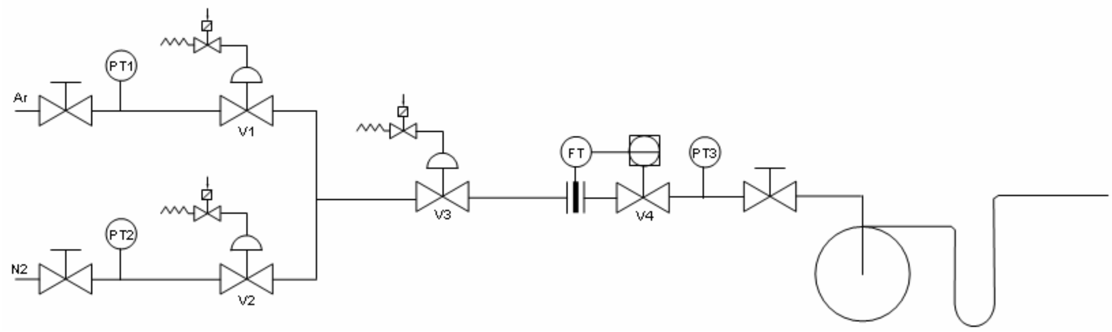

Figure 32 - Simplified scheme of the gas bubbling system at ACERALIA (Avilés LD plant)

The duration of a typical treatment is around 20 minutes but the ladle remains in the CAS station for almost 30 minutes, depending on production schedule. This provides a short time to perform sensor adjustments. **Table 11** summarizes the main features of the bubbling process for CAS treatment at ACERALIA LDA.

Table 11- Main features of treatment at CAS station in ACERALIA LDA

Stage	Operation	Flow rate (l/min)	Typical duration (min)
1	Open-eye formation and snorkel immersion	700	1
2	Performing additions	350	1,5
3	Alloying	500	2
4	Homogenization	360	8
5	Cleanliness bubbling	<50	5

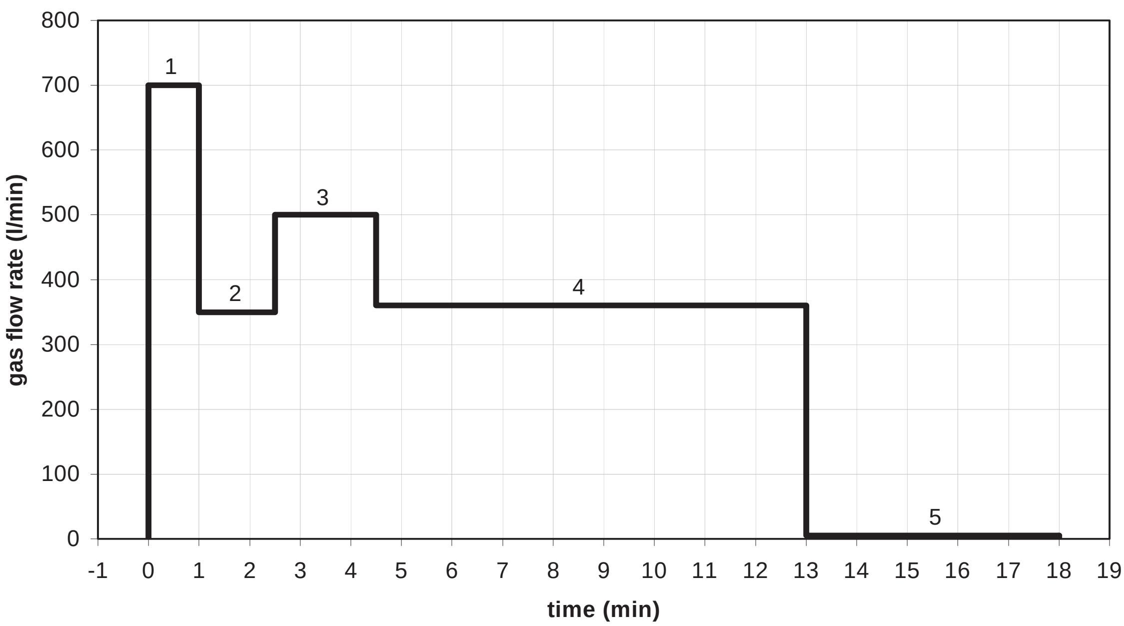

Ladle capacity	Slag amount	Plugs		
		Number	Lifetime	Type
300 t	3 t (mean)	1	1 - 10 heats (mean: 4 heats)	Off-centred (700 mm)

Slag average composition % (based in 8 samples)

Fe	S	CaO	SiO_2	MgO	Al_2O_3	FeO	MnO	P_2O_5	TiO_2
16.76	0.04	15.30	13.18	5.11	28.15	21.06	12.63	0,47	1.17

The following two sub-paragraphs detail the development of advanced assessment techniques, based on the image analysis of open-eye area on one hand and of the ladle vibration on the other hand.

5.2.3.2.1 OPEN-EYE ANALYSIS

5.2.3.2.1.1 On-line image analysis software (BFI)

During medium to strong stirring of liquid steel in a steelmaking ladle, the slag cover is broken open by the ascending stirring gas and an open-eye is formed. Only gas that contributes to the stirring process also contributes to open-eye formation. Gas that escapes through leakages, or otherwise discharges, neither promotes the stirring process nor the open-eye formation. Therefore, the size of the open-eye is a direct indication of the efficiency of the stirring process.

Image processing system

An image processing system was developed by BFI to determine the size of the open-eye. It consists of a camera, a PC, image processing software and auxiliary components like cabling, monitor etc (**Figure 33**). The image processing system was installed on three different locations: On water model, on a laboratory induction furnace and above a ladle stirring station in the turret of a continuous caster. The camera data was transferred to a PC, where it was digitalized and provided to the BFI image processing software.

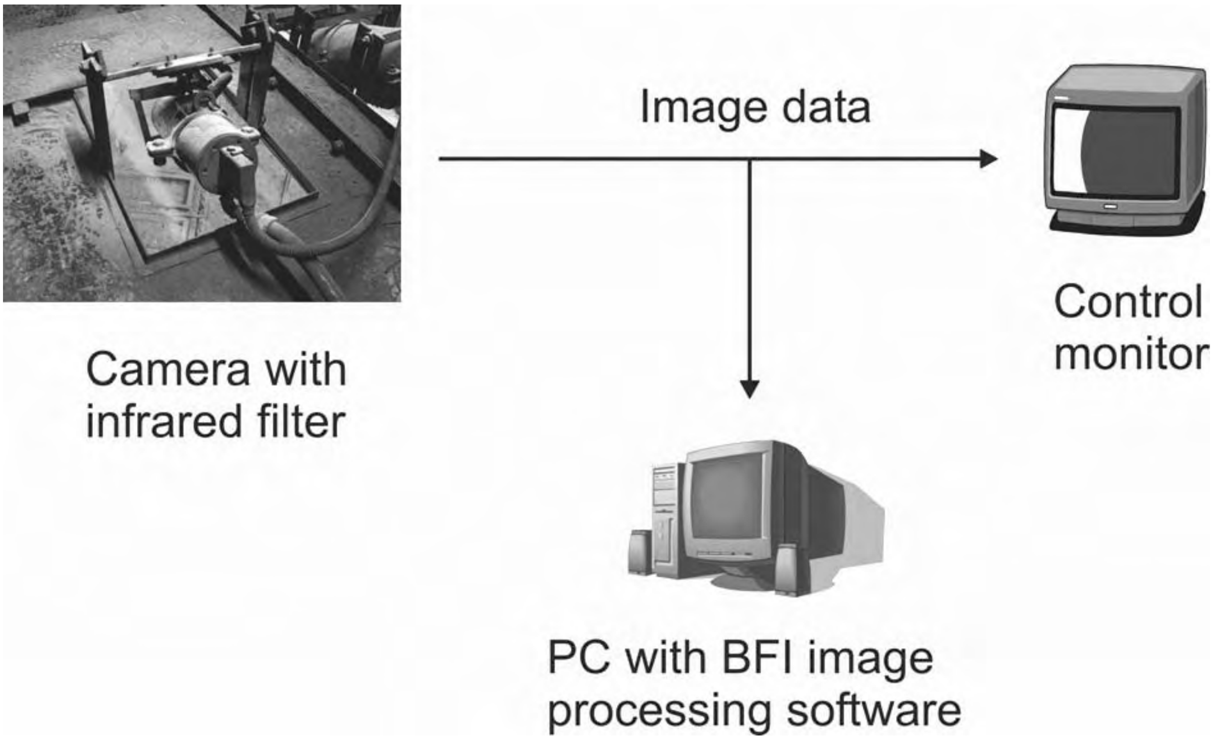

Figure 33 - BFI image processing system

The BFI image processing software (**Figure 34**) was designed to detect the open-eye in the camera images using advanced image processing techniques. It continuously determines and logs the size, position and form factor of the open-eye together with the stirring gas data. At the steel works, this information proves helpful for the stirring operator to accurately judge the actual stirring condition. In addition, the BFI image processing software was trained to detect the start and finish of each stirring charge. After each charge, it provides a stirring summary with classification of open-eye sizes and a good/bad stirring statement in percent of total stirring time. The summary, processed into a diagram, was found to be advantageous for complete evaluation of stirring charges at a glance.

Figure 34 - BFI image processing software

The design of the camera setup was developed during several inspections of ladle stirring stations in the steel plant of Saarstahl AG. Considerations regarding the installation position of the camera are described in the following. **Figure 35** shows a two-dimensional schematic view of a steelmaking ladle and the CCD camera setup. The inner radius of the steelmaking ladle is indicated r, the viewing distance from the camera to the surface of the ladle is labeled d, the height of the camera relative to a mean liquid level of the ladle is labeled x and the horizontal distance of the camera from the ladle wall is given as e. The critical angle of the camera relative to the vertical axis to perform good measurements is given as β, the aperture angle of the camera lens is indicated by γ, the apex angle of the ladle is given as α and its alternate angle is labeled α^I.

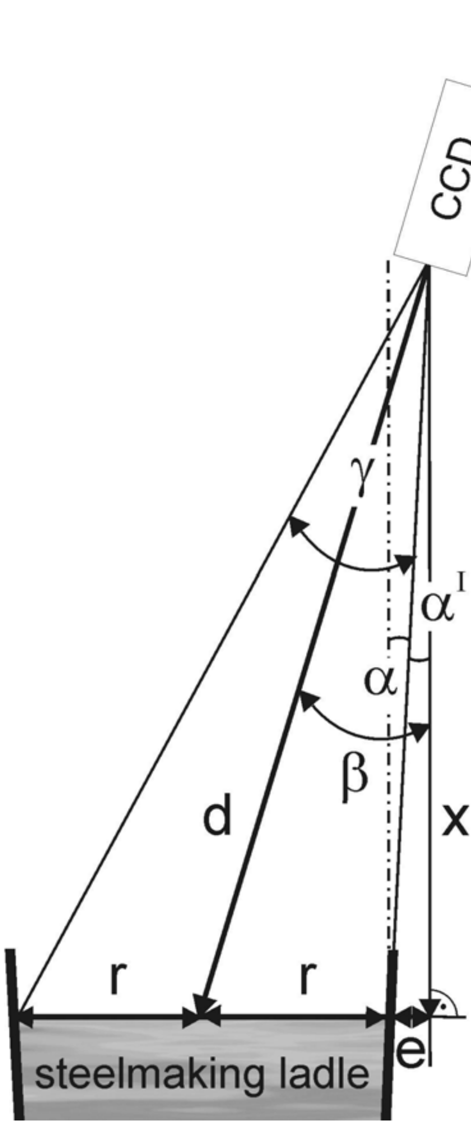

Figure 35 - Schematic view of a steelmaking ladle and the camera setup

The critical angle of the camera β comprises of the apex angle of the steelmaking ladle α and the aperture angle of the optical system of the camera γ

$$\beta \approx \alpha + \frac{\gamma}{2} \qquad (10)$$

The distance of the camera from the steel surface d is defined by the aperture angle of the optical system of the camera γ and the inner radius of the steelmaking ladle r

$$d \approx r / \tan\frac{\gamma}{2} \qquad (11)$$

The height of the camera installation relative to the mean ladle liquid level x is defined by the distance of the camera from the steel surface d and the critical angle of the camera β

$$x = d * \cos\beta \qquad (12)$$

The horizontal distance of the camera installation relative to the outer ladle wall e is defined by the apex angle of the ladle α and the height of the camera installation x

$$e = x * \tan\alpha \quad (13)$$

With these equations, the critical angle of the camera depending on aperture angles and the height and distance of the camera installation relative to the ladle can be determined. For example, using ladles with a 1.8 m steel surface radius r, a ladle apex angle α of 2° and an optical system of the camera with an aperture angle γ of 50°, the critical angle β of the camera is 27°. The ideal relative height of the camera system x should be 3.44 m and the relative horizontal distance from the ladle wall e should be 0.12 m. In practice, as ladles may be positioned differently within a small margin, safety margins should be added.

The distance between the CCD camera and the liquid bath is determined by the liquid level in the ladle. This depends on the amount of liquid steel in the ladle and on the amount of wear of the ladle refractory linings at the bottom and the walls of the ladle. The height of the liquid steel bath may vary in a range of 0.1 m from the mean height due to wear of the ladle refractory. Using the geometry of the example given above, a point at half of the ladle radius will apparently move 0.08 m or approximately 2 % of the image diameter as a result. A variation of the diameter of the liquid steel surface does not affect the image processing system. The diameter of the surface is not used as a length standard. Instead, the system may be calibrated once by recording a geometric pattern installed at the ladle position.

An important step to prepare the camera for installation was to select appropriate optical filters to optimize the visualization of the melt surface patterns. Several optical filters were evaluated during an industrial trial. A mobile CCD camera was used to acquire images of a ladle surface during open-eye stirring of liquid steel. During one stirring sequence, several filters were adapted to the mobile camera alternately. The recorded images were analyzed with an image processing software with the following evaluation criteria in mind:

- Overall brightness of the images,
- Brightness sensitivity between bright and dark parts of the images,
- Visibility of fine structures at the surface of the liquid steel bath.

The results are given in **Table 12**. **The RG 780 infrared filter with 780 nm cut-off wavelength** was chosen for all further hot melt trials because of its superior performance.

Table 12- Evaluation of optical filters for image processing system (BFI)

Name	Type	Overall brightness	Brightness sensitivity	Visibility of fine structures
Neutral filter T = 50 %	Neutral filter with 50 % transmissivity	Acceptable	Poor	Poor
RG 610	Red filter (610 nm cut-off wavelength)	Poor (brightness too high)	Poor	Poor
RG 780	Infrared filter (780 nm cut-off wavelength)	Good	Good	Good

Image processing software for analysis of ladle stirring images was developed by BFI. It is part of the image processing system and was adapted to industrial ladle stirring environments as well as laboratory scale physical models. It works either on-line or off-line and can be used interactively for adaptation of image analysis parameters to the image sequences under evaluation. The BFI image processing software was developed to analyze stirring images on-line according to four consecutive steps as described in the following.

Strategy of image analysis

Image analysis by the BFI image processing system can be divided into four steps: Acquisition of images, segmentation of images, extraction of image features and classification of the open-eye data.

The acquisition of images was realized using a PC-based frame grabber with a frame rate of approx. 10 fps. This frame rate was chosen to ensure that an image processing system was developed successfully within the scope of this research project. Higher frame rates would have resulted in disproportionate demands on the hardware and software of the image processing system. The selected frame rate is still well ahead the needs to control ladle stirring process. Following a multi-second averaging detected open-eye sizes are visualized to the operator.

Detection of the characteristic open-eye pattern in images from gas-stirred ladle treatment is realized using image segmentation. A brightness threshold was chosen to distinguish the bright open-eye from its dark surrounding. The BFI image processing software derives the brightness threshold from the histogram of each image individually. During the operational trials, the value of the brightness threshold was found to be critical for image processing. Values too high result in open-eyes appearing smaller than they are. On the contrary, values too low result in open-eyes appearing larger than they are.

The analysis of image sequences from gas stirred ladle treatment processes showed that brightness thresholds of subsequent images change both long-term and short-term. Long-term changes result from gradual dust contamination of the optical path. Short-term changes are caused by image anomalies, such as burning sampling lances that were often detected during measurement campaigns carried out during this research project. It was found to be very important to adapt to the gradual long-term changes of the brightness threshold and to rule out short-term changes. Therefore, the static brightness threshold was replaced by a “dynamic” or “adaptive” threshold.

The adaptive threshold is realized by comparing the brightness threshold of the image currently under evaluation with an sliding averaged value of brightness thresholds of previous images. The image currently under evaluation is discarded in case of a large and therefore short-term deviation of its brightness threshold from the sliding averaged value. Otherwise, to adapt to the long-term changes, the brightness threshold of the image currently under evaluation is computed into the sliding averaged value.

On the segmented image, a feature extraction method is used to measure the individual features of the open-eye. The area, the form factor (height divided by width) and the location of the open-eye were found to be most suitable to aid the subsequent open-eye classification.

A classification of the open-eye with regard to real operational conditions was developed. Anomalies which occurred during measurement campaigns at gas stirred ladle treatment processes were taken into account for the design of open-eye classification algorithms.

Advantages, performance and environment

The performance of the BFI image processing software for open-eye analysis was investigated during physical modeling, laboratory hot-melt trials and measurement campaigns at Saarstahl AG. The BFI image processing software gave impressive results with image data from industrial trials. The open-eye was detected reliably and image anomalies were ruled out safely. Adaptive threshold was found to be effective.

The BFI image processing system was designed to process about 10 images per second (frequency resolution 10 Hz). In typically 1/10th of a second, an image was grabbed from the camera, evaluated for the open-eye size and, if desired, saved into an AVI movie file. To provide the operators of a ladle stirring station with usable and stable open-eye size information, it was agreed to average the open-eye sizes for several seconds. This greatly improved the acceptance of the novel BFI image processing system among the operators in the steel works, who were more interested in trustworthy information than in sub-second resolution. Therefore, the frequency resolution of 10 Hz was appropriate, or even over-specified, for the measurement problem. However, with high-speed cameras and real-time image processing routines, frequency resolutions of 1 kHz or even 10 kHz are possible. These systems consist of very expensive hardware and software which is without the financial scope of this ECSC research project.

Open-eye classification

Using the feature data extracted in the previous step, a classification of the open-eye with regard to real operational conditions was developed. Anomalies which occurred during measurement campaigns at gas stirred ladle treatment processes were taken into account during the design of open-eye classification algorithms. The feature data of the open-eye is assessed in five steps to identify these anomalies: a) area is within a margin b) area changes dramatically short-term c) position is within a margin d) position changes dramatically short-term and e) form factor is within a margin.

As described before, the BFI image processing system had been used successfully during physical modeling trials where water was used as modeling fluid. To extend the experience with image processing under conditions more comparable to steelmaking but still fully controllable, laboratory trials in liquid steel were carried out.

The laboratory trials on the pilot metal furnace proved that the BFI image processing system works faultlessly under semi-industrial conditions. Analyzing a slag/liquid steel bath surface comparable to that in stirred steelmaking ladles, it detects the open-eyes and determines their area without problems and with good standard deviations. The BFI image processing system was consequently transferred to industrial conditions.

In-plant extensive testing and adaptation of image analysis package

The BFI image processing system was tested during measurement campaigns in the steel plant of Saarstahl AG and image and process data was gathered. Purpose of this task was to further develop the advanced image processing method for the control of ladle stirring process under plant conditions.

Gas stirred ladle treatment processes were recorded and evaluated on-line. An overview of the measurement campaigns is given in **Table 13**. Image anomalies were carefully evaluated to aid the development of the open-eye classification algorithm of the BFI image processing software. A sample image acquired at measurement campaign #669 is shown on **Figure 36**.

Table 13- Measurement campaigns at gas stirred ladle treatment processes (BFI)

Date	ID numbers of measured heats
18. 2. 2004	BFI1-BFI5
14. 9. 2004	503, 509, 511
6. 10. 2004	036
7. 10. 2004	075, 077, 080
18. 11. 2004	289
19. 11. 2004	327, 334, 336, 340
26. 11. 2004	669
12. 4. 2005	029
15. 6. 2005	511, 512

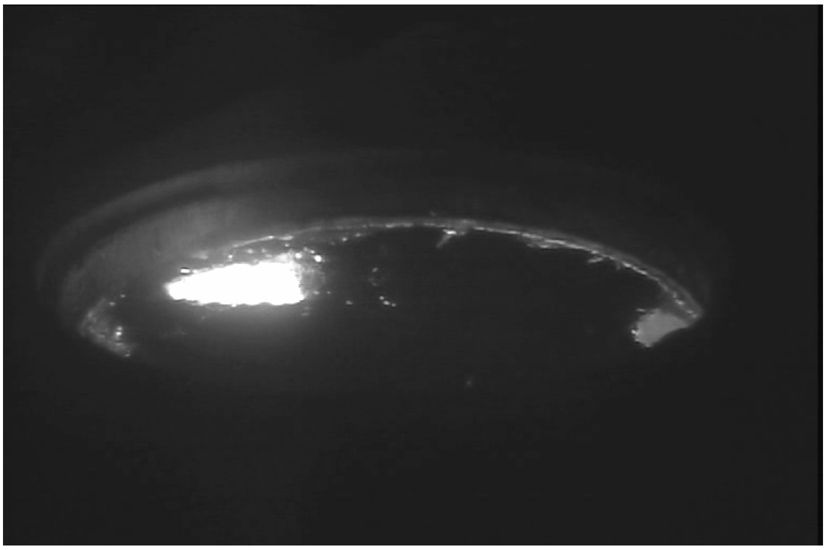

Figure 36 - Sample image taken at measurement campaign 669 at gas stirred ladle treatment process

Image anomalies that were detected during the measurement campaigns were:

- Sampling lances burning brightly when immersed into the liquid metal through the open-eye,
- Sampling lances burning softly on the slag or floating in the open-eye,
- Covering compounds burning on the slag surface and on the open-eye,
- Refractory materials radiating brightly nearby the slag/refractory interface after ladle stirring, still giving the impression of an open-eye.

The anomalies were evaluated and measures to distinguish them from normal operating procedures were developed.

As a result, detection of image anomalies was improved and testing of the BFI image processing system was successful. Vital information was obtained during the measurement campaigns to optimize the detection algorithms of the BFI image processing software.

Industrial transfer of the development

The BFI image processing system was permanently installed in the turret of a continuous caster at Saarstahl AG to improve the ladle treatment process. Additionally, images were acquired separately from a ladle stirring station and processed by the BFI image processing software. According to the results of these investigations, the suitability of the BFI image processing software for both strong and weak stirring was assessed.

The image processing system at the turret of a continuous caster provides for the first time important open-eye size information and helps the operator to maintain a suitable small stirring gas flow rate for optimum open-eye generation.

Margins for the minimum and maximum tolerable open-eye size were defined and a good/bad signal is given as an immediate and easy-to-understand feedback to the operator. In addition to the information provided on-line, the open-eye sizes and stirring parameters are logged for documentation and subsequent rating of the stirring process. The system was applied to the daily steelmaking practice and has been running successfully non-stop and unassisted for several months.

5.2.3.2.1.2 On-line image analysis software (SIDENOR)

The installation of a camera at SIDENOR proved to be more difficult than expected (see Annex). SAARSTAHL AG was also faced to problem regarding the industrial implementation of a video camera in the course of this project.

During image acquisition, different parameter combinations were tried to check their influence on the results and subsequent analysis. Lens and camera parameter tuning has proved to be quite influential on the final image quality, poor parameters give as result images that are not useful for image processing. Most lens and camera parameters are related and must be tuned with liquid steel/slag images, because otherwise they are likely to be inadequate for the difference in the amount of light emitted. Even circumstantial factors as amount of dust in the housing front glass change parameters election. After getting first video records, imageJ processing software was acquired. This processing software allows automation via macros in Java programming. After acquisition start, image analysis procedure learning began too. The image analysis process summary is the following:

- Geometrical transformations of the image to allow length and area measurements,
- Image segmentation by threshold to determine what zones correspond to open-eye,
- Area measurement of zones classified as open eye,
- Automation of measurement procedure for great number of images.

Geometrical transformations of the image

Area measurement in the image consists of counting pixels corresponding to that region and multiplying the sum by the area value assigned to each pixel. For that reason, before starting any measurement, it is helpful to prepare the image and define geometric distances for subsequent correct area description. Due to image acquisition position even if most of the ladle surface is caught, the original circle of the ladle is converted into an oblique ellipse.

Figure 37 shows the procedure followed to obtain pixel area value. The obtained ellipse is 1100 pixel x 645 pixel. The ladle diameter is 3 m, so horizontally the ratio is **366.67 pixels/m**. Vertical ratio is different for the ellipse, therefore there is a pixel ratio of 1.7 between vertical and horizontal axes. After those calculations, area measurement was checked calculating whole area surface. Only 0.7 % difference was found between image analysis and geometric calculations, thus validating measuring technique.

That result and subsequent pixel/area ratio are only valid if all geometric factors remain unchanged. Any modification in image acquisition position, lens zoom or image scaling will change those values and new geometric calculation would be necessary, but the procedure used in this example would be equally valid. The important point is to get reliable geometric references to define pixel length and pixel ratio.

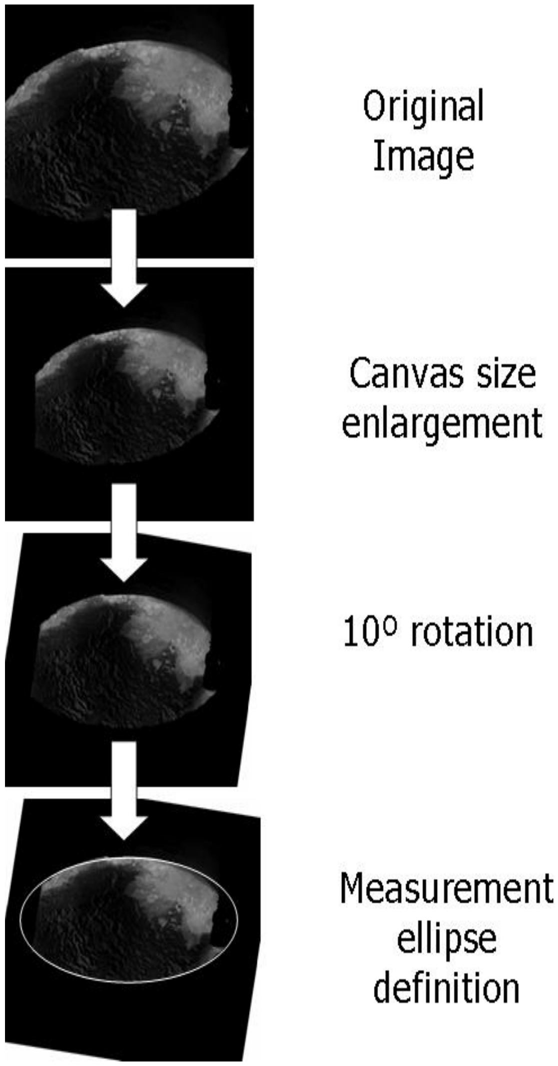

Figure 37 - Geometric transformations to achieve measurable figures

Image threshold

Once pixels are well correlated to real geometry, it is time to define what is wanted to be measured in the images, this is “segmentation”. The purpose of segmentation is to partition the image space into meaningful regions. The definition of “meaningful region” is a function of the problem being considered and in this project the meaningful region is “open-eye”: it is the region we want to distinguish from the rest. Theoretically, it would be possible and meaningful to distinguish three regions really, open-eye, ladle surface without open-eye and outside the ladle. However, in this case it is not needed because ladle surface area does not change and open-eye area is measured (it is geometrically calibrated), so even no open-eye ladle surface area or open-eye percentage with respect to total ladle surface may be easily calculated when desired.

There are several segmentation techniques and the most appropriate for each situation is also highly dependent on the nature of the image itself. In order to choose the most suitable for this case, image histogram was considered. Image histogram classifies all the pixels in the image in function of their brightness, as it is 8-bit image the brightness range is 0-255. The histogram of **Figure 38** is clearly bimodal. It shows two peaks, one around 15 and the other one around 115 of brightness. Open-eye areas are the brightest zone in the figure, they correspond to the bright peak (the 115 brightness peak) of the histogram. So the conclusion after histogram analysis is that outside ladle pixels are very dark, inside ladle pixel range from dark to bright and exhibit a two peak histogram and open eye pixels are the brightest.

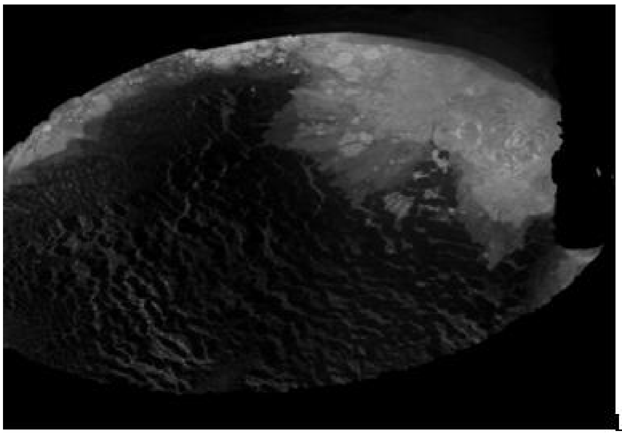

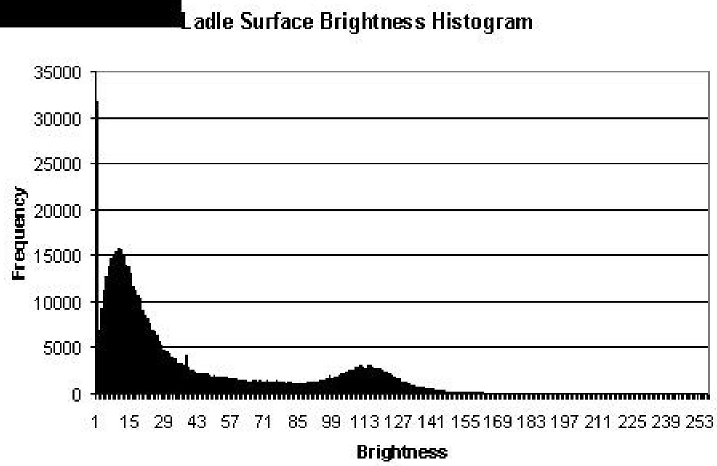

Figure 38 - Histogram of the image in the figure

In consequence, an efficient way to distinguish between open eye and the rest of the image is to establish an appropriate threshold to brightness values, pixel over this value will be considered part of open eye. This segmentation technique is called “threshold”. The main doubt encountered in the image processing has been to find the adequate threshold to decide where the “open-eye” and the slag are. Several ways to calculate the threshold have been searched and they have been tested comparing their results over real data. Tried threshold definition algorithms are the following:

1. <u>Static fixed threshold</u> choice based on histogram and image visual analysis, or other considerations. Considering the histogram in Figure 38 bright values next to the second peak have been considered as meaningful: 75, 95, 110 and 130 brightness values have been checked because they range from the final part of the first peak to the maximum in the second peak. So using this method all the images will be analyzed with the same threshold, once a threshold is selected for a set of images this method required the less computational work because the rest of algorithms calculate a threshold for each image independently. It is possible to apply it adaptively, by changing fixed threshold progressively from image to image.

2. Mixture modeling: This algorithm separates the histogram of an image into two classes using a Gaussian model. Then it calculates the image threshold as the intersection of these two Gaussians.
3. Otsu Threshold: The histogram is divided in two classes and the inter-class variance is minimized.
4. Maximum entropy threshold: Automatic threshold based on the entropy of the histogram. The method is very similar to Otsu's method, but with certain numerical differences, based on histogram.
5. k-means clustering: it performs pixel-based segmentation. The ultimate goal is to classify all the pixels in the image in 3, 4, 5 or the desired number of groups, called clusters. It is based on the statistical clustering technique to classify populations of data, in this case the population are brightness values. Depending of the number of groups decided, the same number of thresholds will be got, in this case only the last one will be used.

The algorithms may be classified in three groups: the fixed threshold, adaptive threshold based on histogram calculations (Otsu threshold, Maximum Entropy and mixed Modeling) and clustering method. Those methods have been compared using image in Figure 38 as reference at first, and with a set of images later. For each of the bimodal histogram methods two tests were carried out, applying the algorithm to the whole image and only to the ladle surface.

An important test to the different algorithm was to use a stack of stirring images with two flow rate changes from 300 l/min towards 400 l/min and then towards 500 l/min (STP); counter-pressure was not too low for that plug, so no major leak should be expected. This way the different threshold techniques could be tested with respect to changing stirring conditions. As dispersion of measured areas was high, moving average of the areas were performed to soften small range peaks and seek more general trends. **Figure 39** shows the results for some fixed thresholds, it is visible that a too high fixed threshold does not allow to distinguish different flow rates or stirring conditions, in this case 110 and 130 threshold areas do not change at all with flow rate; those threshold values were the ones near the second peak in the histogram.

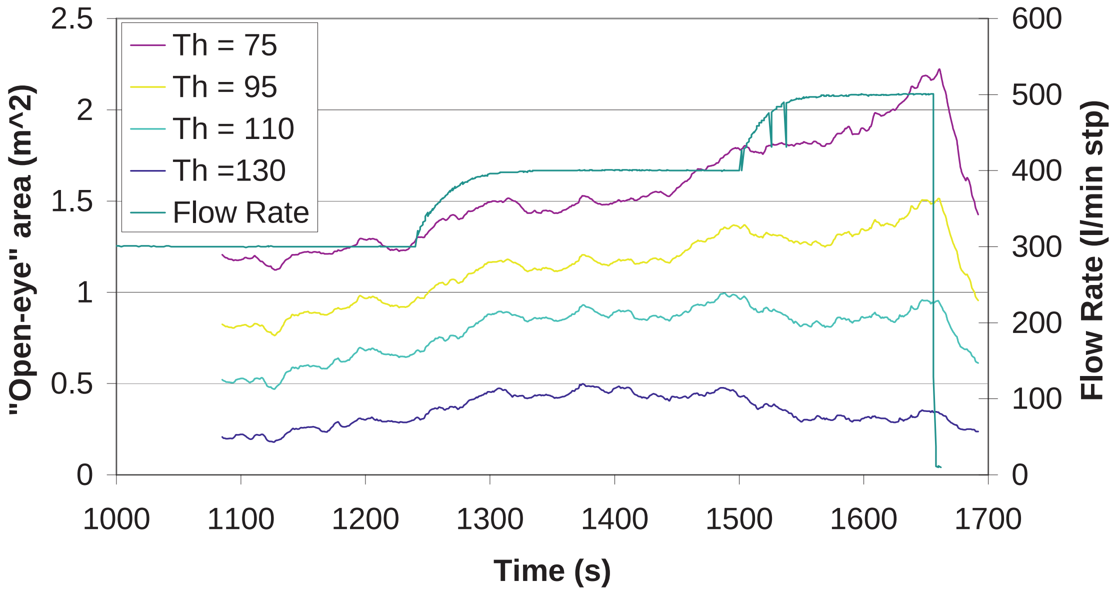

Figure 39 - Area measured with different fixed thresholds and after applying moving average for three consequent flow rates

On the other hand variable threshold methods and 75-95 fixed threshold areas show graphical correlation with flow changes. There are some time shifts in the changes but this is not strange because flow rate and image acquisition time are not perfectly synchronized. Maximum entropy threshold gets a larger area, slightly larger than fixed 75 threshold, and k-means clustering lower area, lower than 95 fixed threshold. The areas measured show a clear correlation between flow rate and measured area changes, not so evident from naked-eye analysis.

Another test was performed comparing threshold technique results with the same heat, plug, flow rate, slag, image acquisition position, exposure time and lens; but changing image acquisition parameters, so the amount of light entering the CCD was different for the same exposure time. This test pretends to simulate a change in optical conditions. Some of the results from this test are exposed in **Figure 40**. Fixed threshold methods are not able to cope with those changes; both 75 and 95 threshold figures are very sensitive to the changes. On the contrary entropy threshold is quite robust for most of the change range but it is strongly affected for great changes. K-means clustering shows moderate influence over the whole range of change, it is clearly more robust than fixed threshold and it behaves worse than entropy threshold for small-moderate changes, but better for strong changes.

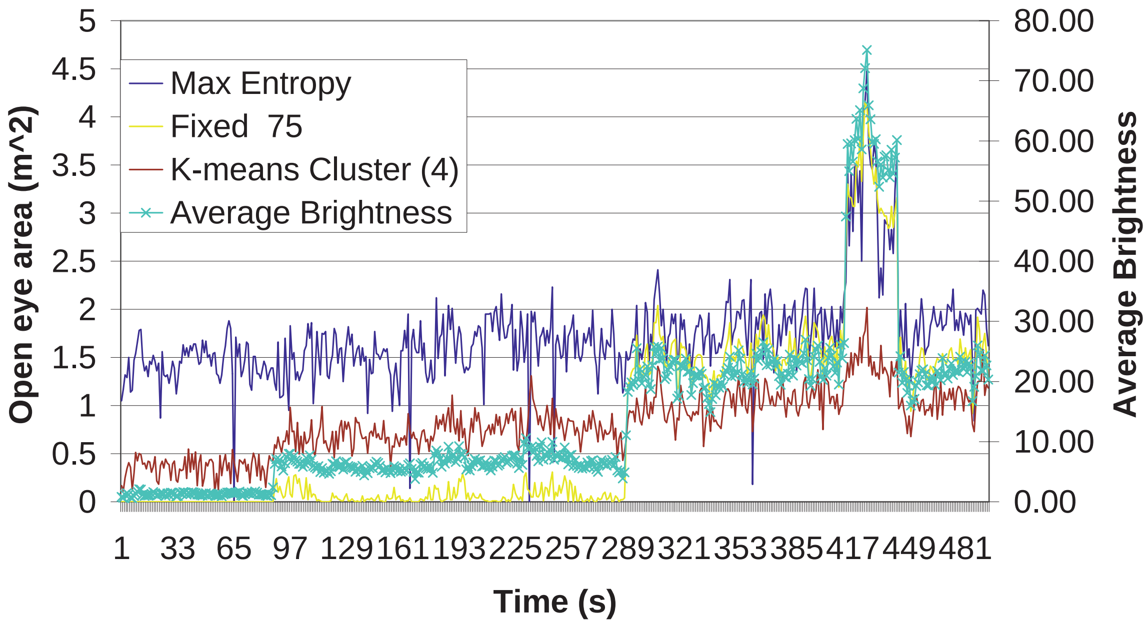

Figure 40 - Area measured with maximum entropy, fixed threshold and k-means clustering for images captured from the same heat, slag condition, plug state and flow rate (300 l/min) but different image acquisition parameters

The overall conclusions from these tests are:

- The k-means clustering method is considered very advantageous in those images analysis because it does not overestimate the open-eye, it is not sensitive to ladle surface outside area and it is not too sensitive to image acquisition parameter changes. With respect to number of clusters used, 4 clusters are preferred to 3 because they are a bit more robust to brightness changes even if open eye areas got with 3 clusters are likely slightly better in the tested images. The main problem of this method is the computation time needed, considerably higher than for any other method considered,
- Fixed thresholds are fast and easy to handle, and for constant acquisition conditions are able to distinguish flow rate in the same degree as any other methods. Their problem is that are very influenced by acquisition parameters (including environmental factors) so for a correct measurement a threshold should be defined in each circumstance,
- Maximum Entropy and Otsu threshold are based in similar theoretical considerations. Maximum Entropy has been more thoroughly studied because it was easier to use to multiple image sequences. The positive aspect of maximum entropy is its robustness for moderate brightness condition changes, on the other side it is quite sensitive to ladle surface outside background and overestimates to some extend the open eye area,
- Mixture modeling overestimates clearly open eye area and it is discarded for this reason.

After algorithm comparison some programming was performed to make it possible to measure automatically large amount of images, this work was very important so as to be able to measure large numbers of images.

5.2.3.2.1.3 Conclusion on on-line image analysis software

Both SIDENOR and BFI used image processing techniques to determine the open-eye size from images taken by a camera. The basic steps of image analysis were obeyed by both partners in similar ways. These steps were defined as acquisition of images, segmentation of images, and extraction of open-eye information from the images and classification of the open-eye information. SIDENOR took a more complex approach on the segmentation step, whereas BFI considered the classification of open-eye data in more detail.

The acquisition of images as the first step of image analysis was of course handled individually with respect to the installed camera type/cabling/computer hardware by each partner. In both cases, the image was available to image processing software, where it was deskewed, calibrated and further examined.

For segmentation of the images, two different approaches were chosen by SIDENOR and BFI. SIDENOR used k-means clustering, which sorted the pixels of each image into four groups according to their brightness. The group with the pixels containing the highest brightness was used as a representation of the open-eye and the number of pixels in that group represented the open-eye size. The other groups were discarded. As k-means clustering is an iterative algorithm, the examination of one picture took about 30 seconds. The advantage of k-means clustering was that the algorithm was insensitive to changing acquisition parameters like image brightness.

BFI used a brightness threshold for image segmentation. This approach allowed much faster segmentation of the images (approx. 1/10th s), but the determination of open-eye size depended much more on the accurate positioning of the threshold value. To ensure this accurateness and allow for changing acquisition parameters (image brightness), the image threshold was calculated from each image first and then compared with a sliding averaged threshold. Only in case of compliance, the sliding averaged threshold was used for image segmentation and re-calculated using the image threshold that had been determined from the actual image. The advantages of this approach were insensitiveness to acquisition parameters and the speed of processing, so that the BFI system can be used on-line during steel treatment with open-eye stirring.

The extraction of open-eye information from the segmented images was handled similarly by the SIDENOR and BFI approaches. The following and final step of image analysis, classification of the open-eye information, was extensively investigated by BFI. Different amounts of image anomalies occurred at SIDENOR and at Saarstahl, where the BFI image processing system was used. Whereas the slag surface in the ladle furnace at SIDENOR was rarely masked by anything except the electrodes, on the slag surface in the turret of a continuous caster at Saarstahl anomalies were to be found regularly.

In conclusion, the approaches of SIDENOR and BFI were both able to solve the image processing problem using different main focuses. The SIDENOR system was developed with strong emphasis on the image segmentation because of unfavorable conditions in the ladle furnace where the open-eye was observed. The BFI system was constructed with fast and accurate image segmentation in mind, as it is used as an on-line system at Saarstahl. Both systems use adaptive algorithms for image segmentation. Open-eye classification is used by BFI to distinguish open-eyes from image anomalies.

5.2.3.2.2 Ladle vibration monitoring by contact and contact-less sensors

ARCELOR Research and ACERALIA have developed vibration-based analyses of gas stirring in ladle (**Figure 41**). Different approaches driven at lab-scale, pilot-scale and industrial scale are used, combined and described in this part.

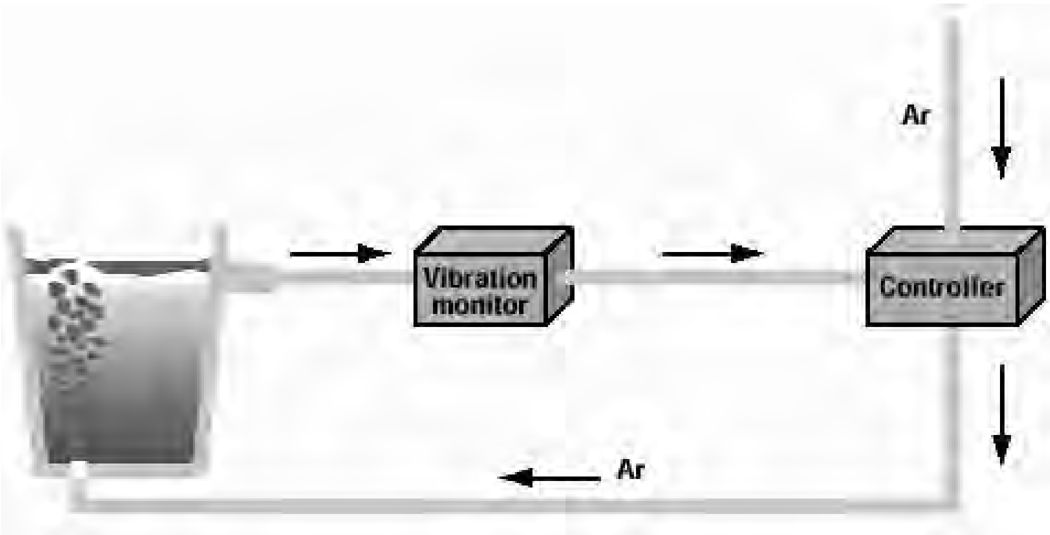

Figure 41 - Principle of the vibration-based analysis of gas stirring in ladle

5.2.3.2.2.1 Contact-less conoscopic holography (ACERALIA)

ACERALIA has implemented a contact-less sensor using Conoscopic Holography (C.H.) distance measurement sensors. These sensors provided signal is digital and they are sensitive to the low frequencies. Apart from that, they give their measurements in distance that can be easily converted to acceleration, and their working range and precision can be easily adapted by simply changing lenses.

CH is a form of incoherent light interferometry, based on the interference that occurs between ordinary and extraordinary rays into which polarized monochromatic light is divided when crossing a uniaxial crystal. When the monochromatic light emitted or reflected by a point is passed through the Conoscope, an interference Gabor Zone Lens figure is obtained, and it can be captured by a standard CCD camera. The frequencies of the fringes that are present in the interferogram are related to the distance of the illuminated point. Once the interferogram has been processed, the distance of the point can be obtained. The basic scheme of the needed setup, called Conoscope, is shown in **Figure 42**. The light for illuminating the point is provided by a laser source installed inside the sensor. A sensor configured like this is called Conoprobe.

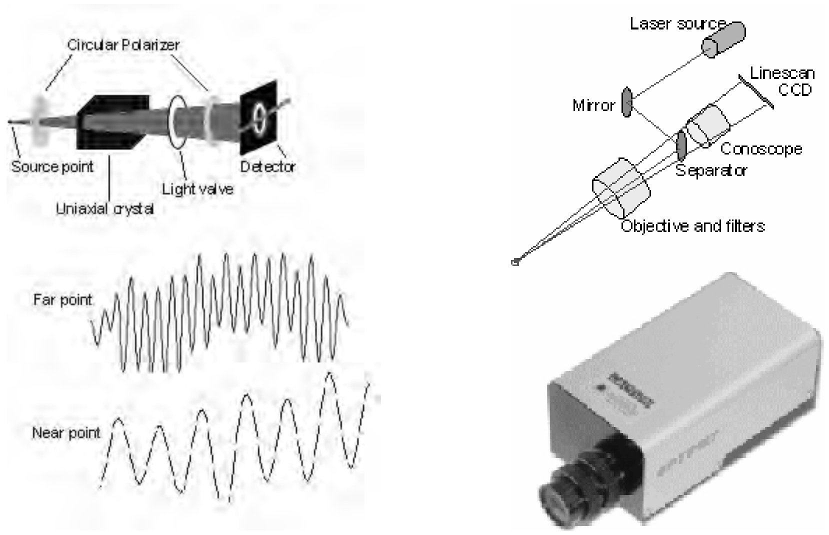

Figure 42 - Configuration of a Conoscope (left) and of a Conoprobe (right)

This technique has many advantages: it is completely collinear and very accurate; the range and consequently the accuracy of measurement can be easily changed by simply using the required lens; it can measure surfaces with a slope of nearly 90º. There are different combinations of range, stand-off and resolution for several lenses. For this project, the goal is to have good sensitivity to detect the relevant vibration features and enough standoff to cover the car positioning tolerance.

Lab-scale tests

Several lab tests to validate the sensitivity of CH were performed. For this purpose, a vibrating surface was constructed by connecting a non-balanced power source to a 3-phase motor: In this way, the vibrations are higher as the source is less symmetrical. An accelerometer was placed in the casing of the motor, and this place is measured with a Conoprobe (CH sensor) using different lenses: 25 mm, 75 mm, and 150 mm. When one phase input of the 3-phase motor is turned off, a higher amplitude vibration, with 100 Hz main frequency, becomes present. It was seen that a high definition Conoprobe can give a more reliable solution than a conventional accelerometer, providing direct amplitude data with higher accuracy. The selection of the probe lens will depend on the amplitude of the vibration to be measured, in order to combine enough stand-off and high range with enough accuracy. Anyway, in the frequency studies lower resolution lenses could be used with results similar to the accelerometer. **Figure 43** shows how the 25 mm Conoprobe appears as much more sensitive, and the 75 mm lens is in the range of the accelerometer.

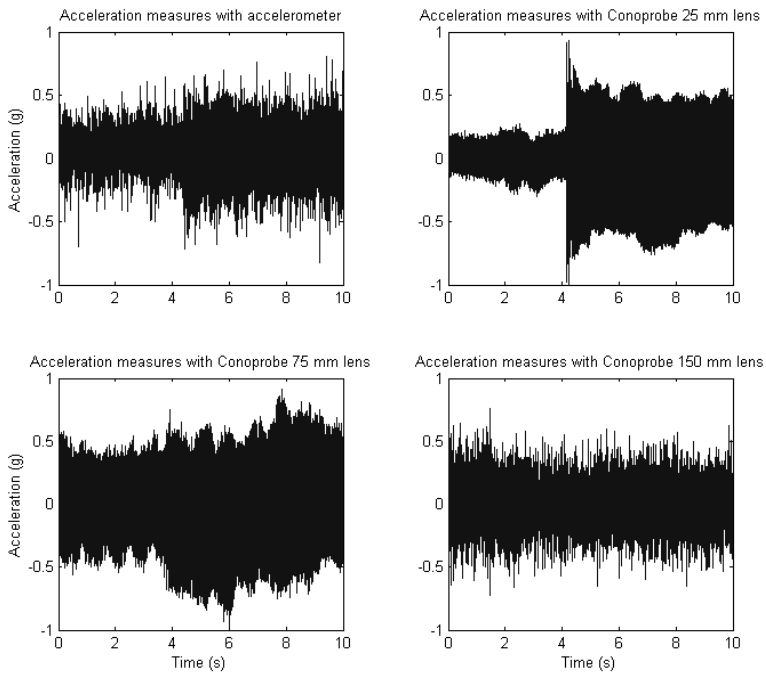

Figure 43 - Comparison of results for different lenses and the accelerometer

In-plant trials

After checking the viability of the C.H. based vibration measurement in the lab, the feasibility of this approach was checked in the real plant. A system was constructed in order to measure the vibration in the ladle car, and software was developed in order to obtain on-line vibration values and the process main parameters simultaneously.

The first trials were performed with a C.H. probe with 75 mm lens (65 mm stand-off, 18 mm working range, 10 µm precision). These tests clearly showed that the amplitude of the vibrating distance signal was related to the gas flow rate. The frequency study of this signal together with the process parameters allowed us to obtain one relevant value representing the stirring.

For example, **Figure 44** shows the acquired signal and the spectrogram obtained through FFT. The different stages of the treatment are clearly marked in the spectrograms, mainly relevant in the medium-higher frequencies distribution. Even some special events, as temperature measurement of the melt, were slightly detected by the system. Frequencies at 8-9 Hz, and 22-26 Hz were dominant at low gas flows (cleanliness bubbling).

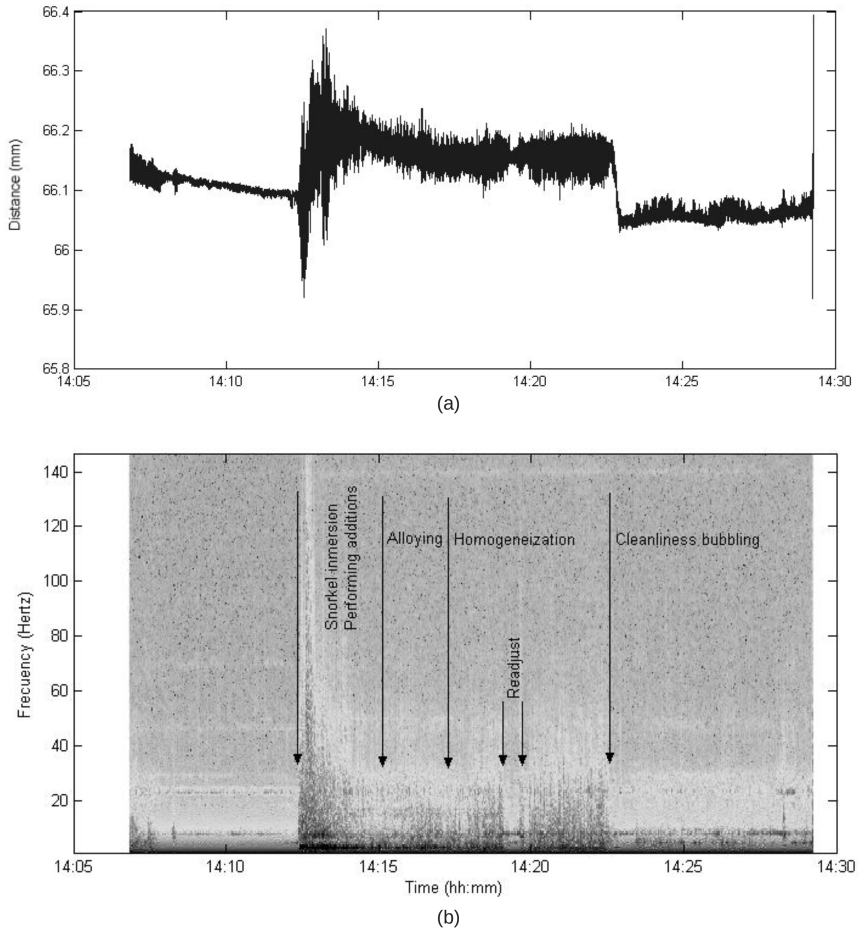

Figure 44 - Vibration diagrams of a complete CAS treatment at ACERALIA: (a) signal and (b) spectrogram

Several tests were also performed with water and steel scale ladles (see §5.2.3.2.2.3). The results were not as interesting as in the plant, due to the fact that the scale models presented similar accelerations as full scale ladles but with smaller displacements of the wall at higher frequencies. This lead to better results in conventional accelerometers and poorer results in C.H. distance measurement sensors.

In order to improve the sensitivity of the system, a prototype using a C.H. probe with 25 mm lens (15 mm stand-off, 1.8 mm working range, 3 µm precision) was constructed and tested. The main advantage of this lens is a higher precision that enables to have good results at higher frequencies; the drawback, the short stand-off and working range, was overcome with a translation stage for the probe, and the development of an automatic positioning for ensuring accurate and robust operation in the plant conditions. The resulting final prototype is showed in **Figure 45**.

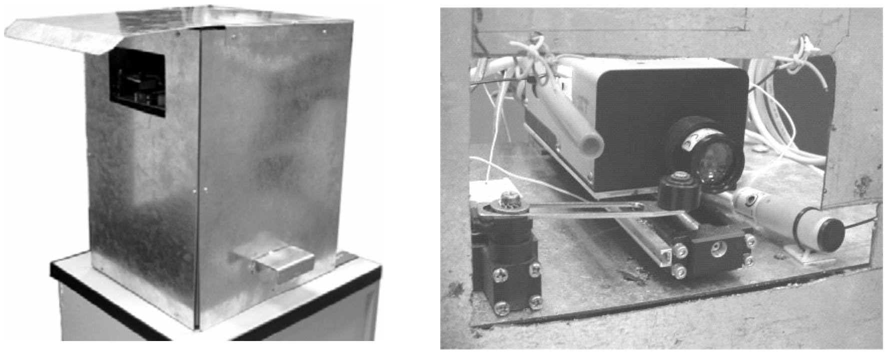

Figure 45 - The final version of CH based sensor (ACERALIA): External view (left) and internal detail showing the 25 mm Conoprobe, the linear translation stage, and proximity sensor (right)

Results

With this system, a measuring campaign of continuous heats was performed, that allowed to improve the interpretation of the results and to look for the relations between the measured vibration and other plant parameters. A number of more than 100 heats were recorded, processed and studied. The main conclusions obtained from this work can be summarized as follows. A good value for the stirring can be obtained from the distance signal of the ladle car, by grouping the frequency components between several ranges. Low frequency ranges (between 3 and 15 Hz) give results that clearly followed the changes in the gas flow rates, but were noisier. Higher frequency components (in the range of 125-150 Hz) look to be less noisy, but are naturally filtered by the distance measurement sensor and give less information. **Figure 46** shows a representative spectrogram where the key frequency ranges can be seen. **Figure 47** shows variation of the measured vibration and the plant parameters in a sample heat.

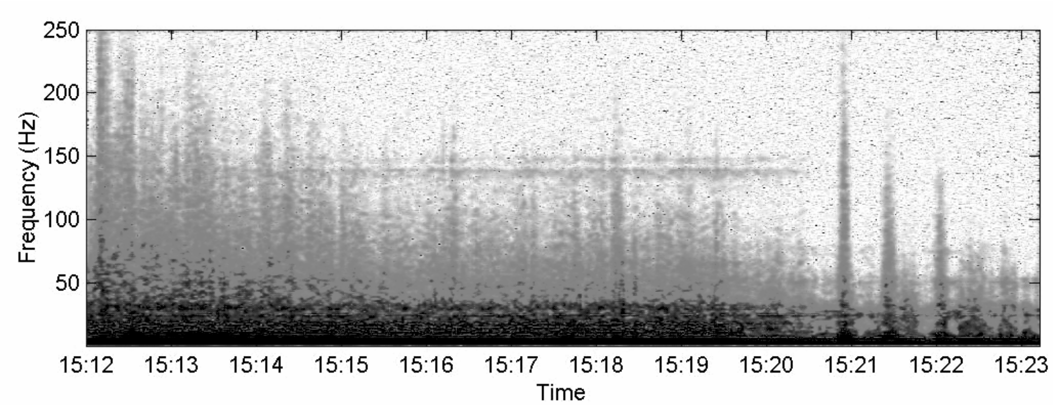

Figure 46 - Spectrogram obtained with the final prototype of ACERALIA vibration sensor based in 25 mm Conoprobe

ACERALIA Grupo Arcelor		Fecha_Trat	Num_Cuch	Vida_Cuch	Vida_tapon	Nivel_Acero	Espesor_Esc
		18/04/2005	1	94	2	4940	100
Ins_Llegada	**Ins_salida**	**Com_burb**	**Fin_burb**	**Com_trat**	**Fin_trat**	**Com_Lim_Inc**	**Fin_Limp_Inc**
15:39:32	16:10:13	15:43:30	16:01:42	15:44:42	15:53:53	15:53:30	16:01:29
Cod_Patron	**Cons_Ar**	**Cons_N2**	**Pres_Rot_Esc**	**Pres_Adic**	**Pres_Agit**	**Pres_Homog**	**Pres_Reaj**
4	4861,75	0,00	8,30	6,25	6,71	6,47	0,00

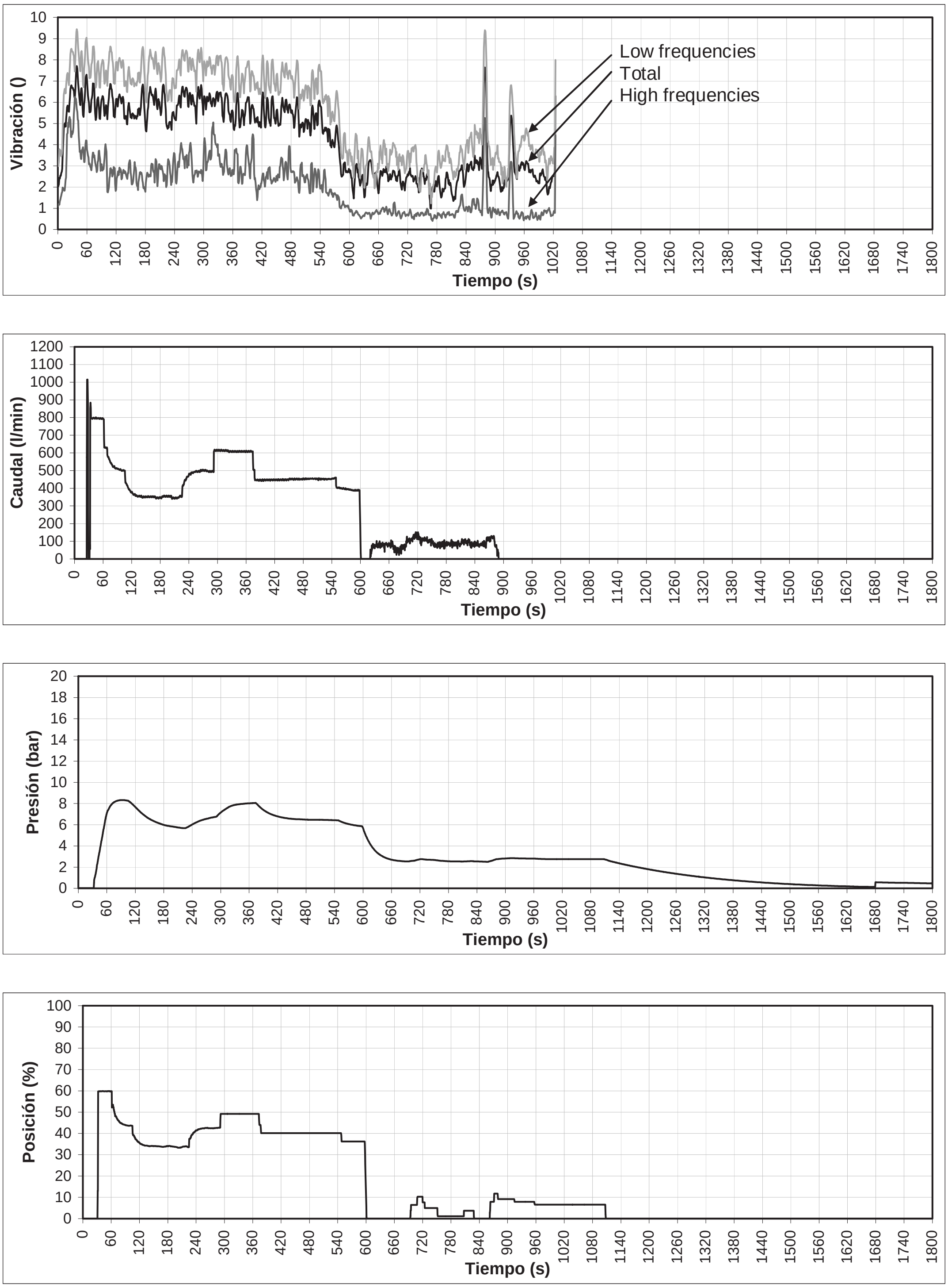

Figure 47 - Evolution of the measured vibration and the relevant stirring variables as can be seen in the standard report. The upper part contains general data: Heat number, date, ladle number, ladle life, plug life, steel level, slag thickness, time of events, bubbling pattern, gas consumption and mean pressures. The curves represent the evolution of the processed vibration, the gas flow rate, pressure and control valve aperture

The obtained static relations between vibration, gas flow rate and gas pressure have been investigated. It has been observed that the dispersion of the results is particularly high for the cases of pressure / flow-rate and vibration / pressure. By contrast, as can be seen in **Figure 48**, the ***correlation vibration / gas flow rate presented a clear logarithmic tendency with less dispersion. This is further discussed in the conclusion paragraph over vibration*** (5.2.3.2.2.4).

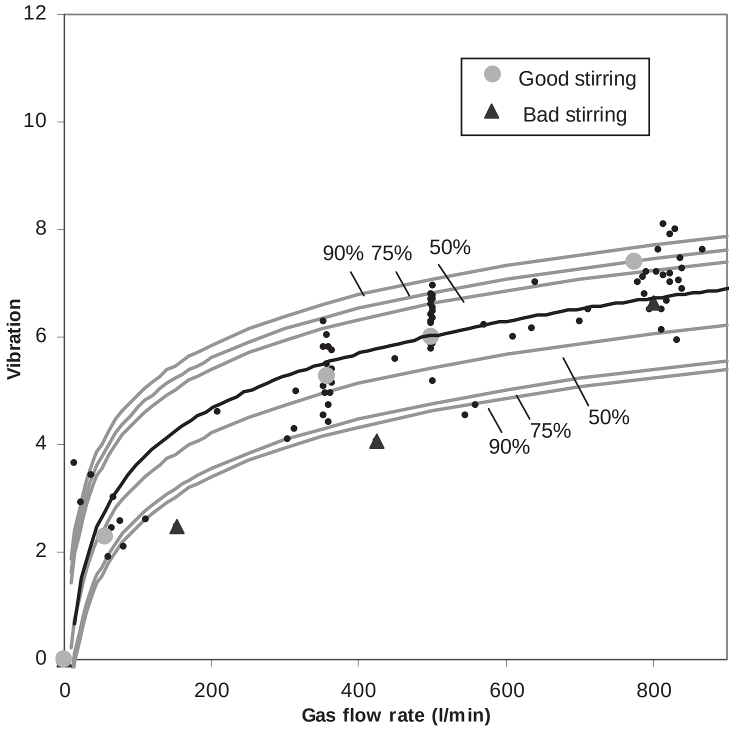

(numbers in the graph indicate the limit of confidence intervals)

Figure 48 - Static relation between the vibration measured and the gas flow rate

It has been statistically shown that problematic heats (for example, heats moved from CAS to the injection treatment due to bad operation of stirring) fell outside the 90 % percentile curves.

Regarding the dynamic relations, the global vibration value looks to follow the gas pressure more than the gas flow rate in the case of heats with good performance of stirring. Both the pressure and the measured vibration have first order dynamic output towards step changes in the gas flow rate input. The dynamics are faster in the increasing steps, and slower in the decreasing steps.

An important effort has been devoted to the analysis of the effect of different process parameters on the correlation between vibration and gas flow rate. The ratio vibration / gas flow rate was compared for different heats taking into account the value of several parameters as porous plug or slag thickness. **Figure 49** shows an example of the results obtained when comparing the ratio between vibration and gas flow rate for different plug life and different slag thickness. In all the cases the dispersion of the values does not give general conclusions, showing again the variability of the actual stirring which depends on a complex combination of several factors that is not easily predictable. For this reason the measurement of stirring is strongly required for a good control of the bubbling processes in the ladle treatment.

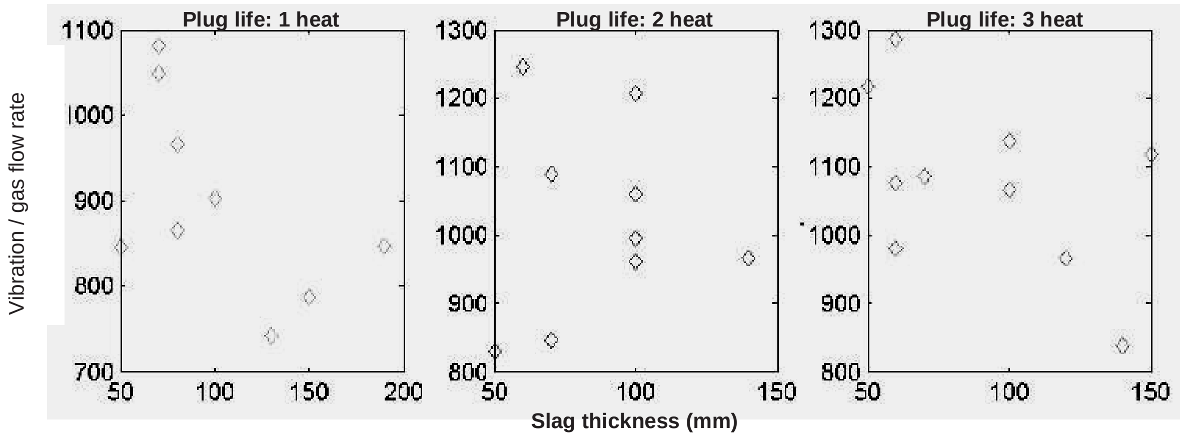

Figure 49 - Effect of slag layer thickness and porous plug life on the ratio stirring / gas flow rate

A relation of the equipment and software used in the final system follows:

- Core sensor:
  - Conoprobe (Opitmet), 25-mm lens,
  - Acquisition unit EC1000,
- Software:
  - Module for acquisition based in MFC Windows application programmed in C++ (Microsoft Visual Studio 6) with TCP/IP socket communication,
  - Module for remote control based in VNC program,
  - Signal processing consisting on periodogram algorithm, filtering and re-composing signal using Matlab,
  - Monitoring module based in Matlab 6.5 with TCP/IP socket communication,
  - Several Matlab 6.5 scripts and Excel macros for statistical analysis of results
- Ancillary equipment:
  - Embedded PC, ultrasonic sensor, linear table 150 mm max stroke, motor 75W DC, motor controller board,
  - Portable computer for configure and boot the sensor in the plant,
  - Portable computer with analogue acquisition board for data logging of process variables.

5.2.3.2.2.2 Contact and contact-less sensors (ARCELOR Research)

Extensive tests with vibration analysis were conducted in ARCELOR Research centre on both a water model (half & full scale of the pilot steel furnace) (**Figure 50**), steel lab and pilot-scales (**Figure 51** and **Figure 52**) and 90-t industrial ladles (**Table 4**).

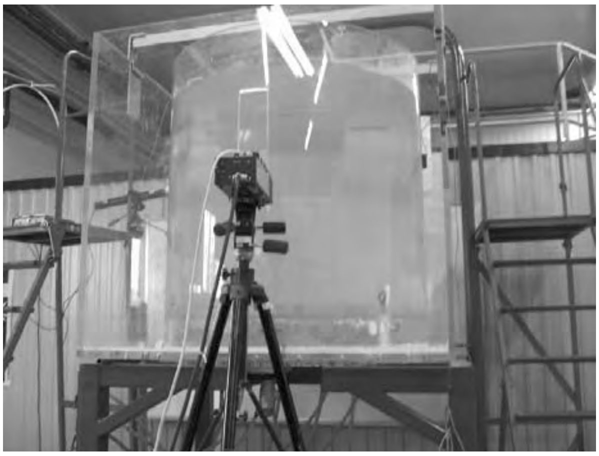

Figure 50 - Full-scale water model of ARCELOR Research centre

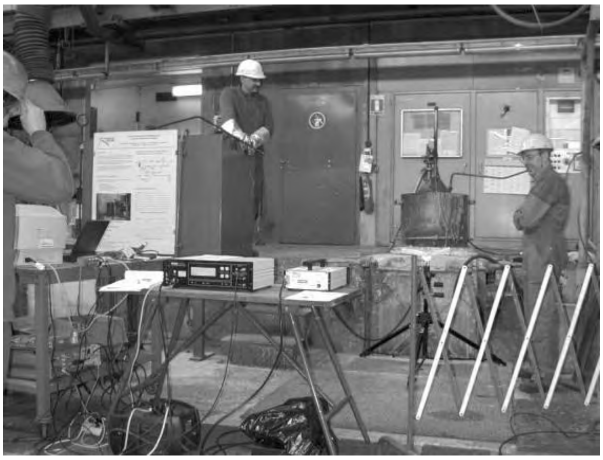

Figure 51 – ARCELOR Research induction furnace (300-kg) used for pilot trials with the laser vibrometer

Figure 52 - 6-t metal capacity ladle used at ARCELOR Research

Calibrated mass flow controllers have been used to control the gas flow rate.

We have placed a calibrated conventional accelerometer at mid-height on the ladle external wall. To ensure the reliability of the conclusions, we have compared the measurement to both laser vibrometer (**Figure 53**) and a reference vibrating gauge (**Figure 54**).

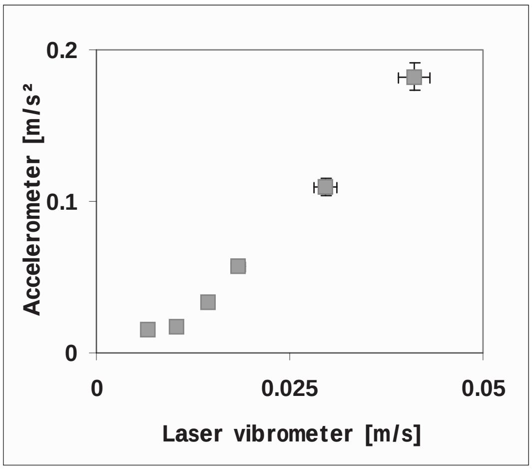

Figure 53 - Accelerometer compares to laser vibrometer

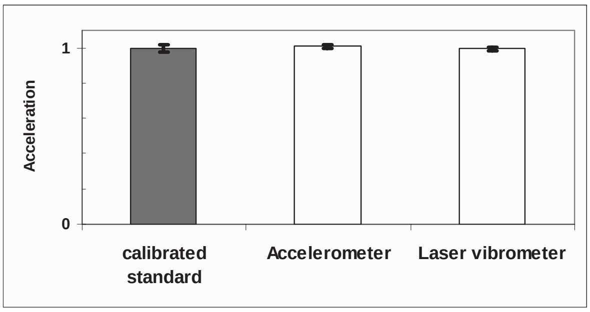

Figure 54 - Accelerometer compares to laser vibrometer and to a reference gauge

We have also used a laser vibrometer, making it easier to cope with the hot temperature of ladle wall. Its power is low (1 mW), so that no drastic protection is needed. The measuring device is 1 to 5 m far from the furnace thanks to an optical fiber: safety problem is minimized.

Analysis of vibration path and vibration origin

The objectives of this part are to get a good understanding of the vibration behavior in a ladle. To estimate the vibration path in a ladle due to gas stirring we have firstly carried out the following tests with/without gas injection:

- Porous plug & ladle external wall: when we hit the porous plug or the internal ladle wall of an empty ladle (**Figure 55**), the signal measured at the ladle outside shell wall is directly correlated to the signal measured on the plug as the coherence between the input and output signals are close to 1, for a large range of frequency (**Figure 56**),
- Connection of argon circuit & ladle support. Coherence between the signal of the argon circuit and ladle wall was sometimes found to be close to 1, meaning a major direct way of vibration transmission, for a large range of frequency (**Figure 57**). This leads to a noised/false measurement. The gas circuit has been modified to avoid this noise in the corresponding configurations.

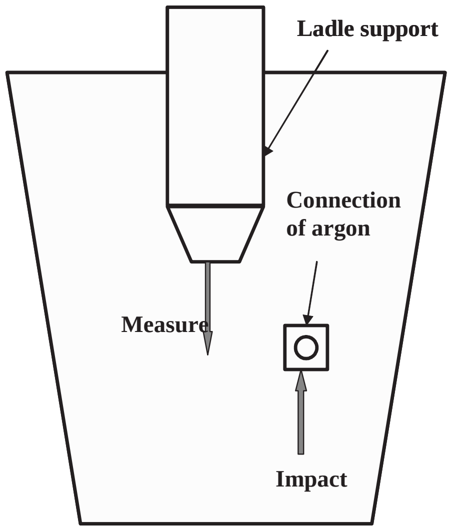

Figure 55 - Schematics of the study of vibration propagation between the argon circuit and ladle support

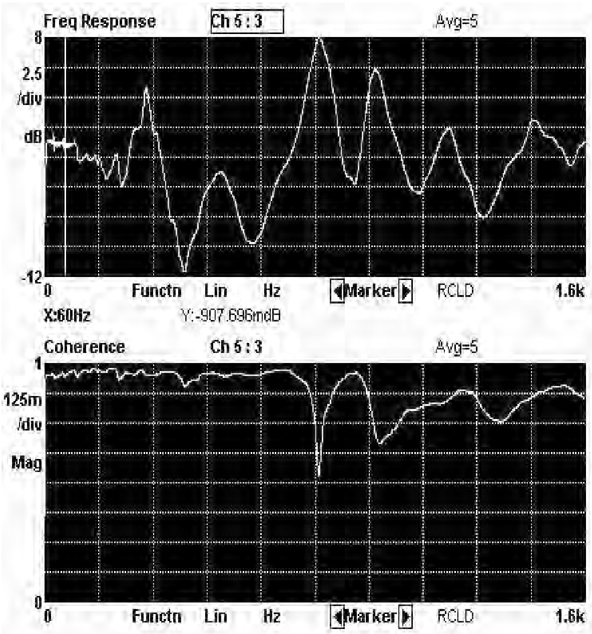

Figure 56 - The coherence between the signal of the porous plug ladle wall is close to 1, meaning a good vibration transmission

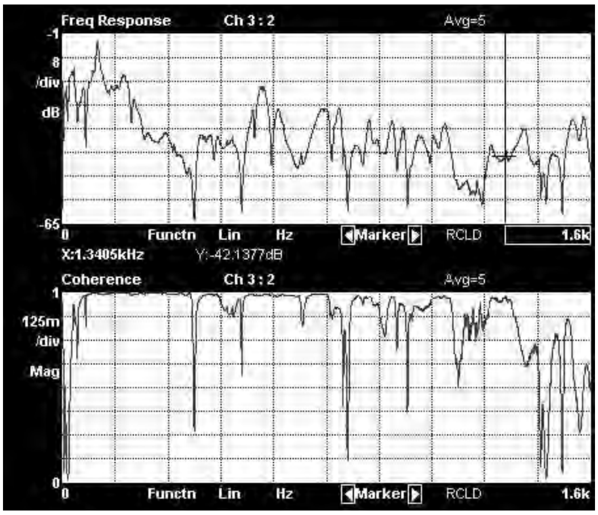

Figure 57 - The coherence between the signal of the argon circuit and ladle support is close to 1, meaning a major direct way of vibration transmission

A second important step was to compare on the water model the vibration measured outside the ladle to the fluctuation of pressure measured by an hydrophone in the liquid pool close to the ladle wall. As a matter of fact, there is a very good correlation between them (**Figure 58**). Moreover we can already notice the increase of the vibrations with the injected gas flow rate according to a logarithmic law. Moreover the agreement between ladle vibration and pressure fluctuation in the liquid is valid for a wide range of frequency, possibly above 200 Hz.

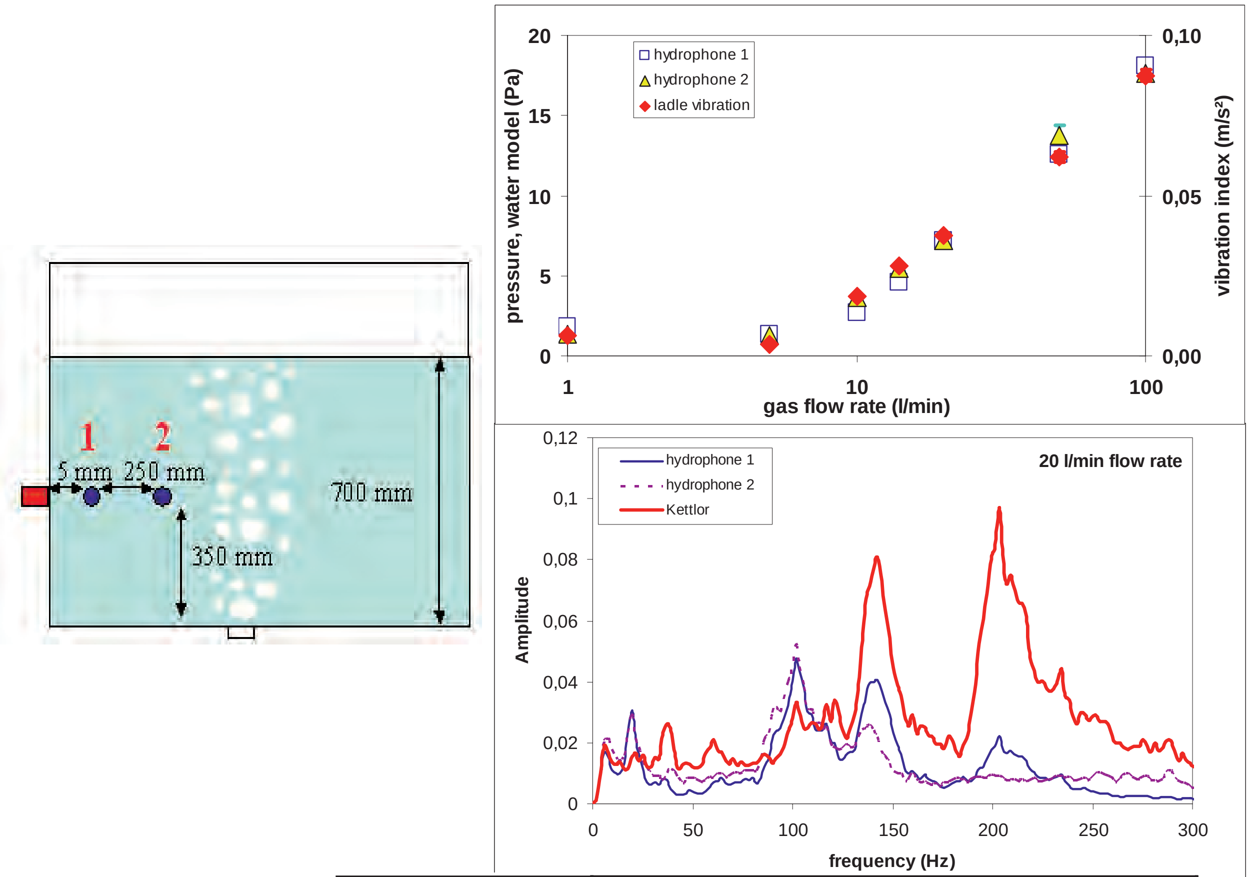

Correlation between Kettlor and hydrophone 1	0.25	0.67	0.57	0.80	0.99	0.91

Figure 58 – Principle of comparison of ladle vibration and of liquid pressure fluctuation. Good agreement between ladle vibration and pressure fluctuation in the liquid bath. Same evolution with gas flow rate

Conclusions: All these tests support the direct relationship between true gas injection and true gas stirring and the true vibration signal measured outside the ladle.

<u>Transient stirring phenomena and industrial trials of vibration monitoring - Gravity mode may develop</u>

The driving question here is: is the gas stirring a steady state phenomenon?

The measured vibration is analyzed in terms of time-dependence. **<u>Figure 59</u>** shows typical energy spectra as determined for gas flow rates between 7 and 30 l/min on the water model. Energy spectra are similar but shifted toward higher energy for higher gas flow rates. Several energetic frequencies are evidenced between 60 and 500 Hz.

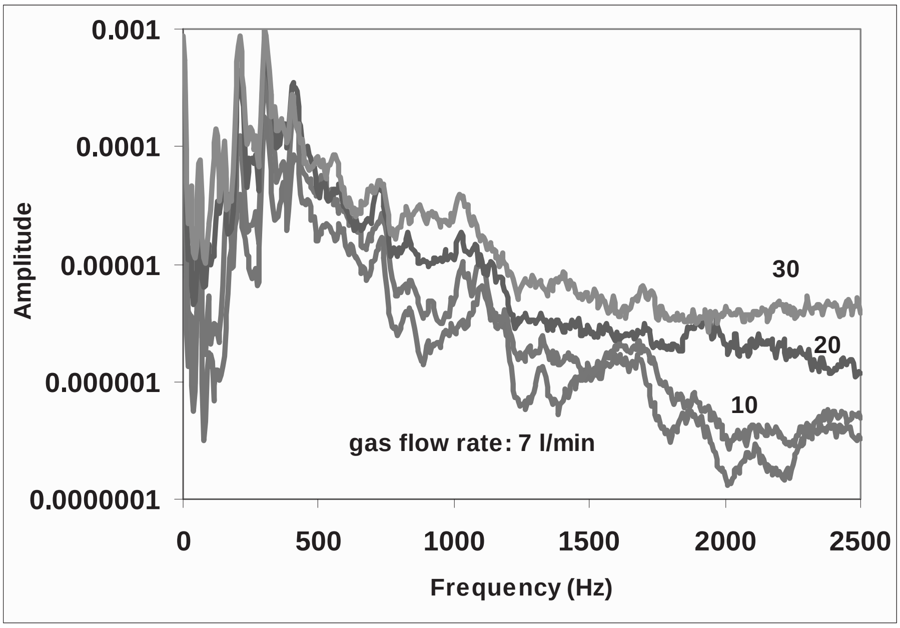

Figure 59 - Energy spectra are similar but shifted for different gas flow rates on IRSID water model. Several frequencies are evidenced which may correspond to gas plume or surface instability

But during first in plant measurements, the vibration measured on the ladle wall was found to be hardly changing with the input gas flow rate (**<u>Figure 60</u>**). The energy spectra exhibit almost an unchanged curve for gas flow rate between 0 and 800 l/min. A fine analysis has indicated a high energy in the very low frequency, namely around 1 Hz. The careful observation of the ladle surface during its transfer to the treatment stand, by removing the thermal protective refractory cover, has put into evidence the existence of visible oscillation of the surface. This does correspond to a **resonance effect** as reported previously in the literature (**<u>Figure 61</u>**) [35]. A solid movement develops in the liquid pool. All the input energy is retransferred to the frequency band close to the main gravity mode. The stirring, mixing and inclusion removal are supposed to be damped. **The transfer procedure of the ladle has been changed so as to minimize sudden movement of the ladle. As a matter of fact, these gravity modes could be avoided.** Such waves have indeed been reported and studied in different phenomena such as **<u>ladle teeming</u>** [35,36], **<u>mechanical agitation</u>** [37-42] and **<u>gas-stirred ladle</u>** [43-51]. As a conclusion, some **low frequency** (of about some Hz) **waves** may develop at the metal surface and in the bulk during gas stirring. The signal treatment to apply to get a **significant bubbling index** should take into consideration the possible existence of such waves.

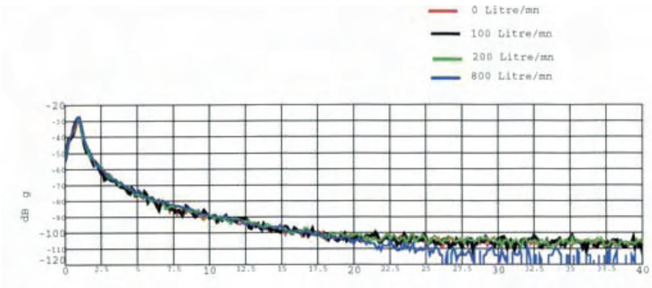

Figure 60 - Gravity mode appears predominant in the first industrial trials, due to ladle transfer procedure

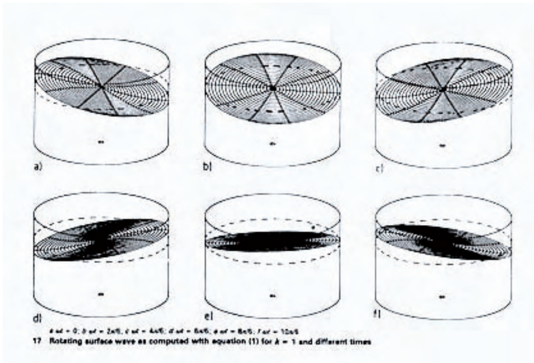

Figure 61 - Solid movement of the liquid pool as observed from the top surface of the ladle ([35])

During the industrial trials, the typical energetic frequency range is about 20 to 200 Hz for gas flow rate between 15 and 90 l/min (**Figure 62**).

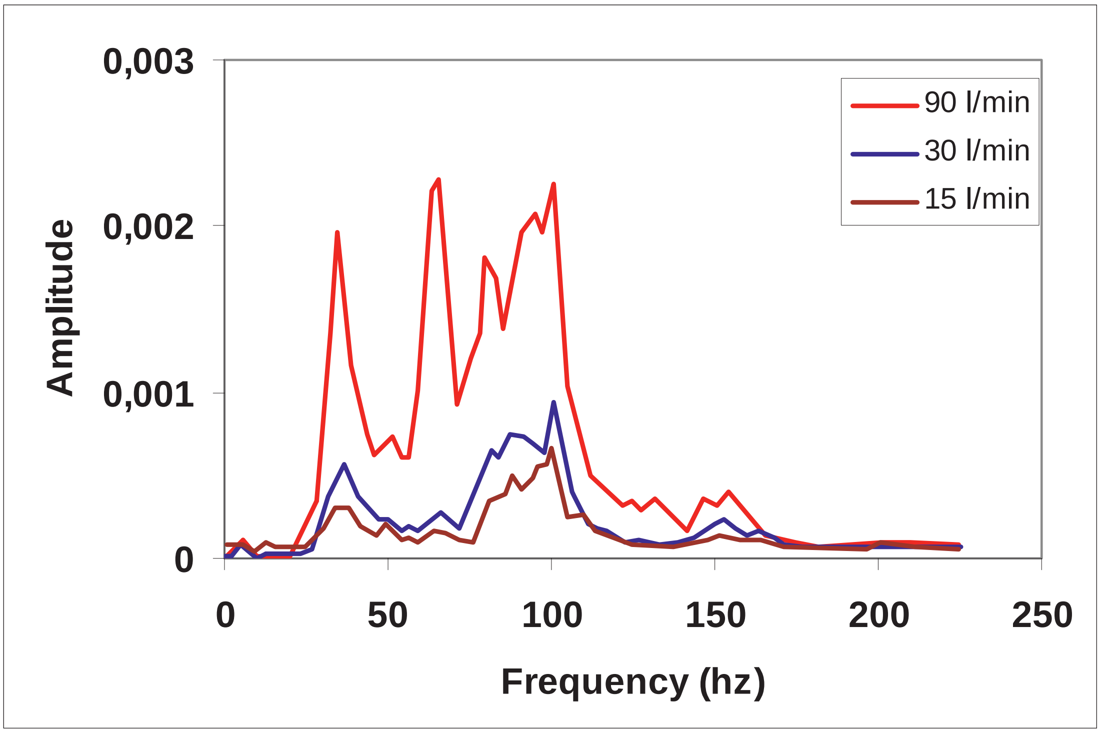

Figure 62 - Industrial spectra revealing energetic frequency range up to 100 Hz or more, depending on the case

Analysis of vibration

The reproducibility of the vibration measurements has always been very high, when varying the gas flow rate at lab and pilot scales. The ensemble of measurement makes it possible to give the following results (**Figure 63**):

- The measured vibrations exhibit a logarithmic increase with the injected gas flow rate on both the 1-m^3 water model, the 300 kg and the 6-t steel pilot ladles,
- Moreover a good agreement is observed between water model and steel ladles, using the Froude similitude (§5.2.3.1.1). Therefore the trend of the curves is very similar, for both full-scale water modeling and experiment of the pilot-scale steel ladle.

- Moreover, we observe a good agreement between measurements with contact-less laser vibrometer and an accelerometer fixed on the ladle.

This is another validation of the relationship between the real gas injection and the measured ladle vibration.

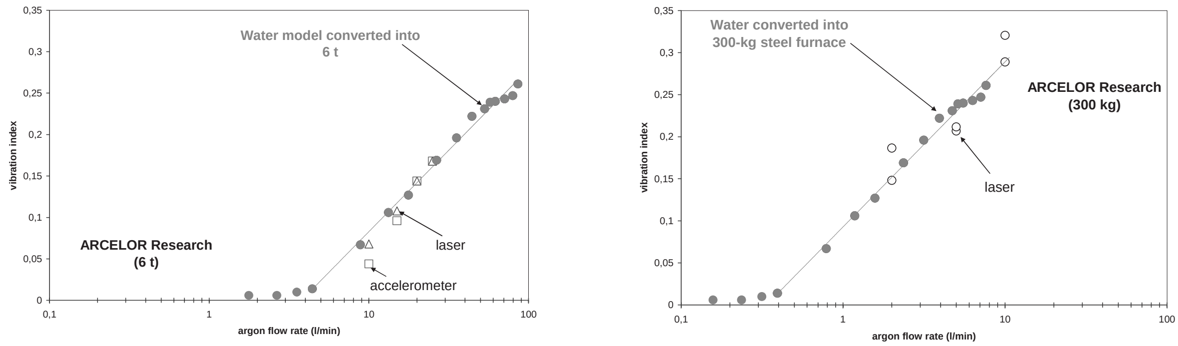

Figure 63 - A logarithmic increase with injected gas flow rate of vibrations is measured on both water model and steel pilot steel ladles. A good agreement is observed between water model and steel ladles

Following these analysis, large scale plant trials have been performed in one ARCELOR plant. The ladle capacity is about 90 t. No problem arose during the measurement campaign. The gas flow rate could be varied in a wide range, from 0 to 1000 l/min. The ladle vibrations were measured using an accelerometer. In addition, the slag surface was observed not only by the operator, but also by a person in charge of metal quality and the person measuring the ladle vibration.

The main conclusions after these trials are summarized on **Figure 64**:

- The measured vibrations increase with the input argon flow rate, accordingly to the law established on the water model (after conversion using the Froude similitude),
- Nevertheless a scattering of the measurements is observed, which is attributed to the quality of the gas injection. For example, a same vibration level is observed for a gas flow rate ranging from 200 and 400 l/min. Reversely, a same gas flow rate can lead to a vibration index between 0.15 and 0.22,
- Failed bubbling can be detected very quickly, when the vibration level is out the standard deviation range. Up to 10% of the treatment could be qualified as failed,
- The open-eye could be observed on one charge or another for gas flow rate higher than 200 l/min or for a vibration index over 0.15. The quite thick slag layer, in average 0.15 m helps to minimize the open-eye as explained previously. For vibration level over 0.32, open-eye is always observed. This confirms the present quality rules which are to apply a 10-min bubbling period if possible at a gas flow rate of 100 l/min, having an open-eye as small as possible. Formerly the operator could be sure of the plug working only through this procedure. And a failed bubbling would mean a downgraded metal. **Figure 65** illustrates the increase of the area of open-eye with the input gas flow rate. The feasibility of getting such data is demonstrated. Some long-term observations have been made in the plant so as to get a feed-back on this point.

These trials confirm the relationship between the gas injection and the vibration level. It offers the possibility to check, adjust and control a given vibration level, supposedly related to a given metal stirring, even a low gas flow rate without open-eye. *The last part of the work has consisted in relating the metal cleanliness to the stirring/vibration level. In other word, is* *it possible to find an optimum stirring condition maximizing the metal cleanliness and to control it in an industrial environment? This is described in the last part (§5.2.3.3).*

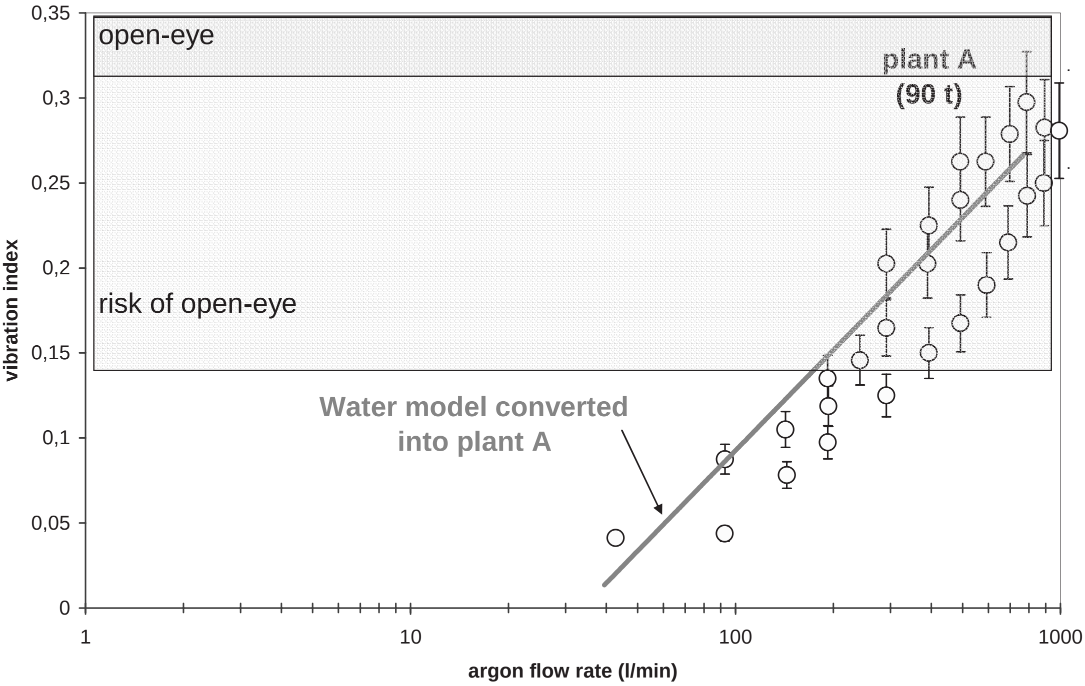

Figure 64 - Measured increase with the argon flow rate of the ladle vibration index in ARCELOR plant. Some scattering is observed

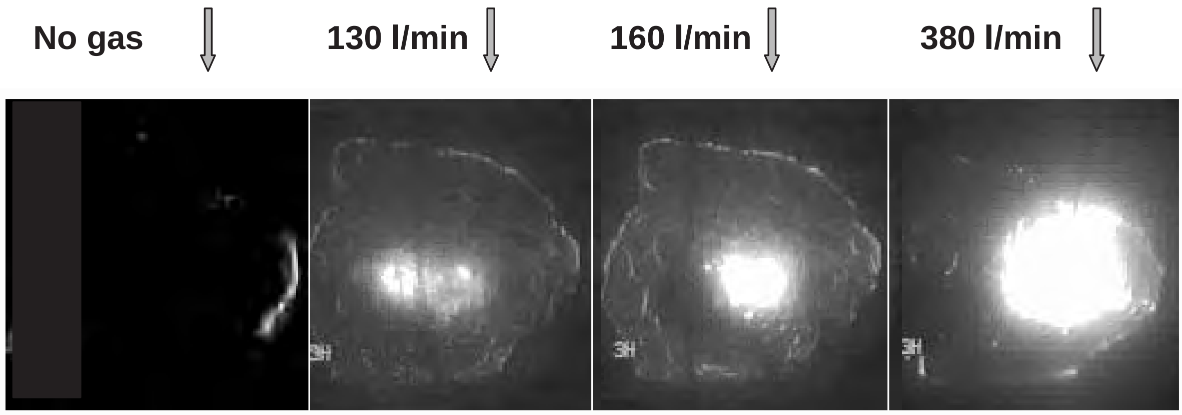

Figure 65 - Increase of the open-eye area as seen during first feasibility trials

5.2.3.2.2.3 Comparison of sensors (ARCELOR Research – ACERALIA)

ARCELOR Research has got good agreement between contact and contact-less sensors, namely accelerometer and laser vibrometer, as already explained (**Figure 53**, **Figure 54**).

Several tests have also been made to compare CH with other technologies, as piezoelectric accelerometers and laser Doppler vibrometers, both in pilot scale and real plant conditions. ARCELOR Research and ACERALIA have driven common tests at ARCELOR Research facilities on water and pilot steel ladles during the project. These trials have shown that CH works fine at low frequencies and high gas flow rates. Moreover, an on-line comparison test has been performed in Aceralia LDA steel plant, with the usual Conoprobe configuration and a piezoelectric accelerometer.

It is very important to note, as said before, that accelerometers and C.H. are measuring different but related magnitudes: the accelerometer measures acceleration, while the C.H. sensor measures distance, so it is needed to derivate twice in order to obtain the same magnitude. This means that, in the frequency domain, the C.H. sensor is much less sensitive to acceleration when frequency grows, as the amplitude of the vibration is reduced by the square of the frequency for the same acceleration.

Acceleration: $a(t) = K \sin(wt)$

Distance (integrating twice the acceleration): $d(t) = -(K/w^2) \sin(wt)$

This means that the Conoprobe will not be able to distinguish vibrations when the frequency grows. For instance, a 0.2 g peak 250 Hz sinusoidal acceleration, as obtained in the tests, gives 0.8 µm peak distance variation, at the limit for the conoscopic system detection with the 75 mm lens used. The same acceleration at 3 Hz means 5.6 µm peak distance variation, easily detectable by the conoscopic system.

Comparisons with accelerometers have been performed in lab and plant trials. All of them have shown the effect indicated before: conoscopic sensor can be used only if low frequency vibrations (0 - 40 Hz) are involved. In these cases it is comparable or better than accelerometers, especially in the very low frequencies.

This has been demonstrated in lab trials with a three-phase motor with a phase fail that induces a 100 Hz oscillation. The **Figure 66** shows the spectrogram of a signal acquired with a high sensitivity accelerometer (Wilcoxon Research 786 F-1; sensitivity 100.0 mV/g +/-5%; low Freq: 0.5 Hz, 30 CPM; High Freq: 13.0 kHz; 780 kCPM; Max Temp: 120 °C), a Conoprobe with 75 mm lens, and the Conoprobe with 25 mm lens. The 100 Hz vibration is induced, and the relative amplitude of the 100 Hz peak is compared to the amplitude of the 25 Hz permanent vibration. The accelerometer is more sensitive in growing frequencies.

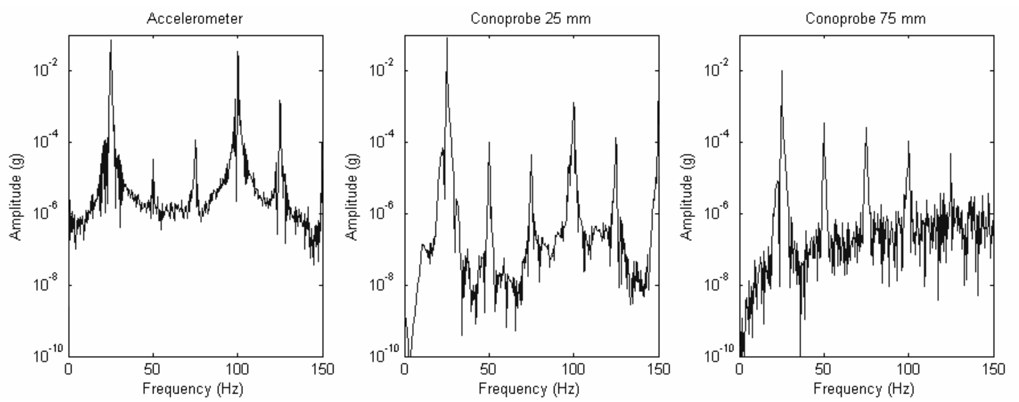

Figure 66 - Comparison of frequency sensitivity of accelerometer and conoscopic sensor with two different lenses. The reduction of sensitivity at higher frequencies is clear for the 100 Hz component of the vibration

In lab-scale model trials (water model and scale steel ladle) the results have also shown that the conoscopic sensor is detecting the low frequencies and discarding the high frequencies. In these cases, due to the ladle configurations, the interesting vibrations appeared in high frequencies (around 100 Hz) as can be seen in **Figure 67**, so are not suitable for the C.H. The frequencies between 7-15 Hz look to be interesting, but they remain after stop. Look to be the residual movement of the steel in the ladle, not interesting for stirring. Frequencies between 70 and 120 Hz appear to be more indicative. The accumulation of the PSD at these frequencies gives a 'measurement' of the stirring, as seen in **Figure 68**.

In plant trials, the ladle is 5 times bigger and the real process relevant frequencies appear to be lower, so C.H. is more useful.

As a conclusion from the tests performed, C.H. looks to be an alternative appropriate approach to low frequency vibration. A laser vibrometer is to be sensitive to dust in the atmosphere and to the quality of the reflection on the measured surface. Accelerometers are simple, cheap and reliable, only its performance can be limited by the temperature of the place where it is located.

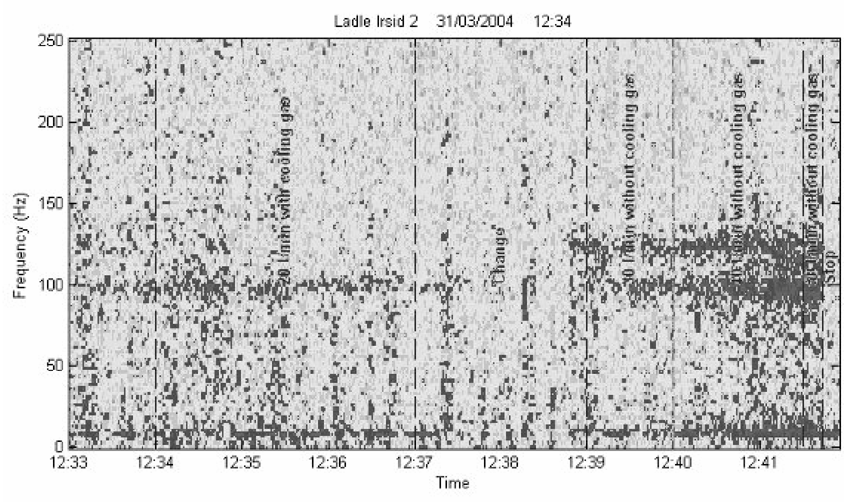

Figure 67 - Spectral distribution variation for a test with a scale ladle, using a conoprobe with 75 mm lens; gas flow rate varies from 20 to 50 l/min. For this configuration the interesting frequencies appear around 100 Hz

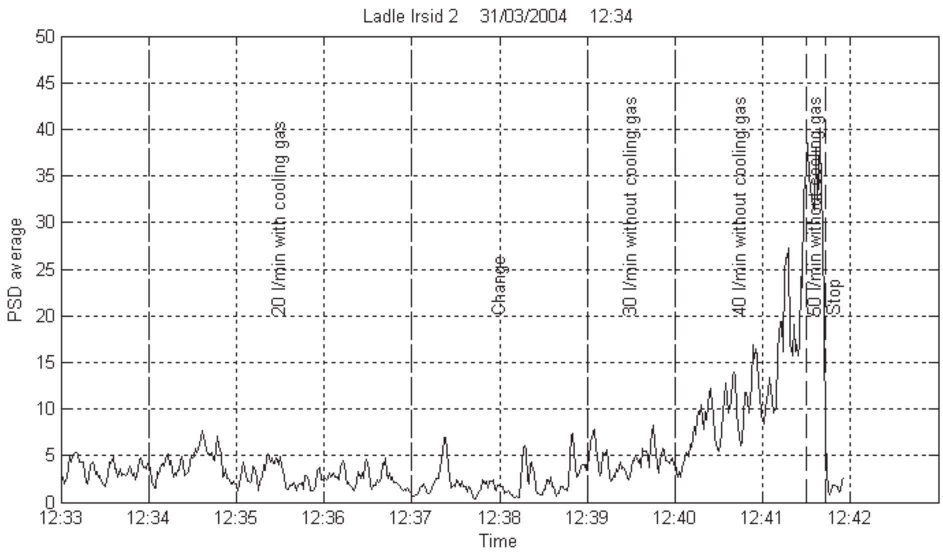

Figure 68 - Results after the processing of the interesting frequencies in the previous trial; sensitivity is low due to the involved frequencies around 100 Hz and the 75 mm lens used

5.2.3.2.2.4 Transient stirring (MEFOS)

The turbulence kinetic energy of the liquid metal is related to the fluctuating velocity u_i. Therefore, the simulated k value close to the ladle wall could be used as an index of the ladle vibration. **Figure 69** shows the transient simulation results of turbulence energy with the different gas flow rate in the 120-t ladle considered by MEFOS. It shows that the fluctuating velocity increases with the increase of gas flow rate. But, it should be pointed out that this simulation can only be used as the qualitative. The reasons are double:

- the turbulence simulation in the gas stirring ladle still needs to be developed,

- the time step in this simulation is 0.01s, which means that the high frequency phenomena (>100 Hz) can not be captured by numerical simulation.

These results are further analyzed in the following paragraph.

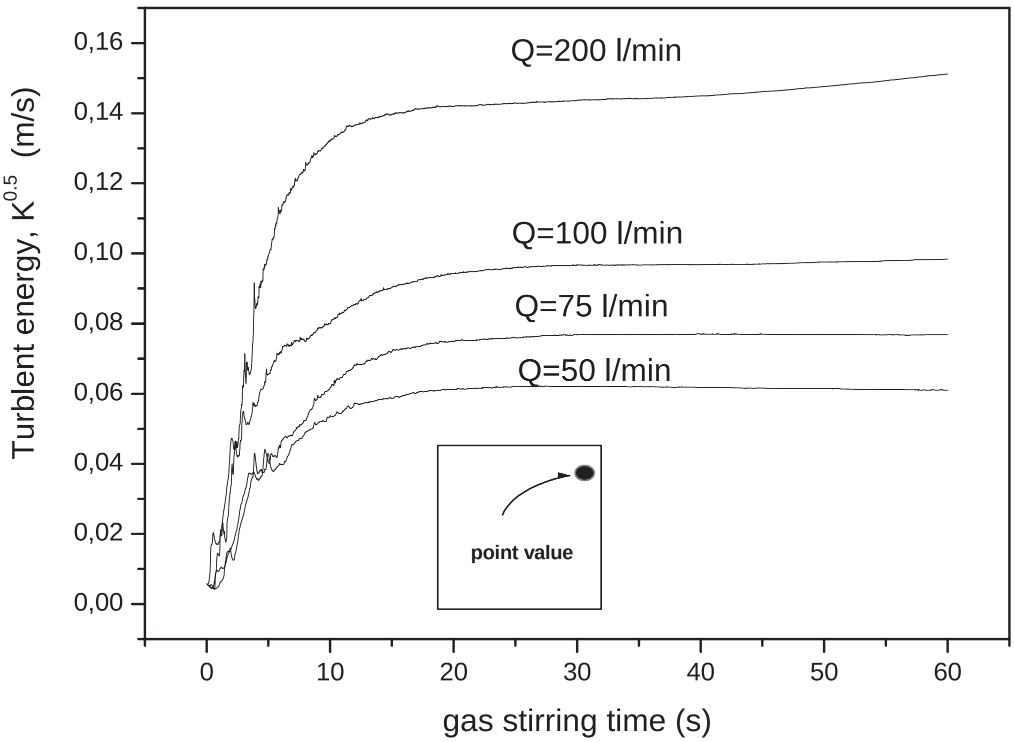

Figure 69 - Transient simulation results of the turbulent energy close to the ladle wall

5.2.3.2.2.5 Conclusion on ladle vibration

As explained at the beginning of the report, the Froude number is generally used as the similitude number for gas stirred ladle model.

Figure 70 shows the ensemble of measurements of ladle vibrations according to this parameter:

- ARCELOR Research water models, of 0.5 or 1 m diameter,
- ARCELOR Research pilot induction furnaces, of 300-kg or 6-t capacity,
- ARCELOR 90-t plant,
- ACERALIA 300-t plant.

Measurements have been performed by laser vibrometer, accelerometers or conoscopy. Moreover, calculated kinetic energy at the ladle in MEFOS 120-t ladle is also considered.

Using the Froude number, all the data are aligned, emphasizing again the validity of the relationship between ladle vibration and true stirring. Deviation from this unique curve would mean either a wrong flow meter calibration, already evidenced in some cases, or an evolution in the true stirring, related to a change of porous plug property for example.

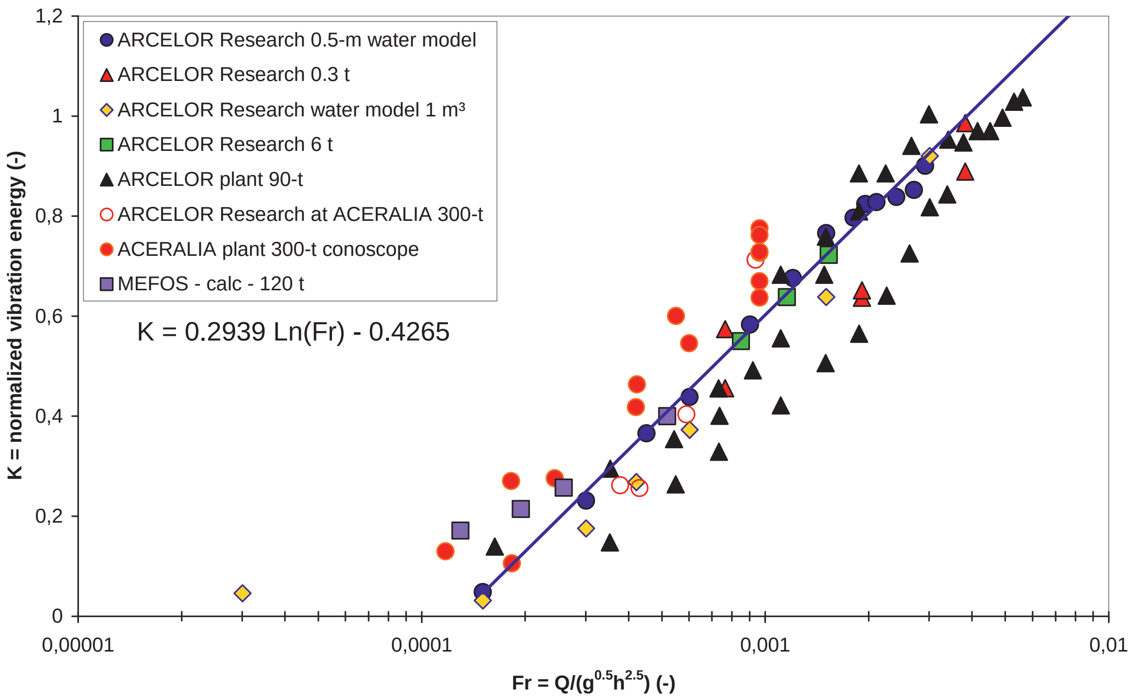

Figure 70 – Increase of ladle vibration with the Froude number – Water scale models, pilot scale steel ladles, industrial plant data and numerical simulation

5.2.3.3 Transient phenomena

Main results over transient phenomena are already given in other sections of the report. They can be summarized as follows:

- Gravity Mode or Resonance Effects as put into evidence by ARCELOR Research (e.g. Figure 60, Figure 61) induced by the ladle transfer procedure. These affects can be (and should be) avoided by minimization of sudden movements of the ladle during transfer.
- Frequency analysis of vibrations (Figure 59, Figure 62) has been done by ARCELOR Research and this is used to filter out the low frequency resonances.
- MEFOS transient CFD modeling of open-eye formation is reported in section 5.2.3.1.4.4 and the results are in (Figure 29). Regarding time-depend calculation of fluid flow, Figure *69* gives the evolution of turbulent kinetic energy (section 5.2.3.2.2.4).

5.2.3.4 Towards improved ladle treatment process

5.2.3.4.1 RESPONSE TIME

The time constant for the vibration response to changes in the set point of gas flow rate has been evaluated by ACERALIA for different situations:

- Increase from 0 to 800 l/min (stage 1, **Table 11**): 40 s,
- Increase from 350 to 500 l/min (stage 3): 30 s,
- Decrease from 360 to approximately 0 l/min (stage 5): 70 s.

It must be taken into account that these estimations are based on real plant data where the bath is not completely stabilized when changes in the gas flow rate take place. Anyhow, it is evident that the dynamics are faster in the increasing steps, and slower in the decreasing steps.

According to MEFOS numerical simulations (Figure *69*), the time-scale for change of flow pattern is some seconds after the real change of gas flow rate through the porous plug, without taking into consideration the time needed to change the real pressure and flow rate in the gas feeding pipe.

Figure 71 shows a typical time evolution of gas flow rate set point and of the corresponding ladle vibration during ARCELOR Research plant trials. A typical global response time, after a change in the flow rate set point is around 1 to 2 minutes. Moreover we can see the real time evolution of the ladle vibration level, in this case well correlated to the input gas flow rate.

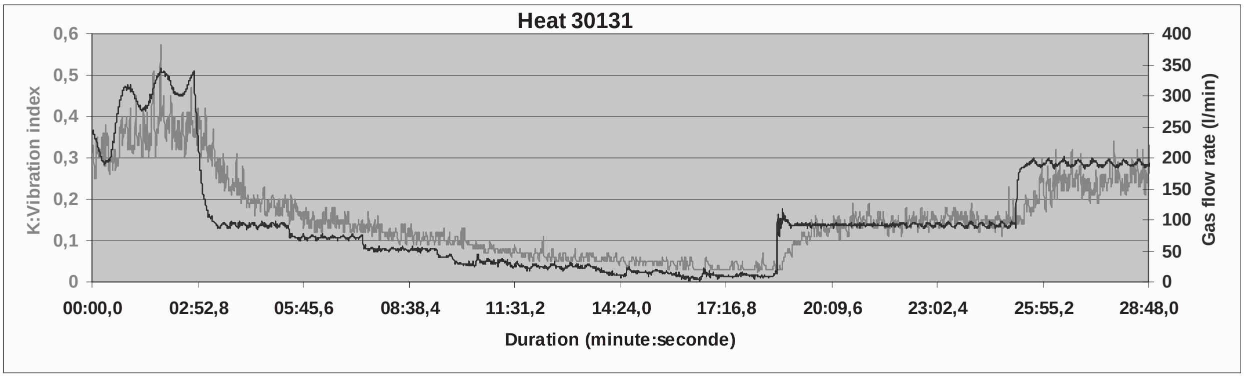

Figure 71 – Time evolution of the gas flow rate and of the ladle vibration (ARCELOR Research)– Response time of 1 to 2 min

5.2.3.4.2 OPTIMUM STIRRING: INDEX OF TRUE STIRRING

5.2.3.4.2.1 Strong stirring for alloying (SAG)

Samples were taken by SAG from the melt immediately after alloying as quick as possible within the periods 5-20 and 30-50 min after tapping (**Figure 72**). The analyses of Al, C, Mn and Si increase finally to the target analyses due to the alloying and argon injection through the porous plug. The influence of the alloying on the content is seen in **Figure 73**. The C content for example increases typically after its addition reaching a “steady state”. The time necessary to reach the “steady state” is approximately 2 – 3 min depending on the flow rate of argon.

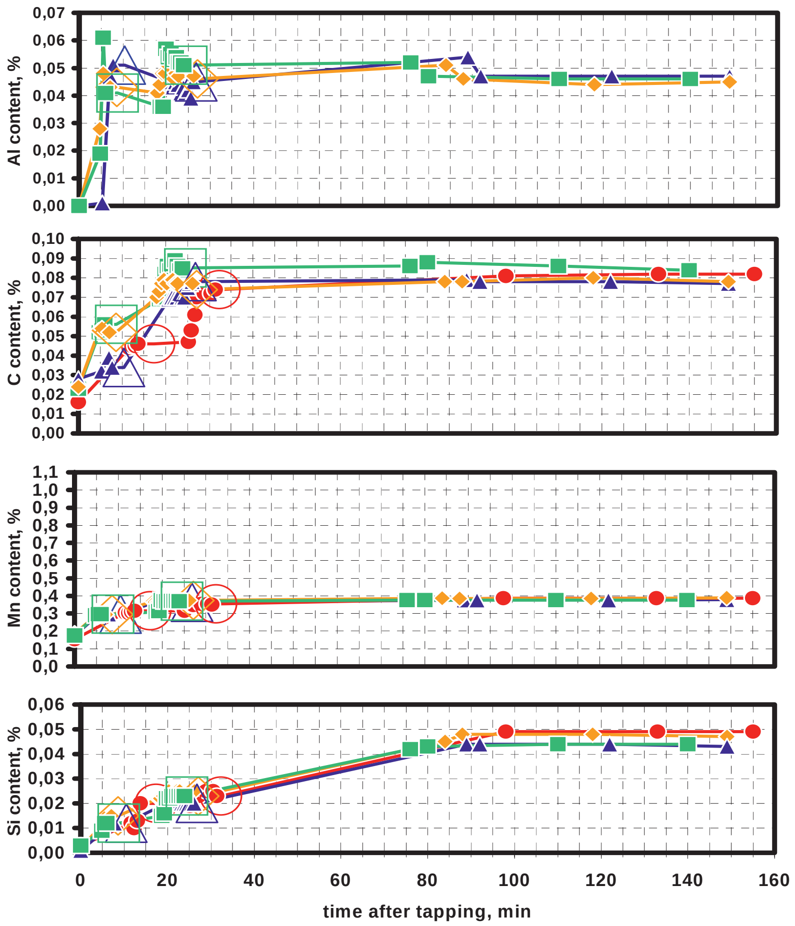

Figure 72 - Analyses of Al, C, Mn and Si

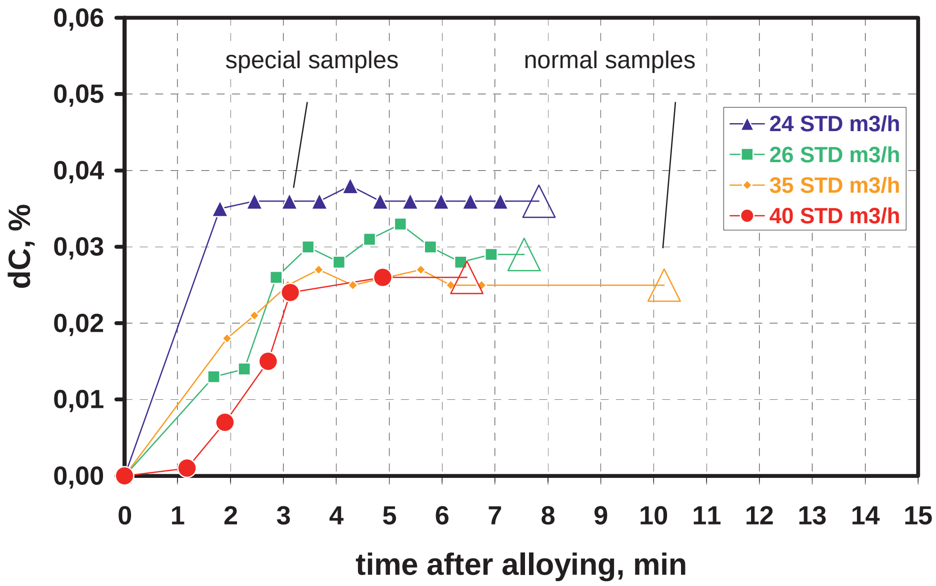

Figure 73 - Influence of the alloying time on the C content (dC = Ct – Cstart)

In addition the time for the normal sampling during melting is in the range of 7 - 11 min. A closer look on the time necessary to reach this “steady state” for each element is done for two selected sections as shown in **Figure 74.** The total time for complete alloying depends on the elements within these experiments. It seems to be that this alloying time increases in the order of Al, C, Mn and Si. Furthermore the alloying time of the first period after tapping is in the order of 4-8 min as the alloying requires only 3-5 minutes in the second period**.** The reason for this behavior might be connected with the fact that under the conditions of SAG the main part of the de-oxidation reaction is coming into existence immediately after tapping. Within this period the necessary time for complete mixing might be influenced by the alloying and particularly by the intensive de-oxidation reactions combined with the removal of the generated inclusions.

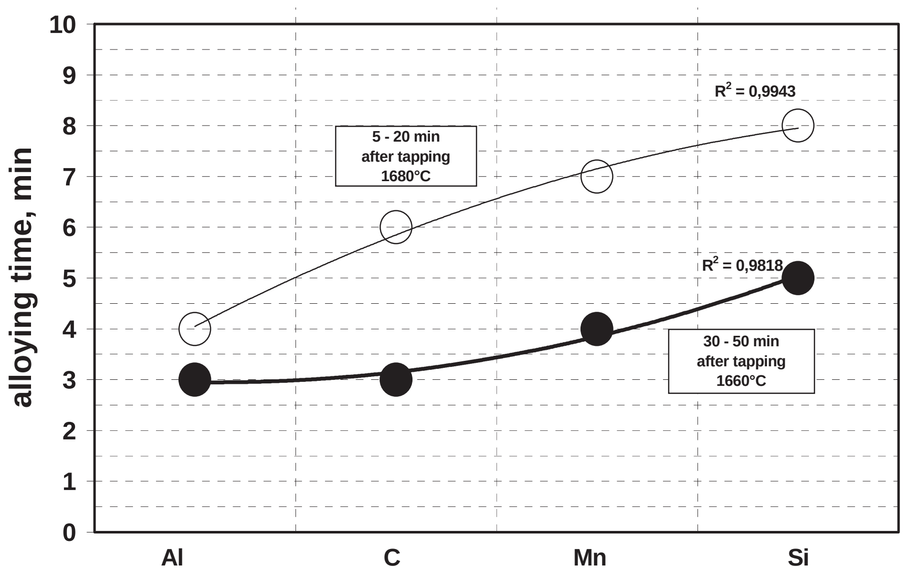

Figure 74 - Alloying time until “steady state” for Al, C, Mn and Si

However, on the other hand the alloying process can be described by the energy introduced by the argon stirring. The rate of energy dissipation in the system is given by [53]:

$$\dot{\varepsilon} = \left(28.5 \cdot \frac{Q \cdot T}{W}\right) \cdot \lg\left(1 + \frac{h}{148}\right) \tag{14}$$

Multiplying the rate of energy dissipation with the rinsing time leads to the total stirring energy introduced into the heat in kJ/t as described in **Figure 75**. The alloying process leads to a constant increase until the final analyses is reached. Once again the time needed to reach a steady state with regard to different elements shows a nearly ideal behavior for Al, C, Mn and Si. The energy required for complete alloying is in the range 10 to 30 kJ/t compared with 30 – 60 kJ/t for the normal procedure in the steel plant. The trials are indicating that it is possible to decrease the rinsing time between alloying and sampling according to **Figure 76**. The decrease of the rinsing time during alloying diminishes both the risk of entrapment of top slag due to the emulsification in the presence of high gas flow rates and the danger of re-oxidation due to the contact between liquid steel and oxygen in the air.

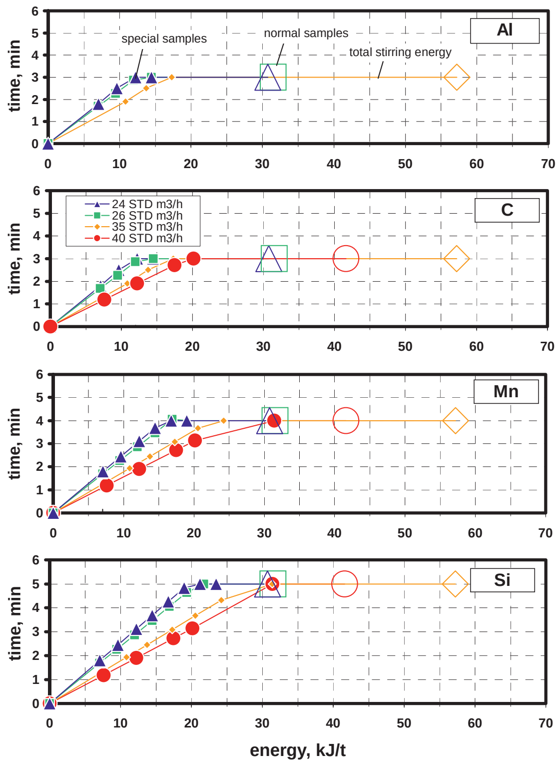

Figure 75 - Influence of stirring energy on complete alloying time

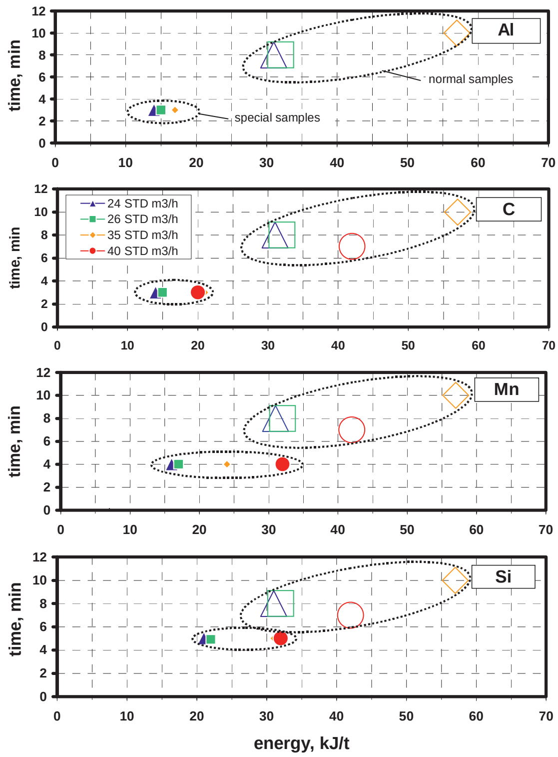

Figure 76 - Comparison between normal and testing sampling

The comparison of the experimental SAG data with those of the literature [53] shows a good agreement (**Figure 77**) as far as the period for "constant analyses" is concerned taking into consideration the rate of energy dissipation in W/t instead of the above mentioned total stirring energy. The normal course of operations needs a larger time as mentioned before. The results are indicating a potential of further optimization.

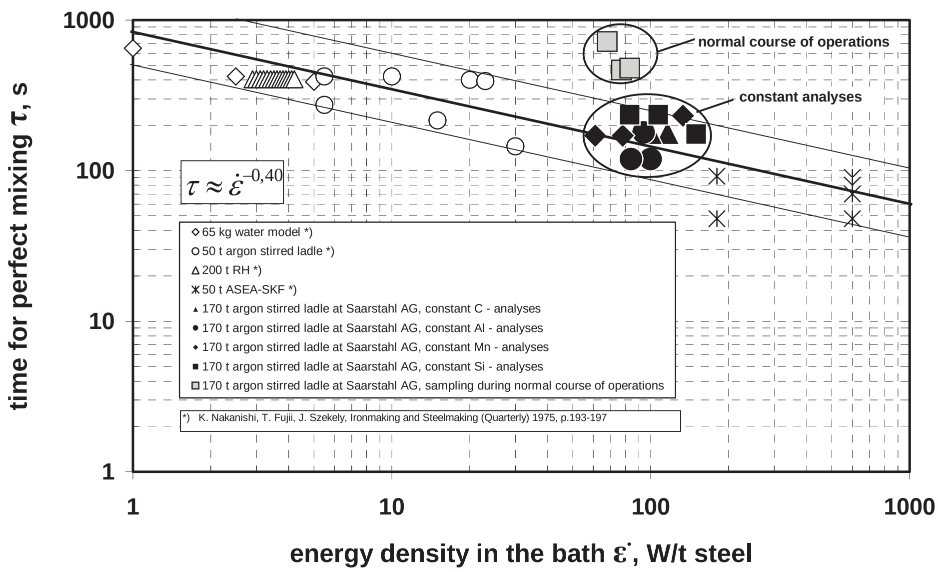

Figure 77 - Relationship between time required for complete mixing and energy density

5.2.3.4.2.2 Towards smaller controlled gas flow rate for cleanliness

Open-eye, stirring and cleanliness (SAG)

Even the measurements of the temperatures with a measuring rod are recorded very precisely by the digital image processing system followed by an increase of the open-eye. This behavior led to additions of ladle cover powder to reduce the size of the open-eye.

According to the research project extensive experiments were carried out with Al de-oxidized heats for the determination of the de-oxidation process during ladle treatment. The oxygen contents of several heats with 0.3 – 0.4% C are shown in **Figure 78**. The total oxygen content varies between 120 and 180 ppm after tapping. Due to the additions of aluminum and the other alloys the oxygen content is lowered to approximately 20 to 25 ppm for the non degassed heats and to 10 – 20 ppm for the RH degassed heats. Sometimes a slight increase of the oxygen content is coming into appearance during the rinsing period at the end of ladle treatment, shown in the lower part of the figure. The oxygen activities, the solved and oxidic oxygen content reach very low values particularly at the end of the ladle metallurgy as shown in **Figure 79**. Following the decreasing temperature between start and end of the ladle treatment it is clearly to be seen in **Figure 80** that the position of the industrial 170-t heats in the metallic system Fe – a(O) – Al is located closely to the equilibrium. On the other hand the frequency distribution of the total oxygen content during the rinsing period shows clearly in **Figure 81** an increase, attributed to a re-oxidation after the formation of an open-eye.

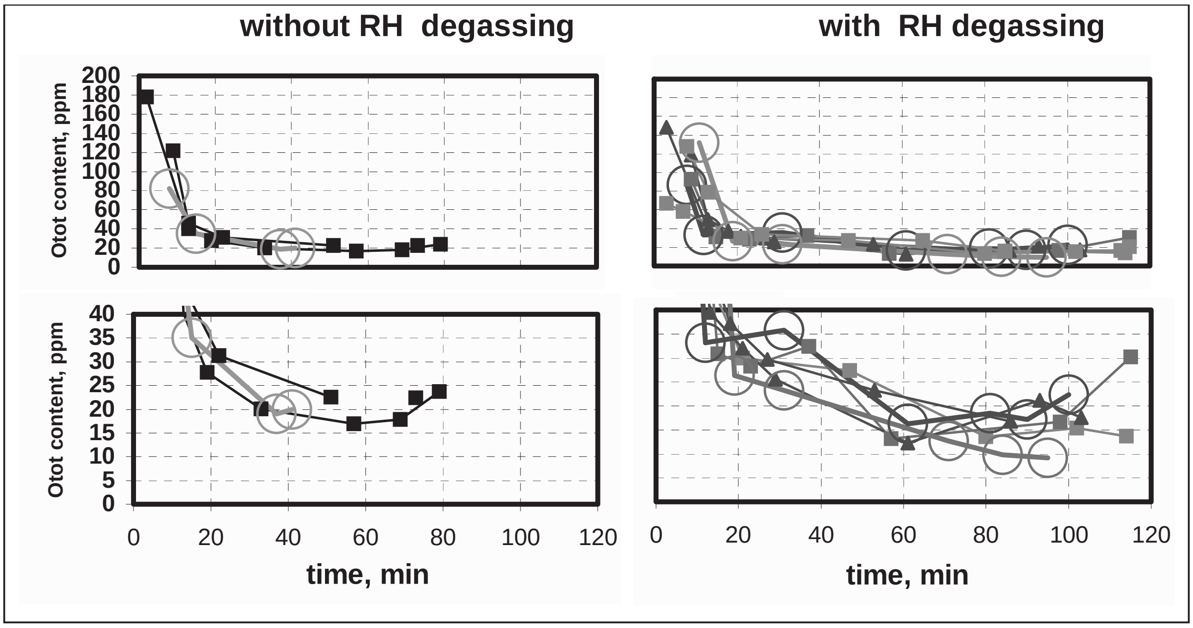

Figure 78 - Oxygen content of Al deoxidized heats

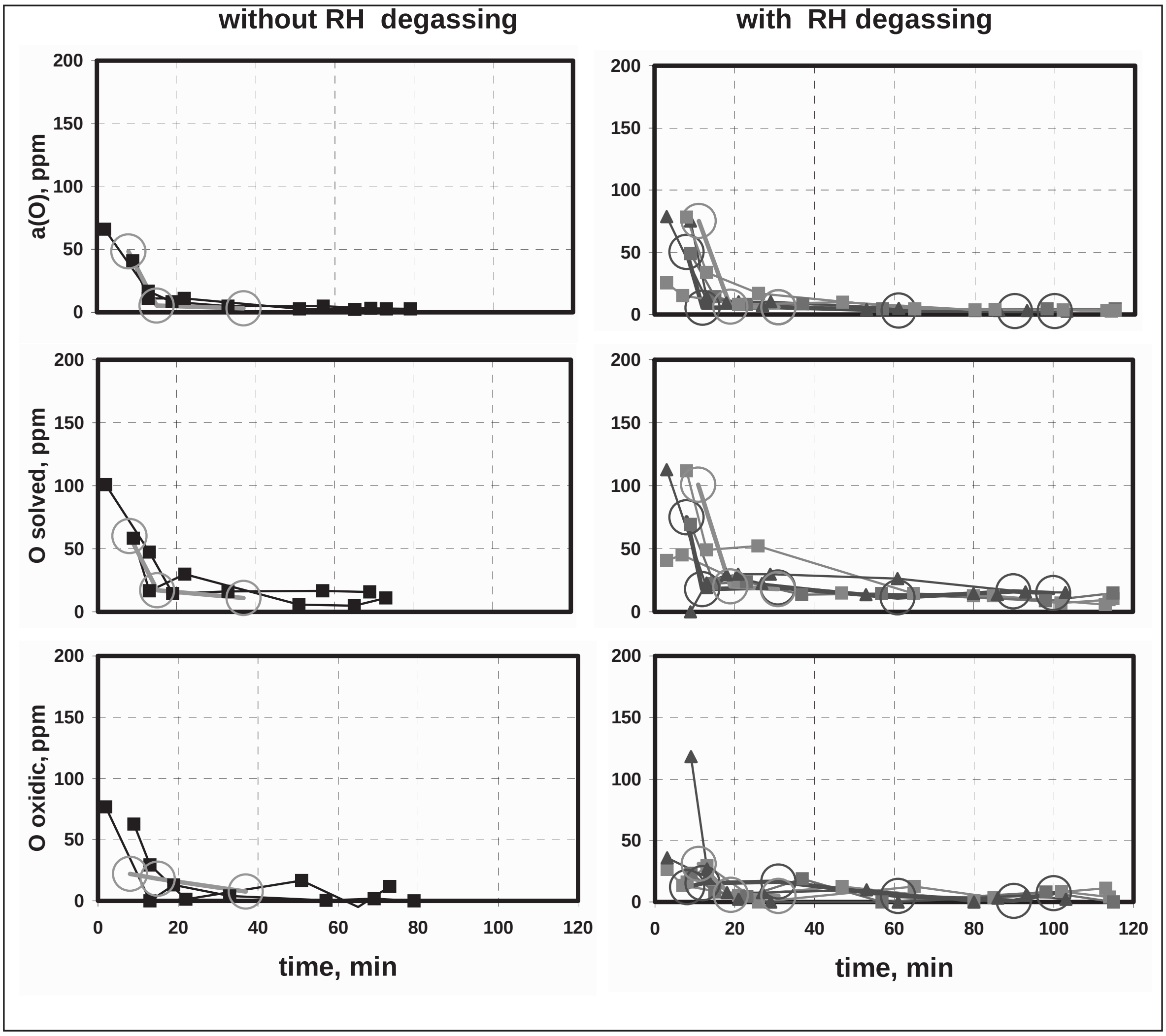

Figure 79 - Oxygen activity, solved and oxidic oxygen content

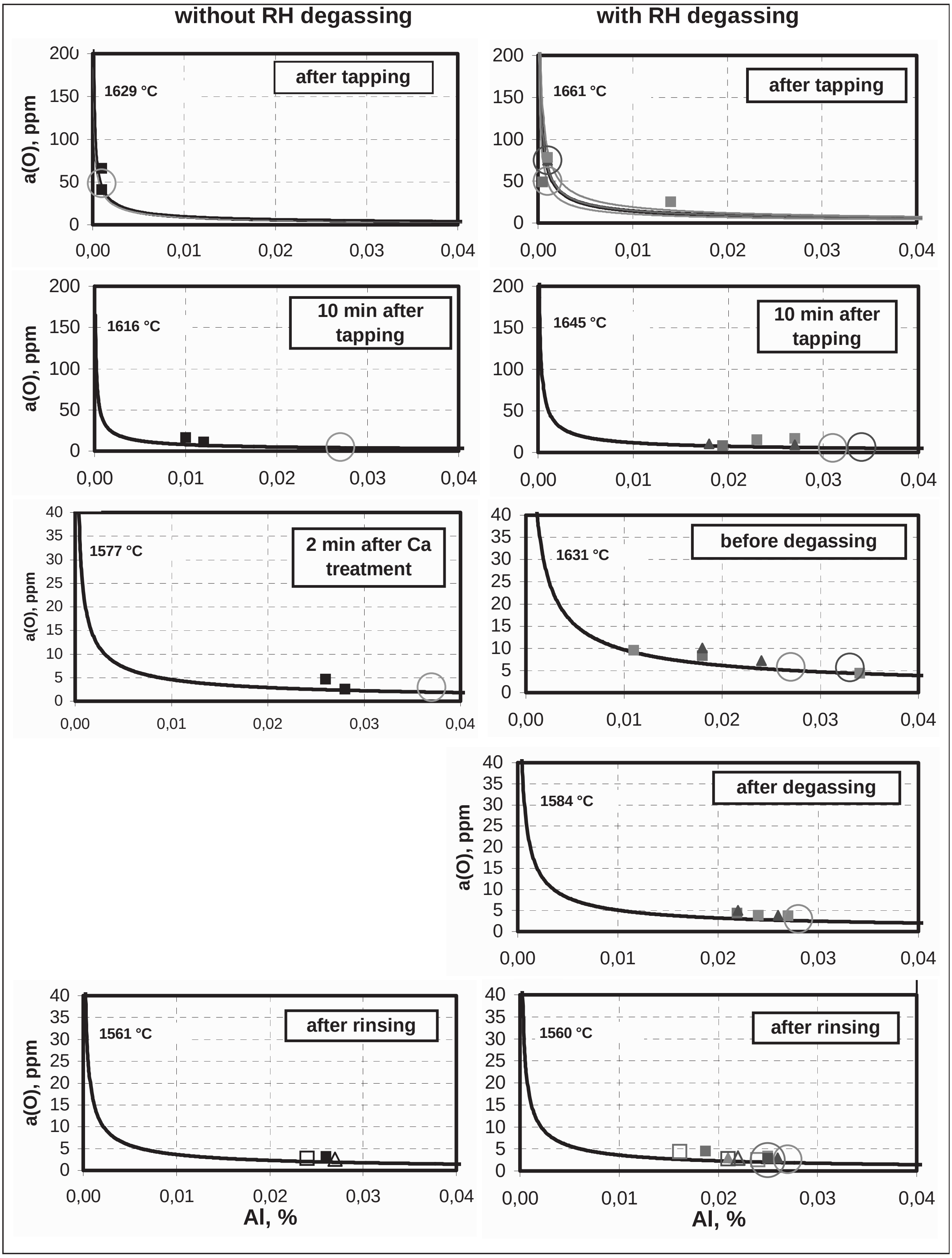

Figure 80 - Position of 170-t heats in the system Fe – a(O) – Al

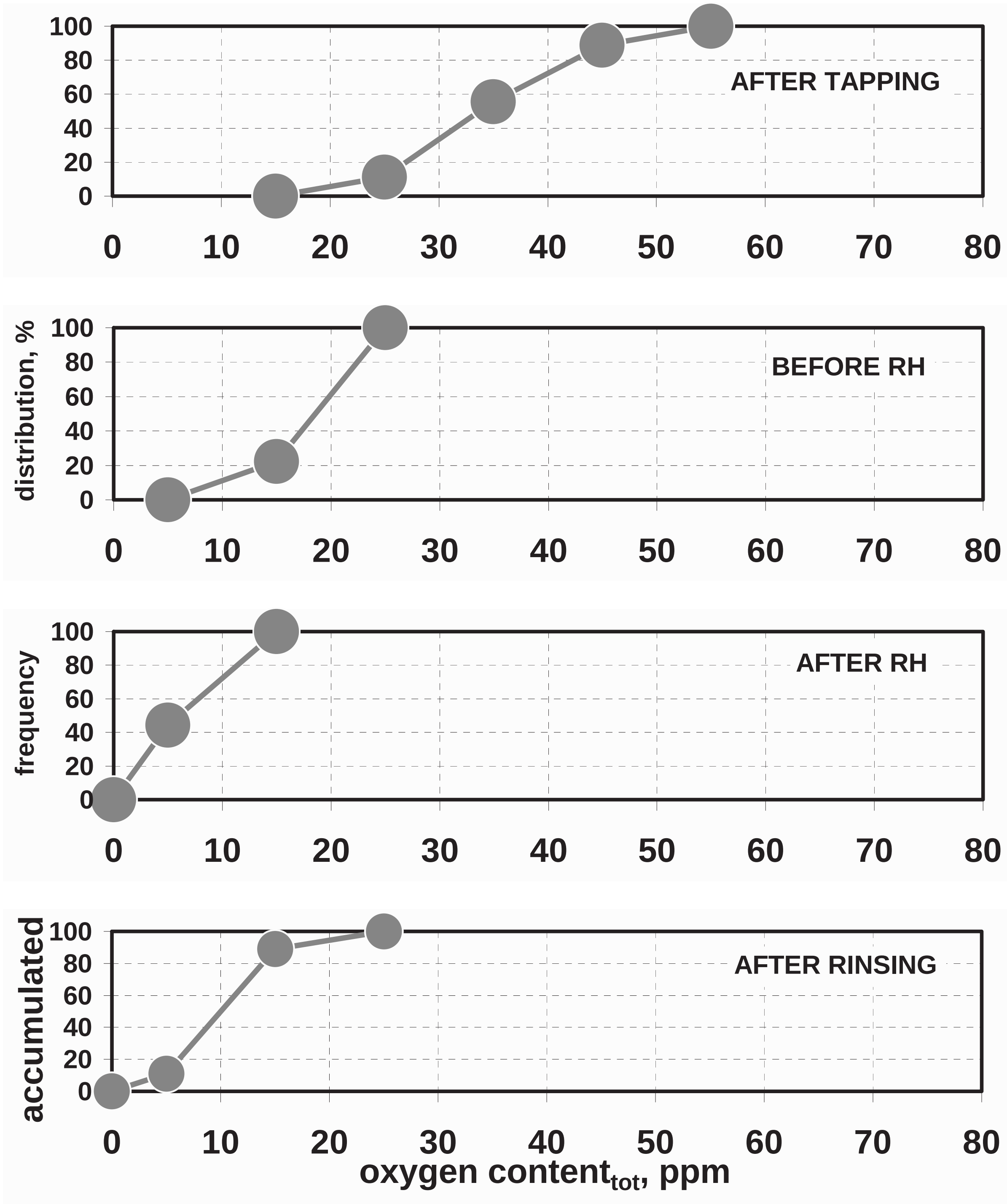

Figure 81 - Oxygen removal during ladle treatment of RH treated heats

Tests were performed with regard to the inclusion coming into existence at the end of ladle treatment. The analyses of typical inclusions of a Ca treated cold heading quality are shown in the pseudo-ternary system CaO´- Al_2O_3´- MgO´ (**Figure 82**). The Al_2O_3 rich inclusions are located mostly between C12A7 and Al_2O_3 in the edge system CaO – Al_2O_3. They contain CaS and some additions of MgO. During these experiments the attempt was conducted to minimize the size of the open-eye by lowering the rate of the stirring gas at the end of the ladle treatment. The results of the trials are summarized in **Figure 83** showing that there is a quite good correlation between gas flow and size indicating the larger the gas flow rate the bigger the open-eye diameter.

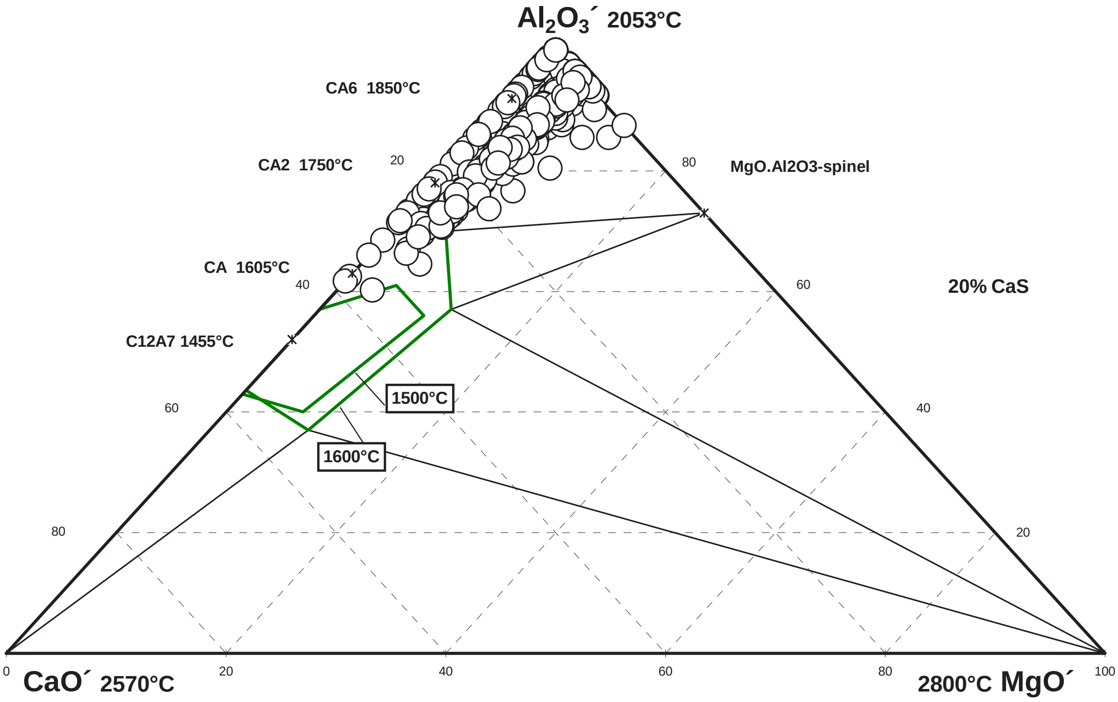

Figure 82 - Typical inclusions at the end of ladle treatment in the pseudo-ternary system CaO´- Al_2O_3´- MgO´

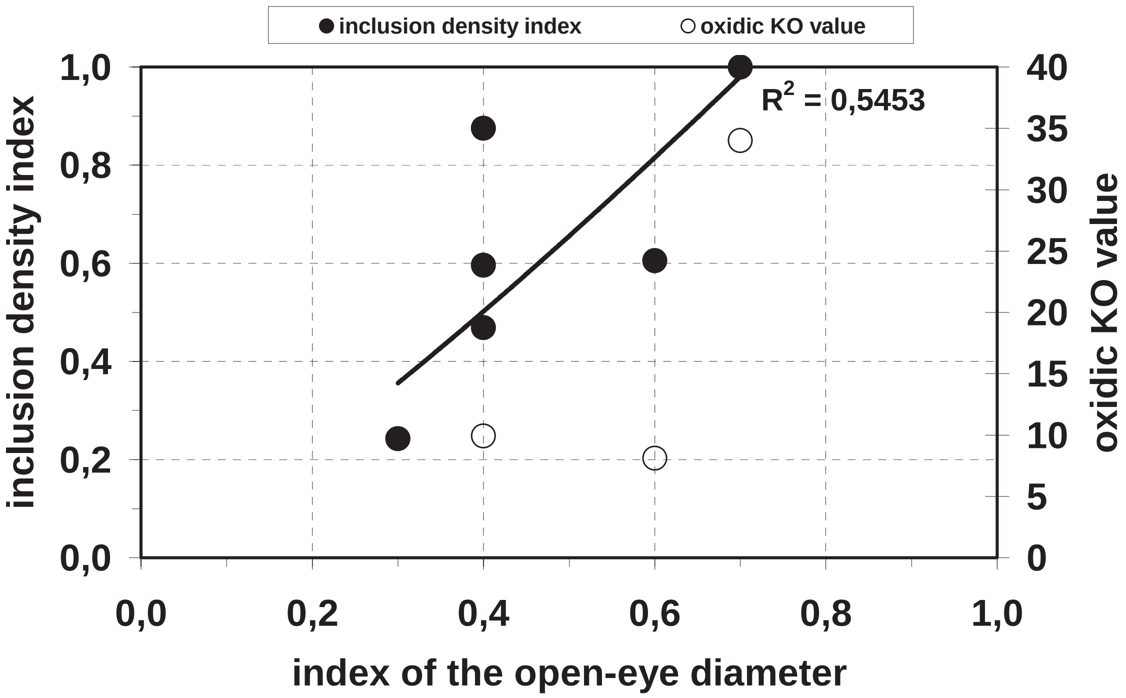

Figure 83 - Correlation between cleanness and open-eye

In addition the cleanness of these heats was determined by intensive blue brittle tests. The inclusion length index is plotted versus the aforementioned stirring energy in **Figure 84**.

There seems to be only a slight correlation between both stirring energy and inclusion length index. But as soon as an open-eye is coming into existence the inclusion length is higher compared to those heats produced under a closed top slag.

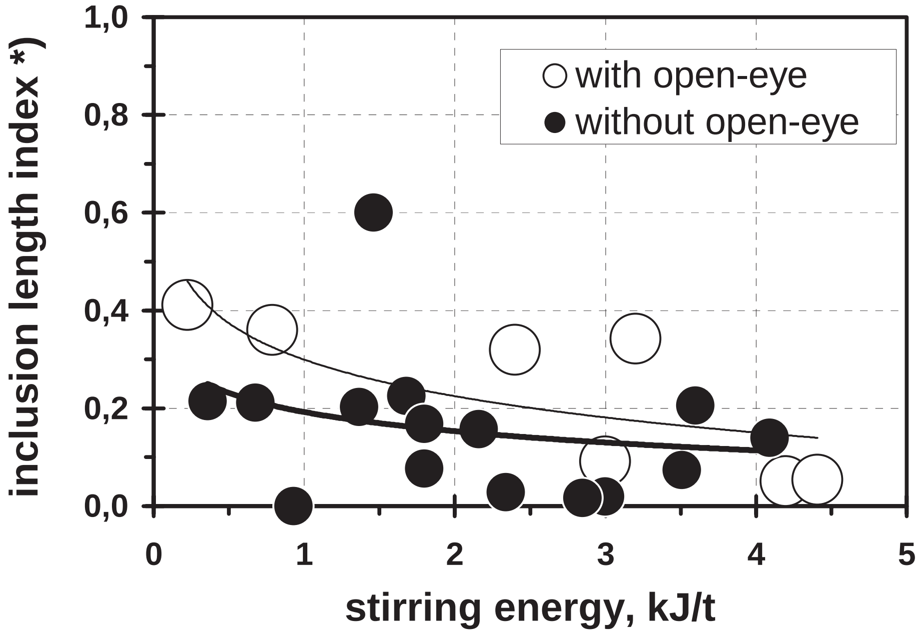

Figure 84 - Inclusion cleanness versus stirring energy [*) blue brittle method]

Evaluation of stirring effect over cleanliness (SIDENOR)

As several maintenance problems made it difficult a direct use of image analysis to relate open-eye to cleanliness, an indirect approach was selected in SIDENOR, based in expression (8). More than 200 heats were selected and on-line production data with 0.5 Hz frequency were collected. With those calculations, stdA values every 2 s were obtained and finally they were averaged and multiplied by time unit after vacuum before end of secondary metallurgy. This way, a unique parameter was got, including open-eye size estimation and time. This parameter is called open-eye risk. Results for 200 heats from different steel grades exhibit many points with no inclusion even for large open-eye risk index values. No clear trend could be evidenced. ***The reason for this poor correlation is likely the variability and measurement error of the slag thickness and fluidity, because slag carry-over is variable and no deslagging is generally applied.***

Criteria for plug change/choice (ACERALIA – ARCELOR Research)

The obtained static relations between vibration, gas flow rate and gas pressure have been investigated by ARCELOR Research and ACERALIA. The dispersion of the results is particularly high for the cases of “pressure/flow-rate” and “vibration/pressure”. By contrast, the correlation “vibration/gas flow rate” presents a clear logarithmic tendency with less dispersion as previously shown. Problematic heats statistically fell outside the 90 % percentile curves: it helps to define the time for plug change and evaluate different plug suppliers.

Correlation vibration versus cleanliness (ARCELOR Research)

As explained in the paragraph 5.2.3.2.2.2, this aimed at relating the metal cleanliness to the stirring/vibration level. In other word, is it possible to find an optimum stirring condition maximizing the metal cleanliness and to control it in an industrial environment?

Heats were elaborated with an aimed 10-min cleanliness bubbling with a gas flow rate of 100 and 200 l/min. The ladle vibrations were monitored. No open-eye could be observed during theses tests. Samples of metal were taken every minute during this phase. The evaluation of the inclusion population has been made by the total oxygen content present as oxides, by image analysis and using PDA-OES technique. The main conclusions after these trials are summarized on **Figure 85**:

- The kinetic of inclusion removal rate is variable from one heat to another. It can be quick or slow even leading to some global re-oxidation of the bath,
- The relationship between gas flow rate and inclusion removal rate is not very clear, although better results are obtained for gas flow rate around 100 l/min,
- A good relationship exists between the ladle vibration level and inclusion removal rate. An optimum range of vibration level is found, namely 0.015 to 0.022 m/s^2 in the present case. Over this range, the inclusion removal is either null or negative. Below this range, the inclusion removal is damped. This is in agreement with a recent publication [52],

Finally, **Figure 86** illustrates the conclusions of this development:

- The ladle vibration gives access to the true stirring,
- An optimum vibration range exist for maximizing inclusion removal rate,
- A higher vibration index corresponds to the risk of open-eye formation.

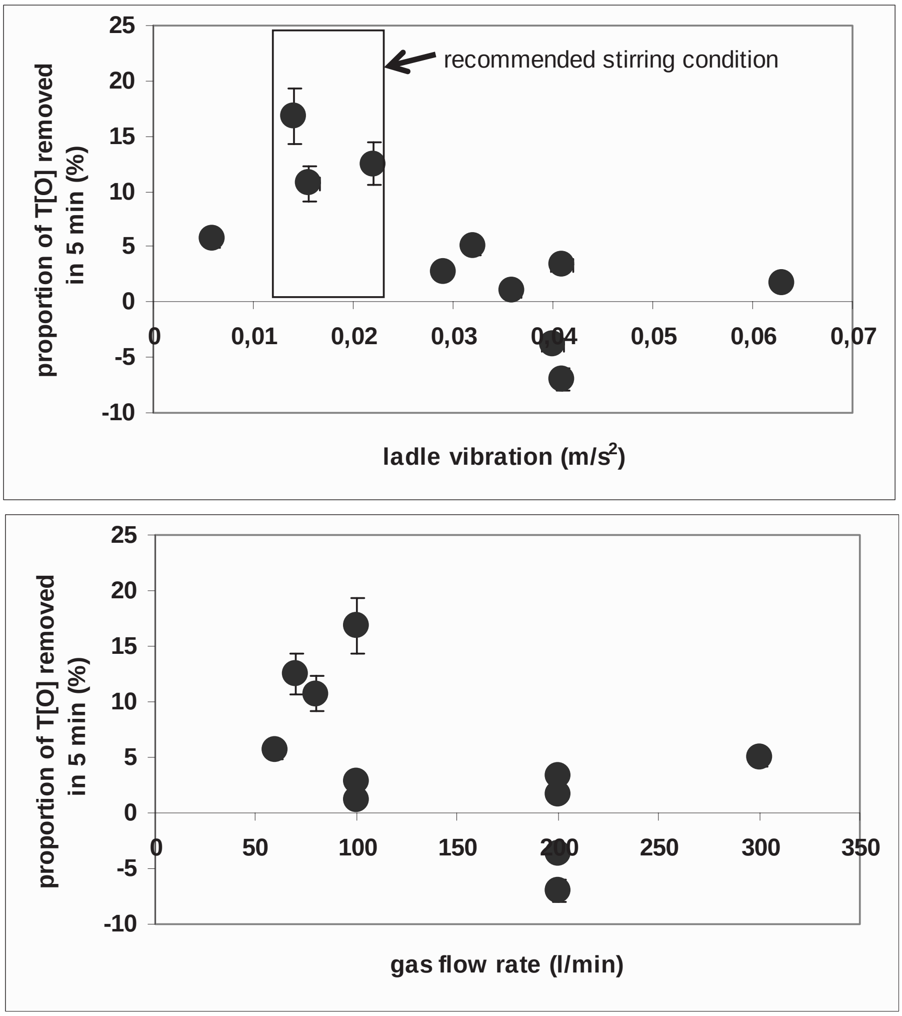

Figure 85 – Optimum rate of inclusion removal for a given ladle vibration range (ARCELOR Research)

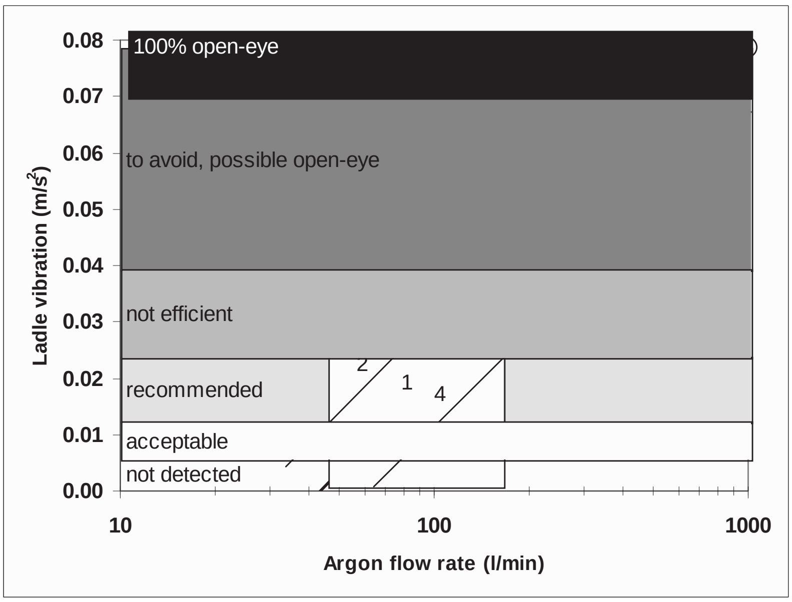

Figure 86 – Optimum ladle vibration range regarding quality control of the metal (ARCELOR Research)

5.3 Conclusions

The general objective of this multi-national multi-partner research project, involving ARCELOR Research, MEFOS, BFI, ACERALIA, SAARSTAHL AG and SIDENOR is to develop advanced methods and systems for on-line control of gas stirred ladle treatment processes in order to improve refining reactions, removal of inclusions and homogenization during alloying and to minimize slag entrapment and re-oxidation.

This project has reached its objectives. Activities were driven in agreement with the planning of the project. The developments and cooperation between the partners had led to a much clearer understanding of the gas stirred ladle treatments.

A correlation giving the open-eye area as a function of a slag Froude number, relating the gas flow rate and the metal and slag thicknesses, was selected. It fits well with all the data obtained on water scale models, at lab-scale hot metal experiments, with numerical simulations and with industrial data.

Image analysis procedures have been developed for automatic threshold and elimination of noised images. The implementation in plant of video camera proved to be more difficult than expected.

The ladle vibration increases with the Froude number, relating the gas flow rate and ladle diameter. This is true for a wide range of experiments driven on both pilot-scale steel ladle and water scale models and also for industrial plants. This assessment technique of the true stirring can evidence possible resonance effect related to the development of gravity mode. Finally a high vibration level corresponds to a risk of open-eye.

Contact and contact-less sensors give similar results. Their advantages and drawbacks are clarified.

The analysis of inclusion population during cleanliness bubbling in the plants made it possible to recommend to

- apply a soft bubbling, avoiding open-eye thanks to image analysis and/or based on a low vibration-level,
- generate a minimum stirring to get an effective inclusion removal, by aiming at a given defined range of ladle vibration.

Future developments are proposed in order to take into consideration the slag physical property and especially its viscosity to describe the open-eye.

5.4 Exploitation and impact of the research results

Regarding the exploitation of the results, we can mention:

- Actual applications are: image analysis at Saarstahl plant and vibration monitoring in Arcelor plants,
- Technical and economic potential for the use of the results: the main outcomes and possible applications in European steel plants are underlined:
  - The concept of soft bubbling procedure,
  - The similarity criteria and the advanced methods to monitor to bubbling favors the transferability,
  - Note that all type of gas-stirred treatment can be controlled through the vibration monitoring.
  - All this contributes to productivity increase and energy saving thanks to better tuning of the treatment time. It impacts positively as well the steel quality.
- ARCELOR has patented the vibration monitoring, under the keyword of Kettlor [54].
- Results of vibration monitoring were published by ARCELOR in June 2006 at the EOSC conference in Aachen [55]. Other presentations of the project work are foreseen in the coming years.

6 REFERENCES

1 J. Szekely: *Metal. Trans. B*, 1988, vol.19B, pp.525

2 D. Mazumdar and R. I. L. Guthrie: *ISIJ Int.,* 1995, vol.35, pp.1

3 S. H. Kim and R. J. Fruehan: *Metal. Trans. B*, 1987, vol.18B, pp.381

4 T. Stapurewicz and N. J. Themelis: *Can, Metall. Q.*, vol.26, pp.123

5 H. Tokunaga, M. Iguchi and H. Tatemichi: *ISIJ Int.,* 1995, vol.35, pp.21

6 Y. Xie and F. Oeters: *Steel Res.*, 1992, vol.63 , pp.93

7 A. H. Castillejos, M. Salcudean and J. K. Brimacombe: *Metal. Trans. B*, 1987, vol.18B, pp. 647

8 S. T. Johansen and F. Boysan: *Metal. Trans. B*, 1988, vol.19B, pp.755

9 Illegbusi O. J. and Szekely J.: *ISIJ Int.,* 1990, vol.30, pp.731

10 H. Turkoglu and B. Farouk: *Metal. Trans. B*, 1990, vol.21B, pp.771

11 D. Y. Sheng, L. Jonsson: *Proc. Of International Conference on Applied Computational Fluid Dynamics*, ACFD 2000, Beijing, Oct. 17-20, pp. 162

12 M. Wakoh, K. Fuchigami, K. Endoh, N. Imamura, A. Kiyose, I. Sawada: *Proc. Of SCANMET I* , Lulea, 7-8 June, 1999, pp. 267

13 Sivaramakrishnan, S., B.G. Thomas, S.P. Vanka, *Materials Processing in the Computer Age III*, V. oller and H. Henein, eds., TMS Annual Meeting, Nashville, TN, March 12-16, 2000, pp. 189-198

14 Hallberg M., Jonsson L. and Alexis J*.: Proc. of SCANMET 1*, pp.119-169., 1999, MEFOS, Lulea, Sweden

15 R.L.Minion, C. F. Leckie, K. J. Legeard and B. D. Richardson: *81st Steelmaking Conference Proceedings*, ISS, (1998), pp. 459-466.

16 Krajcik, W J, Kelly J E, Dorricott J D, Heaslip L J: *79th Steelmaking Conference Proceedings*, ISS, (1996), pp.475-480.

17 http://www.kisstechnologies.com

18 Dipak Mazumdar: "Some Fundamental Considerations Concerning Gas Injection Operations in Steelmaking Ladles", 59th Ironmaking Conference Proceedings, Pittsburgh, PA, March 26-29, 2000, pp. 531-540

19 Y. Sahai and R. I. L. Guthrie: Metall. Trans., 1982, vol. 13B, pp.193

20 Yuhua Pan, Bo Björkman: “Numerical Analysis on the Similarity between Steel Ladles and Hot-water Models Regarding Natural Convection Phenomena”, ISIJ Int. Vol 42 (2002), No. 1, pp. 53-62

21 Zhang, L., Taniguchi, Fundamentals of inclusion removal from liquid steel by bubble flotation, Int. Mat. Rev., Vol. 45 (2000), No. 2, S. 59-82

22 M. Lopez, S. J. Lee, R. T. Lahey, and D. A. Drew: *J. of Fluid Eng.,* 1990, pp.107

23 L. Jonsson and P. Jönsson: *ISIJ International*, 1996, vol. 36, pp. 1127

24 B.E. Launder and D.B. Spalding: *Comp Meth Appl Mech Eng*, 1974, pp.269.

25 B. Spalding et.al: *Phoenics Encyclopedia*, 1997, CHAM

26 D. Mazumdar, J. W. Ewans: “A Model for Estimating Exposed Plume Eye Area in Steel Refining Ladles Covered with Thin Slag”, Metallurgical and Materials Transactions B Vol. 35B (2004), Nr. 4, pp. 400-404

27 K. Yonezawa, K. Schwerdtfeger: “Spout Eyes Formed by an Emerging Gas Plume at the Surface of a Slag-Covered Metal Melt”, Metallurgical and Materials Transactions B Vol. 30B (1999), Nr. 6, pp. 411-418

28 Subgayo, G. A. Brooks, G. A. Irons: “Spout Eyes Area Correlation in Ladle Metallurgy”, ISIJ Int. Vol. 43 (2003), Nr. 2, pp. 262-263

29 K. Yonezawa, K. Schwerdtfeger: “Correlation for Area of Spout Eyes in Ladle Metallurgy”, ISIJ Int. Vol. 44 (2004), Nr. 1, pp. 217-219

30 Oeters F., Metallurgy of steelmaking, 1994, Verlag Stahleisen mbH, Düsseldorf

31 Weckes, J., Verbesserung des mikroskopischen Reinheitsgrades von Stahlschmelzen durch feine Blasen, Dissertation RWTH Aachen, 2002

32 T. Buhles: Modellierung und Simulation der Entschwefelung von Stahlschmelzen Dissertation TU Clausthal, 2002

33 Xiao Z., Peng Y. and Liu C.: *Chin. J. Mater. Sci. Technical*, 1987, vol.**3**, pp.187

34 T. Lehner, G. Carlsson and T. C. Hsiao: SCANINJECT II, June 12-13, 1980, Luleå,Sweden, pp.22, Technology, Göteborg, Sweden

35 M. Dubke, K. Schwerdtfeger I&S making, 1990, vol 17, 3, pp 184-192

36 H. Lamb Hydrodynamics, Dover Publication, New-York, 1932

37 M. Faraday: Phil. Trans. R. Soc. Lond., 121, 1835, 319

38 T.B. Benjamin, F. Ursell: Proc. R. Soc. Lond., A225, 1954, 505

39 C.P Tai, Z.M. Quian: Trans. ISU, 1986, 26, p 139

40 J.P. Gollub, C.W. Meyer: Physica 6D, p 337, 1983

41 S. Ciliberto, J.P. Gollub: Physical Review Letters, 52, n01 1, pp 922-925, 1984

42 S. Ciliberto, J.P. Gollub: J. Fluid Mechanics, 158, pp 381-398, 1985

43 M. Burty et al. Isij Congress, Nagoya, Japan, 1, p 444, 1990

44 G.G. Krishna Munhy, S.P. Mehrotra, A. Ghosh: Met. Trans. B, 19B, 1988, 839

45 A.H. Castillejos, J.K. Brimacombe : Met. Trans. B, 20E, 1989, 595

46 G.G. Krishna Murthy, A. Ghoshi, S.P. Mehrotra: Met. Trans. B, 19E, 1988, 885

47 S.C. Koria, S. Singh: Steel Research, 7, 1990, 287

48 G. Ebneth, W. Pluschkell: Steel Research, 56, 1985, 513

49 J. Pietzka, E. Steinmetz, H. Wilhelmi : Steel Research, 58, 1987, 538

50 V. Sahajwalia, A.H. Castillejos, J.K. Brimacombe: Met. Trans. B, 21B, 1990, 71

51 M.A. Soares: Ph. D. Clausthal, Germany, 1988

52 DS.Kim, Joo H.Park, Jong H.Park, HG. Lee, SB.Lee, Improvement of cleanliness of 16%Cr-containing Stainless Steel in AOD processes, Journées sidérurgiques Internationales, Paris, 10-11 December 2003

53 Nakanishi K., Fujii T., and Szekely J., Possible relationship between energy dissipation and agitation in steel processing operations, Ironmaking and Steelmaking (Quarterly) (1975), No. 3. p. 193-197

54 M. Burty, et al., "Procédé de controle du bullage en poche et installation de mise en oeuvre", PCT/FR2005/001460, 14 June 2005

55 M. Burty, C. Pussé, C. Bertoletti, P. Wetta, E. Carioli, Kettlor: Efficient stirring in ladle metallurgy, Proceeding EOSC2006, Aachen - Germany, June 2006

7 TECHNICAL ANNEX

TITLE: DEVELOPMENT OF ADVANCED METHODS FOR THE CONTROL OF LADLE STIRRING PROCESS

1. OBJECTIVES

The general objective of this multi-national multi-partner research project, involving IRSID, MEFOS, BFI, ACERALIA, Saarstahl AG and SIDENOR is to develop advanced methods and systems for on-line control of gas stirred ladle treatment processes in order to improve refining reactions, removal of inclusions and homogenization during alloying and to minimize slag entrapment and re-oxidation.

The optimization of the steelmaking conditions will lead to an increase of the yield of addition (of about 20%), to an increase of the product quality (by 25 %) and to an increase of the length of casting sequences (of about 25%).

Different sensors will be used and compared, in terms of resolution and performance. Different ladle scales will be used to be able to define general rules for metal uncovering and optimum working conditions of sensors. Soft stirring metal inclusion removal and strong stirring for alloying will be considered.

The main benefits of the proposed research are to:

- increase the steelmaking and casting productivity by reducing the nozzle clogging phenomena linked to the global cleanliness of the steel arriving at the continuous caster,
- improve product quality,
- decrease the steelmaking cost by increasing the yield of addition and by decreasing the thermal losses (by about 15%).

2. WORK PROGRAMME AND DISTRIBUTION OF TASKS

The specific axes of work in this research are the following:

2.1. INTERACTION BETWEEN STEEL AND SLAG

- Gas stirring experiments measuring open-eye and surface oscillations
- Numerical simulation of "open-eye stirring", small scale experiments
- Numerical simulation of "open-eye stirring", plant conditions
- Lab scale and pilot scale trials

2.2. DEVELOPMENT OF SENSORS

- Vibration based sensors
- Image processing of slag surface

2.3. TRANSIENT STIRRING PHENOMENA

- Analysis of surface oscillations with and without slag using fluid mechanics
- Development of models describing time depending behavior of the flow pattern in the ladle
- Verification and validation of transient numerical model

2.4. INDUSTRIAL TRIALS

- Plant measurements of vibrations, oscillations and open-eye formation
- Assessment of metal cleanliness

3. WAYS AND MEANS

In order to reach the objectives, investigations using numerical and physical models as well as plant trials will be combined. The activities will proceed as follows:

3.1– IRSID contribution

IRSID will focus on the following aspects:

- comparison of vibration based sensors,
- stirring and vibration in lab scale and pilot scale ladles,
- analysis of stirring condition in full scale water model of lab and pilot scale ladles,
- industrial tests and impact on metal cleanliness,
- comparison of vibration based sensor and image processing,

Moreover, IRSID will be in charge of the co-ordination of the present project.

3.2– MEFOS contribution

The work of MEFOS is based on two themes:

Interaction between steel and slag during stirring in a steel ladle

The first theme and objective is expected to be achieved by studying the free surface and the steel/slag interaction in small-scale experiments and numerical modelling. Small-scale experiments are planned to be done with a low temperature melting metal system. The characteristics of the open-eye are measured under different conditions, like slag thickness, slag properties, stirring intensity. Beside experiments, a numerical model is planned to simulate the metal/slag/ behaviour in the model and in a plant ladle. Special attention is focused on the "open-eye stirring" at the melt surface. Results from model experiments are used to calibrate the numerical model. Model predictions are also carried out for true plant situations, possibly measured by other partners.

Time-dependent behaviour of gas injection, gas plume shape, general flow pattern and oscillation of metal/slag interface during stirring

The second theme deals with all the time dependent phenomena, which could cause measurable vibrations or oscillations during the stirring process.

The complete gas stirring process is analysed including the gas injection system, the bulk of liquid steel and the metal/slag interface using several methods, fluid mechanics analysis, physical modeling, numerical modeling and plant measurements. Plant measurements of vibrations are foreseen by using a non-contact laser or other measurement technique suitable for industrial applications, like pressure fluctuations in the gas injection system.

3.3– ACERALIA contribution

The following tasks are planned by ACERALIA:

1. Test of sensor in inclusion flotation period at industrial scale

- Different patterns of stirring, verifying with metallographic analysis.
- Check of the result with those made with the accelerometer.
- Trials and analysis for different steel and patterns.

2. Test of sensor in strong stirring for metal-slag

- Test and trials and cross-check: sensor and laboratory.
- Trials and analysis for different steel and patterns.

3. Definition of best sensor location and best signal treatment

- Perform of the trials in different positions in RH-OB, CAS & INJ station.

•Depending of the results of the trials in different conditions, the best location will be defined as well as the best condition for signal treatment.

The sensor is based on image analysis.

3.4- BFI contribution

The following tasks are planned by BFI:

a) Development of prototype image processing system for on-line control and analysis of melt surface during ladle stirring

•Definition and selection of appropriate optical filters and detectors to visualize melt surface patterns.

•Classifying characteristic surface patterns during ladle stirring with respect to different slag layer properties at pre-defined stirring conditions.

•Developing and testing of an image processing tool for on-line detection and analysis of surface patterns.

b) Physical modeling for extensive testing, validation and improvement of the image processing unit

•Set-up of a gas stirred ladle model using water as modeling fluid.

•Definition of a suitable physical model for slag layer properties, like e.g. slag layer thickness and slag composition.

•Detection of surface patterns for different stirring intensities and different slag layer properties.

c) Development and implementation of a theoretical model for on-line evaluation of stirring efficiency by observing surface patterns at different stages of gas stirred ladle treatment

•Experimental investigations on interactions between characteristic surface patterns, slag layer properties and bubble forced flow inside the physical model.

•Definition of suitable correlation between characteristic surface patterns and stirring efficiency. (In addition to the results of physical modeling, this subtask makes use of results from numerical simulations by Mefos and parametric description of observed gas stirring efficiency extracted by SAG).

•Implementation of the theoretical model into the image processing system.

•Extensive testing of the image processing system under well defined conditions in the physical model.

d) Laboratory trials in hot melts with well defined gas stirring intensities and slag layer properties

•Definition of characteristic gas stirring intensities and slag layer properties from operational practice.

•Extensive testing and improvement of the image processing system under defined operational conditions.

e) Operational trials at different gas stirred ladle treatment processes and under varying operating conditions for improvement of image processing system

•Extensive testing of the image processing system under different operating conditions, like e.g. alloying and cleanliness stirring. (This subtask will be undertaken in close collaboration of BFI and SAG.)

•Improvement of the theoretical model and the entire image processing system.

f) Extensive testing during measurement campaigns at gas stirred ladle treatment processes

3.5– Saarstahl AG contribution

The following tasks are planned by Saarstahl AG, concerning using Al- and Si-de-oxidised steels:

•Definition of the “open-eye“ and the melt surface pattern by the evaluation of the stirring process data.

•Parametric description of the efficiency of gas stirring with regard to the requirements of different stages of ladle treatment.

•Installation of camera and recording system.

•Recording and classifying characteristic surface patterns during ladle stirring with respect to different slag layer properties at pre-defined stirring conditions.

•Validation by sampling: analysis of the top slag particularly with regard to steel grade, amount of the slag former added during tapping and temperature.

Operational experiments will be carried out together with BFI with regard to:

•testing of the image processing system under the SAG condition with 170t-heats (ladle data : diameter: 3.5 m, height: 3.8 m) like alloying and cleanliness stirring using different top slags.

•Comparison and validation of the evaluated gas stirring efficiency with operational experience and chemical analysis during ladle treatment.

•evaluation of the evolution of the total, solved and oxidic oxygen

•control of the nitrogen content as tracer either for a normal oxygen decrease or for the entrapment of oxygen due to re-oxidation originated by the air before and after each stirring.

•control of the inclusions before and after each stirring as tracer for the emulsifying of top slag.

•determination of the reaction kinetics and the rate controlling step.

•Evaluation of the cleanness in the final product : micro cleanness according to DIN 50602 and the macro cleanness according to blue brittle tests and ultrasonic tests.

•Determination by SEM analyses of size and composition of the inclusions in the liquid steel and in the bar or wire rod.

3.6– SIDENOR contribution

The following tasks are planned by SIDENOR:

•Definition of the stirring standards at the new LFV station at Basauri plant; Different flow rates are set up according to the process:

- strong stirring (>1200 l/min) after ferroalloys addition, for quick mixing;
- “normal” (200 – 500 l/min, depending on plug and stirring system condition);
- soft for vacuum process;
- soft for inclusion flotation.

A large range of steel grades are produced and slag condition are different as to the oxygen tapping content or if deslagging is carried out after tapping.

•Installation of a camera for "open-eye" observation;

•Analysis of the image by digital processing;

•Data exchange with other partners (for possible models validation with plant data, industrial trials, etc.);

•Determination of the “real” stirring based on bath "open-eye" and its surface movement, inlet gas pressure and slag condition;

•Development and installation of an on-line model to implement automatic stirring programs at LFV;

•Evaluation of the stirring programs reliability;

4. PROGRAMME BAR CHART

N°	Themes		Semester of the activity						
			2002 S2	2003 S1	2003 S2	2004 S1	2004 S2	2005 S1	2005 S2
			I	II	III	IV	V	VI	VII
1	**Interaction between steel and slag**								
1.1	Design and construction of a small ladle	MEFOS		■	■				
1.2	Gas stirring experiments measuring open-eye and surface oscillations	MEFOS				■	■		
1.3	Numerical simulation of "open-eye stirring", small scale experiments	MEFOS		■	■	■			
1.4	Numerical simulation of "open-eye stirring", plant conditions	MEFOS				■	■		
1.5	Initial situation assessment Recording and classifying of suitable parameters describing efficiency of gas stirring	SAG	■	■					
1.6	Physical modeling for extensive testing, validation and improvement of the image processing unit	BFI		■	■				
1.7	Laboratory trials in hot melts with well defined gas stirring intensities and slag layer properties	BFI					■		
1.8	Analysis of stirring condition in full scale water model and pilot scale ladles	IRSID			■	■			
1.9	Definition of the stirring standards	SIDENOR	■						
1.10	Installation of a camera for "open-eye" observation	SIDENOR	■						
1.11	Analysis of the image by digital processing	SIDENOR		■					
1.12	Determination of the “real” stirring based on bath "open-eye" and its surface movement, inlet gas pressure and slag condition	SIDENOR			■	■			
1.13	Global analysis of metal-slag interaction during bubbling process	All partners		■	■	■	■	■	

2.	**Development of sensors**								
2.1	Comparison of vibration based sensors	IRSID			■	■	■		
2.2	Stirring and vibration in lab scale and pilot scale ladles	IRSID	■	■	■				
2.3	Comparison of vibration based sensor and image processing	IRSID				■	■		
2.4	Development of prototype image processing system for on-line control and analysis of melt surface during ladle stirring	BFI	■	■					
2.5	Operational trials at different gas stirred ladle treatment processes and under varying operating conditions for improvement of image processing system	BFI					■	■	
2.6	Functional Specifications of the sensors	ACERALIA	■						
2.7	Technical Specifications of the sensors	ACERALIA		■	■				
2.8	Detailed Requirements	ACERALIA		■	■				
2.9	Performing individual trials and tests	ACERALIA			■	■	■	■	
2.10	Comparison of sensors and of signal treatment	All partners	■	■	■	■	■	■	

N°	Themes		Semester of the activity						
			2002 S2	2003 S1	2003 S2	2004 S1	2004 S2	2005 S1	2005 S2
			I	II	III	IV	V	VI	VII
3.	**Transient stirring phenomena**								
3.1	Analysis of surface oscillations with and without slag using fluid mechanics	MEFOS							
3.2	Development of models describing time depending behavior of the flow pattern in the ladle	MEFOS							
3.3	Verification and validation of transient numerical model	MEFOS							
3.4	Analysis of stirring and interface deformation according to the bubbling conditions	IRSID							
4.	**Industrial trials**								
4.1	Industrial test of sensors and evaluation of impact on metal cleanliness	IRSID							
4.2	Plant measurements of vibrations, oscillations.	MEFOS							
4.3	Adaptation and installation of the digital image processing system Verification and validation of defined efficiency parameters	SAG							
4.3	Development and implementation of a theoretical model for on-line evaluation of stirring efficiency by observing surface patterns at different stages of gas stirred ladle treatment	BFI							
4.4	Extensive testing during measurement campaigns at gas stirred ladle treatment processes	BFI / SAG							
4.5	long term operational experiments to verify classified characteristic surface pattern and defined efficiency parameters and final adjustment of the on-line digital image processing system	SAG							
4.6	Test of sensor in inclusion flotation period at industrial scale	ACERALIA							
4.7	Test of sensor in strong stirring for metal-slag	ACERALIA							
4.8	Definition of best sensor location and best signal treatment	ACERALIA							
4.9	Interpreting results	ACERALIA							
4.10	Check of values with those from real conditions of the process	ACERALIA							
4.11	Integration of the measurements	ACERALIA							
4.12	Integration in the steel plant application	ACERALIA							
4.13	Development and installation of an on-line model to implement automatic stirring programs at LFV	SIDENOR							
4.14	Evaluation of the stirring programs reliability	SIDENOR							
4.15	Exchange of results between the partners and common analysis and interpretation	All partners							
5.	**Evaluation, documentation and reporting**	All partners							

8 ANNEX OF DETAILS

Some details of the partners' contributions are given hereafter.

8.1 SAG theoretical calculations - Flow pattern in the ladle

3D calculations with Computational Fluid Dynamics, CFD, were carried out to evaluate the flow pattern under real conditions with different gas flow rates at the steel plant of Saarstahl AG. Fluctuating velocity fields characterize turbulent flows. These fluctuations cause transported quantities such as momentum, energy and concentration to fluctuate as well. In almost all metallurgical processes, the Reynolds numbers are very high, in the ratio 10^3-10^5. These very high numbers are indicating turbulence, which lead to an exchange of momentum from faster to slower moving regions of the liquid [sag1]. To mathematically calculate the rate of change in the continuity and momentum equations, the Navier-Stokes equation has to be solved. Solving the transient forms of Navier-Stokes equation numerically demands micrometer-sized volume elements and it is not practical with existing computer technology [sag1-sag3].

The Navier-Stokes equation can be simplified using time average values and knowing that $\nabla \cdot \overline{v} = 0$. Using this, the N-S equation can be written in the x-direction as [sag4]:

$$\frac{\partial \overline{v}_x}{\partial t} + \overline{v}_x \frac{\partial \overline{v}_x}{\partial x} + \overline{v}_y \frac{\partial \overline{v}_x}{\partial y} + \overline{v}_z \frac{\partial \overline{v}_x}{\partial z} =$$

$$-\frac{1}{\rho}\frac{\partial \overline{p}}{\partial x} + g_x + \nu\left(\frac{\partial^2 \overline{v}_x}{\partial x^2} + \frac{\partial^2 \overline{v}_x}{\partial y^2} + \frac{\partial^2 \overline{v}_x}{\partial z^2} + \right) - \frac{\partial}{\partial x}\left(\overline{v'_x\, v'_x}\right) - \frac{\partial}{\partial y}\left(\overline{v'_x\, v'_y}\right) - \frac{\partial}{\partial z}\left(\overline{v'_x\, v'_z}\right)$$

where $\nu_t = \frac{\mu_t}{\rho}$ and $\mu_t = \rho l k^{0,5} = C_D \frac{\rho k^2}{\dot{\varepsilon}}$.

The three last components, including the terms of the form $\left(\overline{v'_x\, v'_x}\right)$, are known as Reynolds stresses or turbulent shear stresses. Reynolds stresses are caused by turbulence. To solve the terms, a turbulence model is needed to describe the turbulence energy.

The turbulence energy transport, k, Equation [sag1]:

$$\frac{\partial k}{\partial t} \quad + \quad v_i \frac{\partial k}{\partial x_i} \quad = \quad \frac{\partial}{\partial x_i}\left(\frac{\nu_t}{\sigma_k}\frac{\partial k}{\partial x_i}\right) \quad + \quad \nu_t\left(\frac{\partial v_i}{\partial x_j} + \frac{\partial v_j}{\partial x_i}\right)\frac{\partial v_i}{\partial x_j} \quad - \quad \dot{\varepsilon}$$

rate of

change convection diffusion generation destruction

The turbulence energy dissipation, ε, Equation [sag1]:

$$\frac{\partial \dot{\varepsilon}}{\partial t} \quad + \quad v_i \frac{\partial \dot{\varepsilon}}{\partial x_i} \quad = \quad \frac{\partial}{\partial x_i}\left(\frac{\nu_\varepsilon}{\sigma_\varepsilon}\frac{\partial \dot{\varepsilon}}{\partial x_i}\right) \quad + \quad C_1 \frac{\dot{\varepsilon}}{k}(G) \quad - \quad C_2 \frac{\dot{\varepsilon}^2}{k}$$

rate of

change convection diffusion generation destruction

where G describes the generation of turbulence energy. These two equations are known as the k-ε equations. The turbulent kinetic energy, k, is described by the k-equation and its dissipation rate by the ε-equation. k is proportional to the Reynolds stresses. Appropriate values for the empirical constants C_1, C_2, C_D, σ_k and σ_ε in the Equations (2.7) and (2.8) are presented in Table 2.2.

Table 2.2 Appropriate values for the constants in equations (2.7) and (2.8) [sag1]

C_1	C_2	C_D	σ_k	σ_ε
1.44	1.92	0.09	1.0	1.3

The k-ε model has some weaknesses. It is derived assuming full turbulence and problems can therefore appear when k and $\varepsilon \to 0$. The k-ε model is an isotropic model and as a consequence of that it is not able to respond to neither concave nor convex curvature effects. Other consequences are that it is not good in predicting the normal stresses, the square terms, and it is unable to account for irrotational strains. The advantages of the k-ε model are that it is simple due to that it is an isotropic model. It is stable, well established and works well for several kinds of engineering problems [sag2,sag5].

An alternative to solve the turbulence energy equations is to use the "Reynolds Stress Model", RSM. The RSM model is not an isotropic model and can therefore selectively damp the stresses due to buoyancy, acceleration/retardation, curvature effects and swirling flow. The main disadvantages of the RSM model are that it is numerically unstable and more computational expensive to use due to the complexity. The RSM model is favorable to use where curvature effects are important and it is necessary to accurately predict all Reynolds stresses, not only the shear stresses [sag2,sag5].

For the three-dimensional calculations, a ladle with the measures of the ones in the steel plant of Saarstahl AG was created. This ladle is divided into 53 964 volume elements, mainly cubes of 100×100×100 mm. Smaller elements are used closest to the walls, due to near wall turbulence. The eccentric position of the porous plug is 1.035 m from the centre. The positions of the different planes being used in the following figures are shown in **Figure S1**.

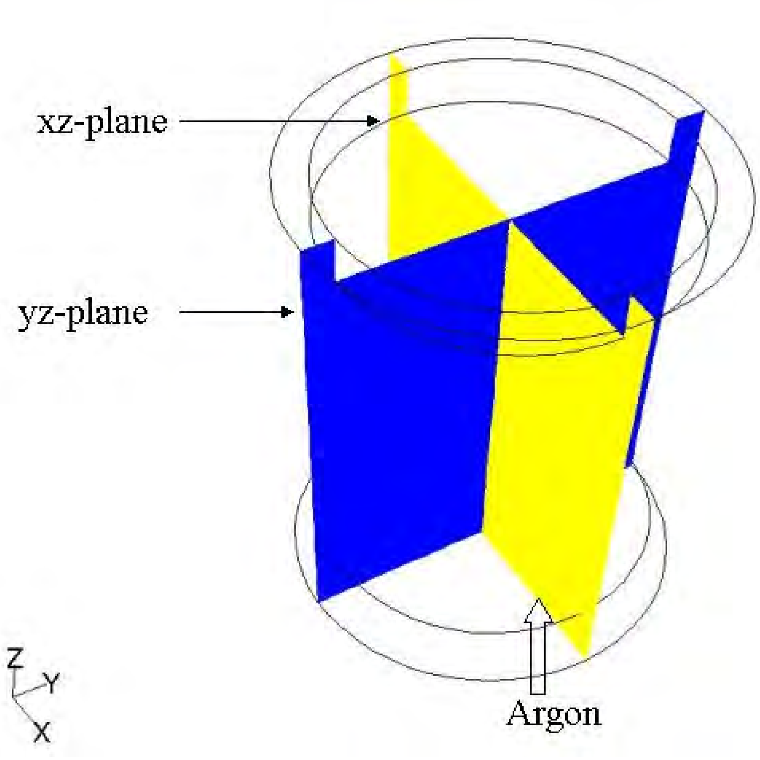

Figure S1 **Planes of the 170t ladle used for the 3D evaluation of steel flow pattern**

The generated flow pattern without the injection of a stirring gas consists of two circulating loops (**Figure S2)**. The steel flows upward in the centre of the ladle and downward along the walls due to heat transfer from the steel to atmosphere or to refractory of the ladle. The hot steel in the centre flows up to the top surface and the colder and heavier steel flows downward along the walls. The maximum velocity observed is 0.11 m/s. The introduction of a stirring gas with a gas flow rate of 3 STP m^3/h generates a larger circulating flow as indicated in **Figure S3**. An upward flow is seen where the argon is injected and a downward flow along all the walls. An upward flow is also observed to the left in Figure S3b. The maximum velocity of the steel is 0.9 m/s and is seen along the walls and in the middle at the top surface. The lowest velocity of 1 cm/s is in this case to be expected in the centre and at the bottom along the walls.

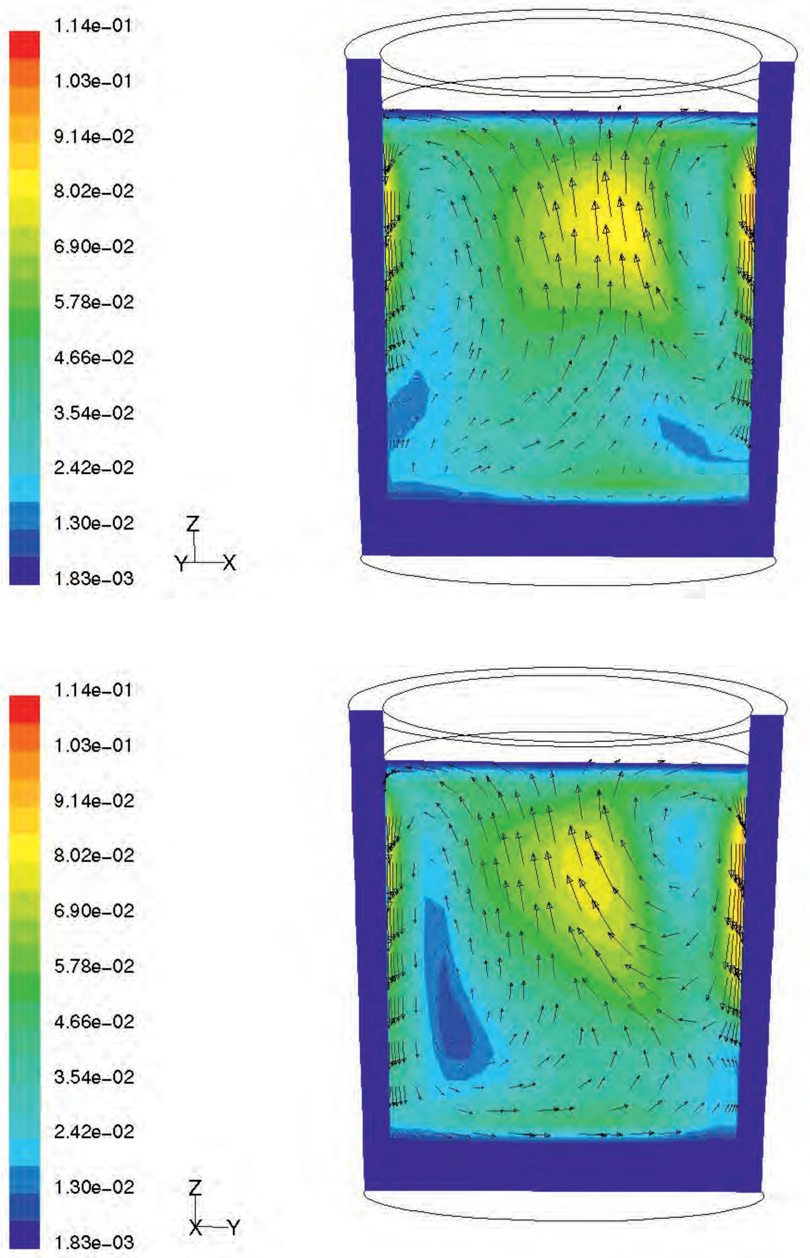

a) xz-plane

b) yz-plane

The coloured scale indicates the velocity in m/s and the arrows indicate the direction of the flow.

Figure S2 **Flow pattern in the 170t ladle without stirring**

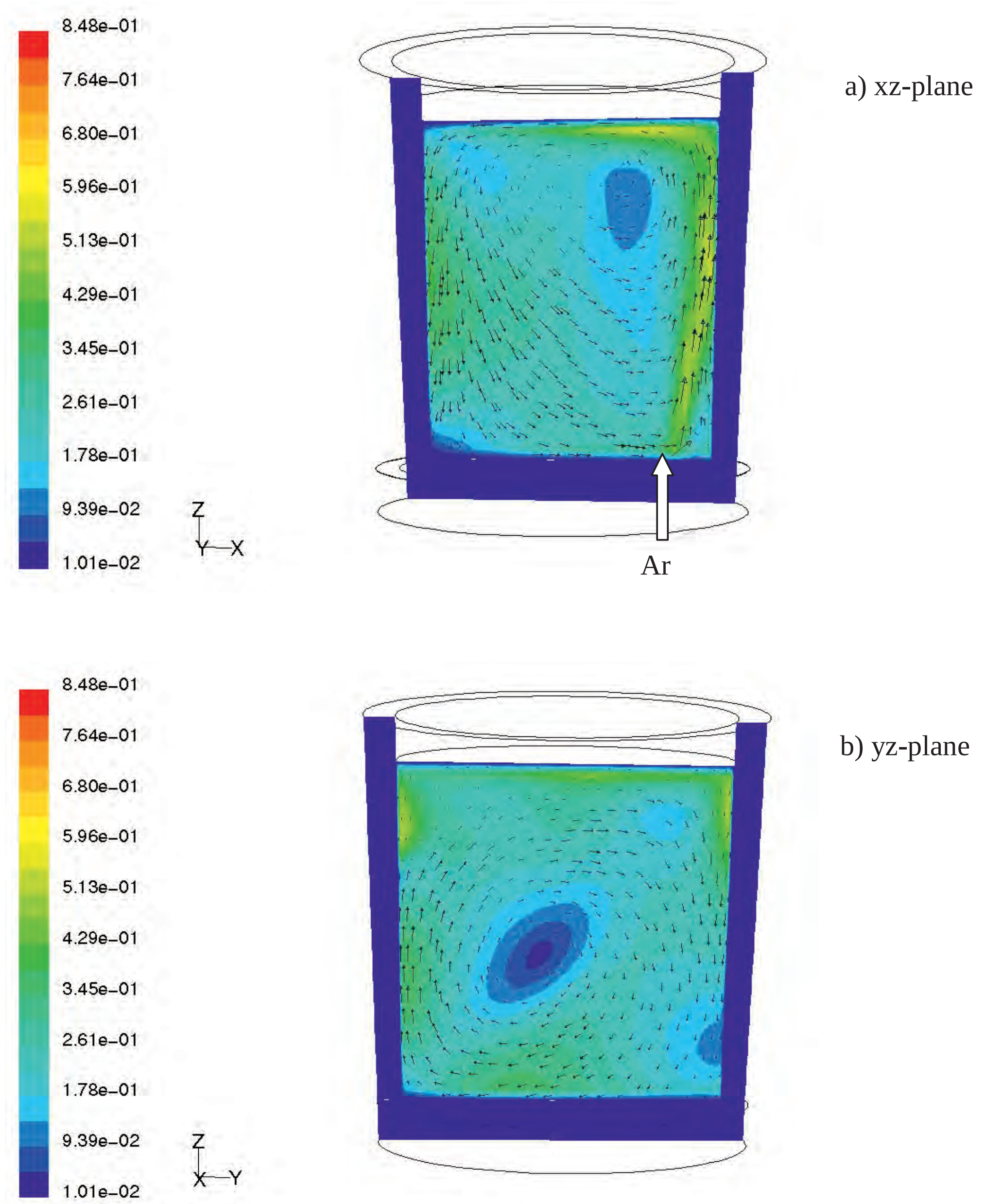

The coloured scale indicates the velocity in m/s and the arrows indicate the direction of the flow.

Figure S3 **Flow pattern in the 170t ladle using a gas flow rate of 3 STD m^3/h**

The last step is to calculate the flow variables at high stirring rate conditions, 27 STP m^3/h. This case represents the stirring used in the ladle after tapping and during alloying. The generated flow pattern consists of a distinguished circulating loop. In **Figure S4** there is an upward flow driven by the argon gas and a downward flow close to the walls in the case of a gas flow rate of 27 STP m^3/h. In the orthogonal plane, Figure S4b, an upward flow is also observed on the left hand side. The maximum velocity of the steel is 2.4 m/s and is found in the xz-plane where the stirring gas is injected. Lower velocities are observed in the centre and very close to the bottom in the orthogonal yz-plane. It can be clearly seen, that the eccentric position of the porous plug leads also to a very eccentric steel flow pattern as the light gas bubbles follow the flow pattern of the heavy steel in such a way that the higher the gas flow rate the closer the upward flow to the wall of the ladle.

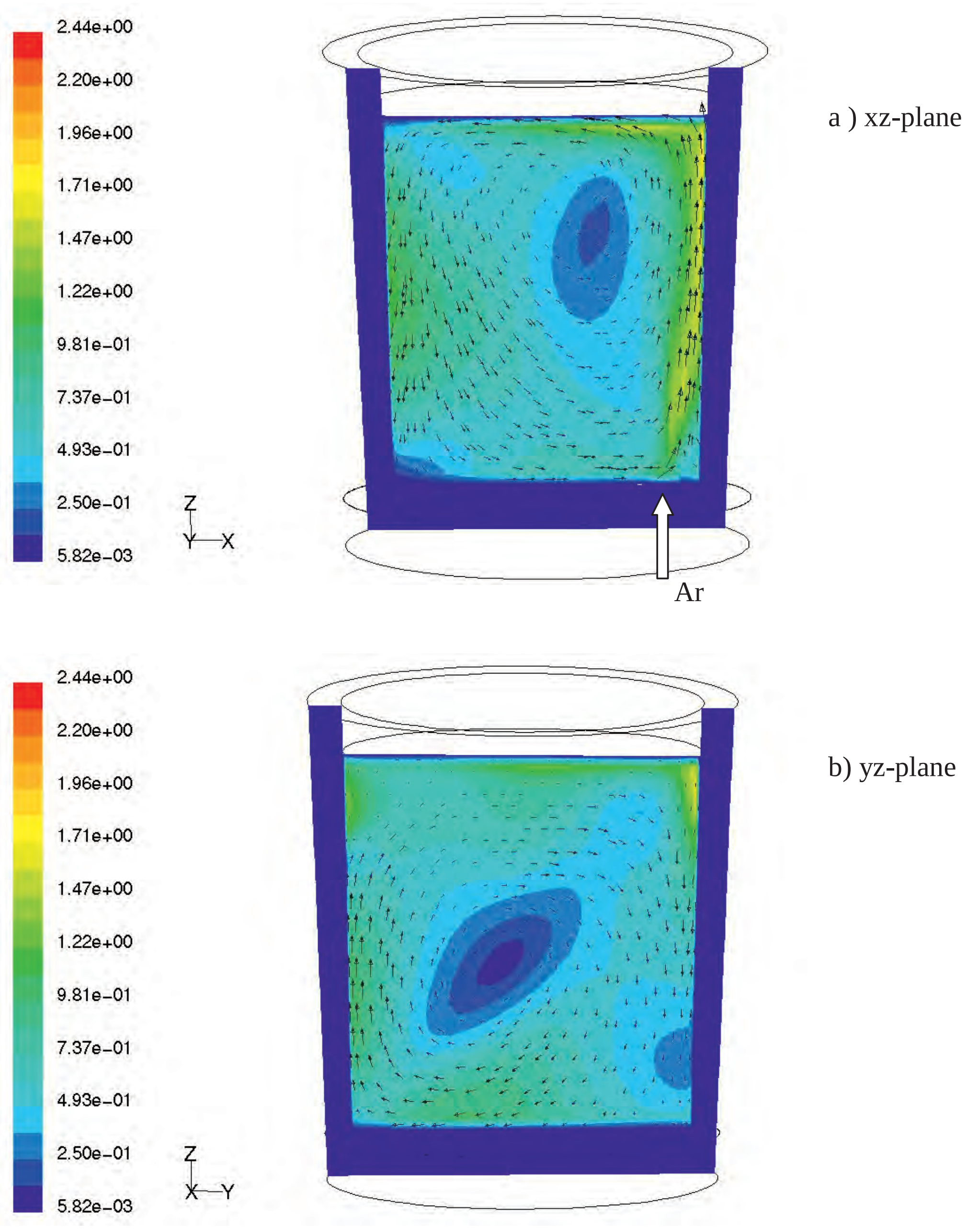

The coloured scale indicates the velocity in m/s and the arrows indicate the direction of the flow

Figure S4 **Flow pattern in the 170t ladle using a gas flow rate of 27 STD m^3/h**

This phenomenon is demonstrated in **Figure S5**. To get a better view of the bottom area in case of low gas flow rates such as 3 STD m^3/h, the velocity < 3 cm/s is plotted only 1 cm above the bottom (Figure S5a). The application of high gas flow rates (27 STP m^3/h, Figure S5b) leads to low velocities at the bottom, the flow being parallel to it. The upward flow in the zone close to the gas flow is clearly indicated by the arrows, which show the direction of the flow. On the opposite side to the gas flow, the arrows indicate a downward flow. The flow is mainly in the direction upward or downward, which means that the steel is transported from the bottom and up to the top surface and it is not circulating at a specific height. The surface area is characterized by a steel flow pattern directed from the right to left side confirming the circulation of the steel along the xz-plane in Figure S4a.

For evaluation of the mixing of the steel, turbulence intensity is used. Turbulence intensity, I, is defined as the ratio of the mean-root-square of the velocity fluctuations, v', to the mean flow velocity, v_{avg}.

$$I = \frac{v'}{v_{avg}} \qquad (1)$$

Generally, turbulence intensity less than 1% is considered as low and turbulence intensity larger than 10% is considered as high. The turbulence intensities at the identical heights of the ladle are plotted in **Figure S6**. In general, high turbulence intensities are seen in the upper part while lower intensities, < 10%, are found in the lowest part of the ladle. The conclusion is that the gas flow rate influences the turbulent intensities very much, particularly when the gas bubbles reach the surface. In such a case an open-eye is generated in the vicinity of wall of the ladle since the porous plug is situated eccentrically. This is confirmed very clearly by the turbulent intensities plotted in **Figure S7**. But generally speaking the higher the gas flow rate the higher also the turbulences in the melt. Relatively high velocities and turbulence intensities are observed, which indicate a low risk that volumes with low mass and energy exchange exist in this case.

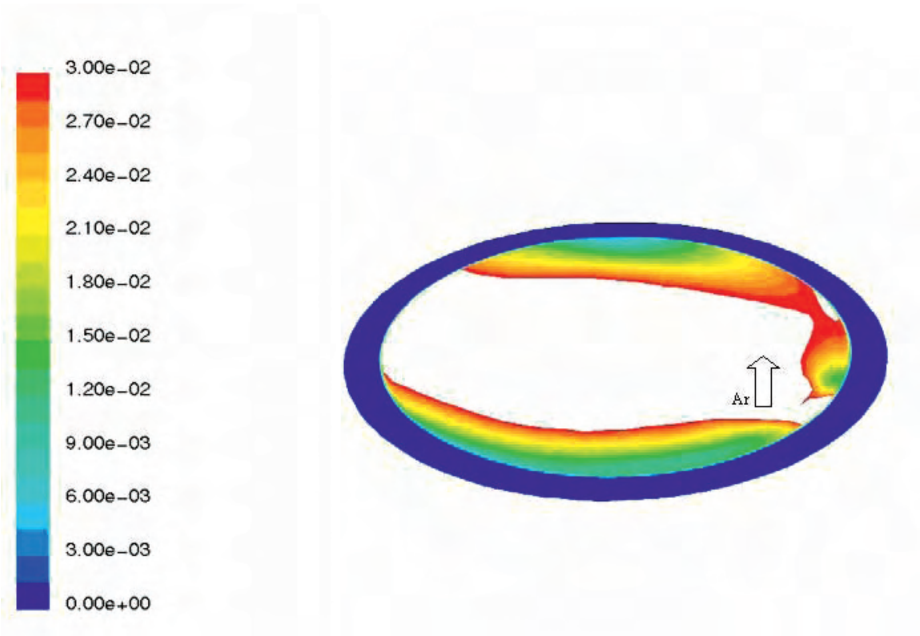

a) gas flow rate : 3 STD m³/h, velocity < 3 cm/s, 1 cm above ladle bottom

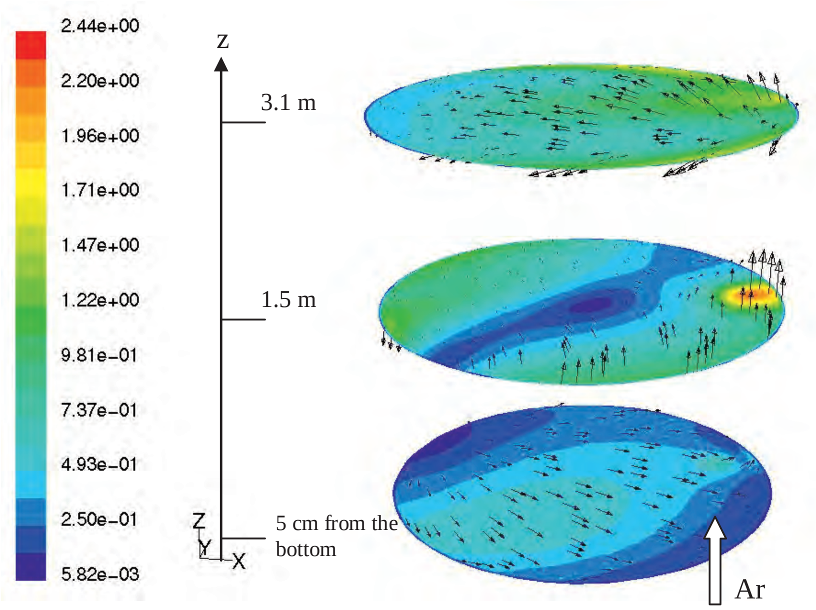

b) gas flow rate : 27 STD m³/h

Figure S5 **Contours and vectors of the velocity in the xy – plane of the 170 t ladle at different gas flow rates**

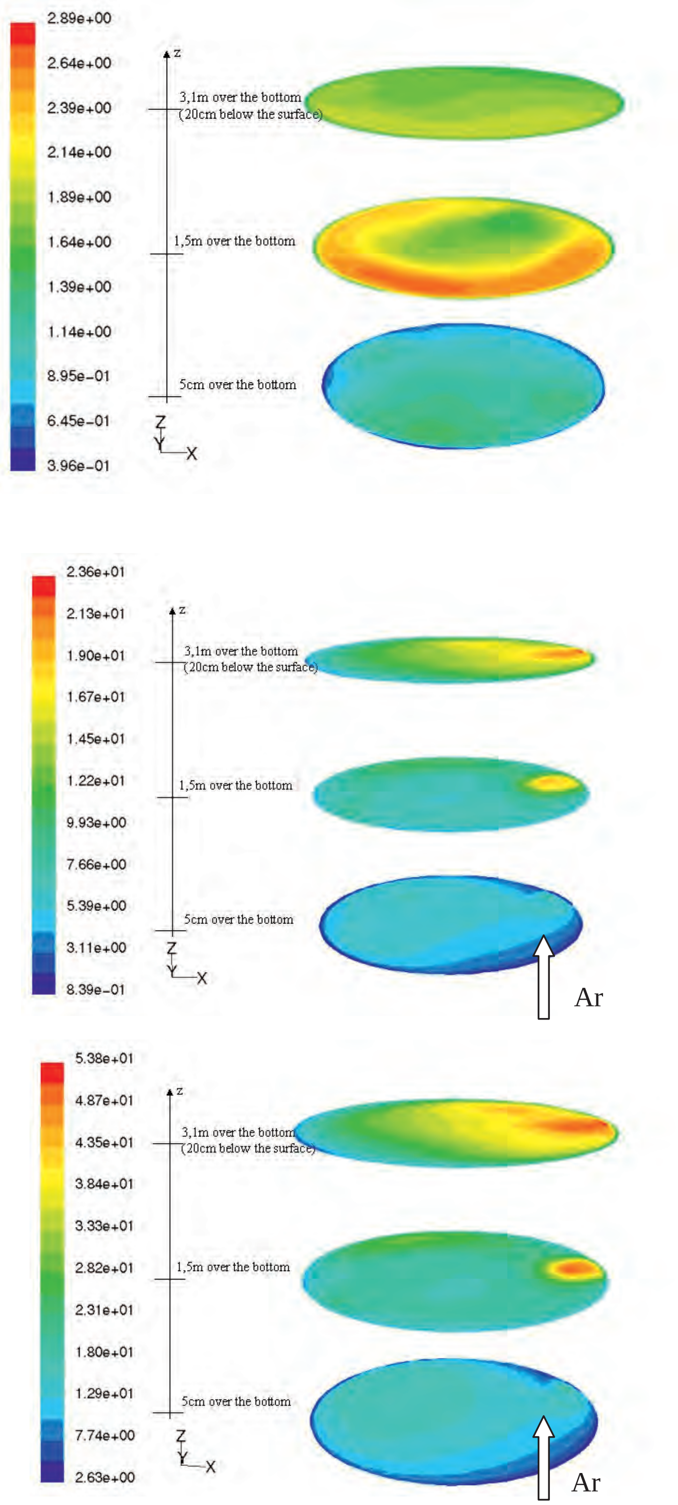

a) without stirring

b) gas flow rate: 3 STD m³/h Ar

c) gas flow rate: 27 STD m³/h

The coloured scale indicates the intensity in percent

Figure S6 **Turbulent intensities in the xy-plane of the 170 t ladle at different a gas flow rates**

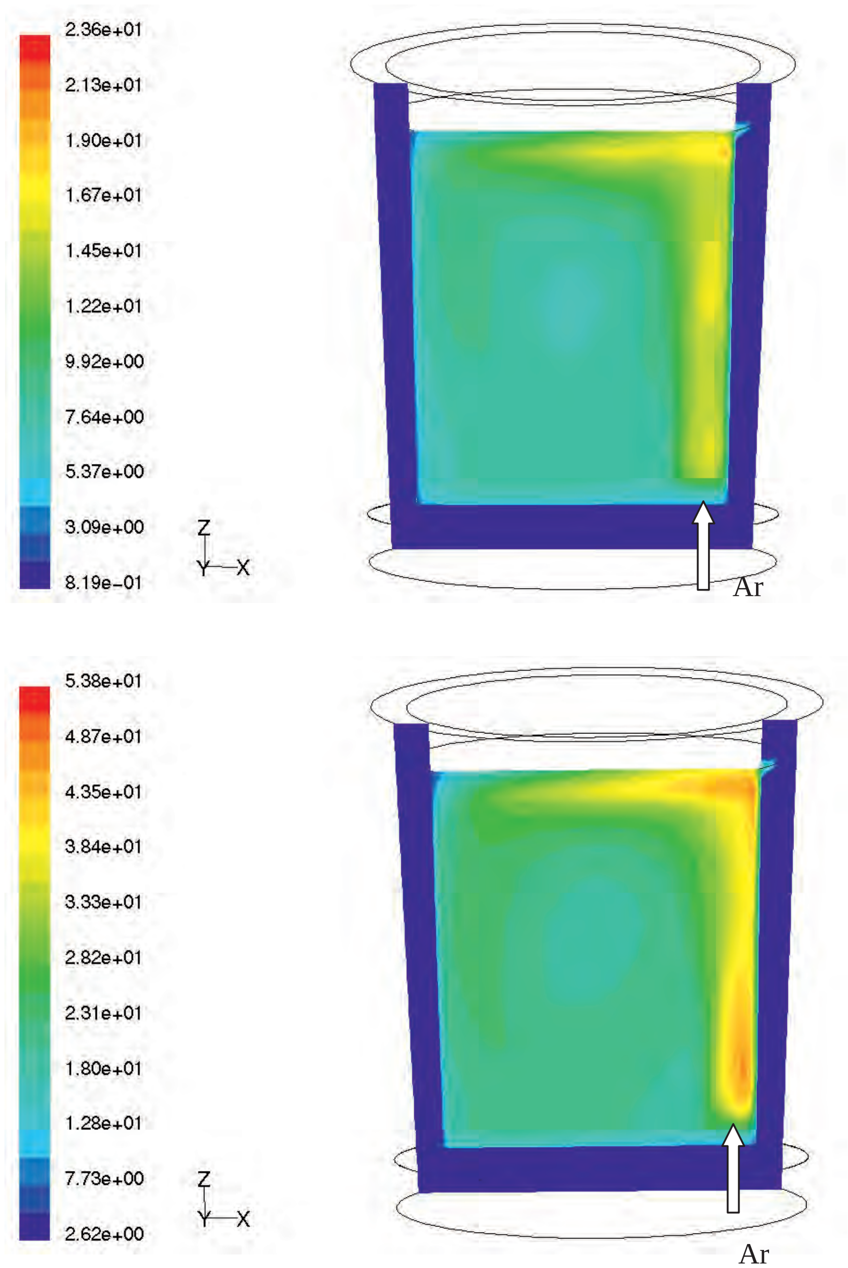

a) gas flow rate:
3 STD m³/h

b) gas flow rate:
27 STD m³/h

The coloured scale indicates the intensity in percent

Figure S7 **Turbulent intensities in the 170 t ladle with different gas flow rates**

Typical tracks of rising gas bubbles are plotted in **Figure S8**. When a high gas flow rate is used, the gas bubbles are taking a straight way from the inlet, but further up the momentum from the circulating steel is affecting the path of the gas bubbles. Followed by that, the breakthrough zone at the top surface is larger and more widely spread than at low stirring rate. In other words this leads to the formation of the open eye during ladle treatment.

To study the backflow behind the gas bubbles, the Reynolds number are plotted as seen in **Figure S9**. The Reynolds numbers are in general high, > 3000. The backflow of the bubbles is turbulent and the conditions are favorable to collision, agglomeration and flotation of inclusions. The results from the calculation where a low gas flow rate of 3 m^3/h is used, show a flow pattern of a large circulating loop with an upward flow driven by the injected gas. The velocity of the flow varies between 0.006 – 2.4 m/s. The turbulence intensity is low close to the bottom. Stagnant zones exist in the centre of the ladle and close to the bottom. In the case of 27 STP m^3/h velocities and turbulence intensities are roughly doubled while the gas flow is almost 10 times larger. The risk that stagnant zones exist in this case is small due to the high velocities and turbulences, which cause a strong mixing of the steel.

However the result of the 3D calculation is that mean and maximum velocity of the steel melt is influenced very strongly by the gas flow rate.

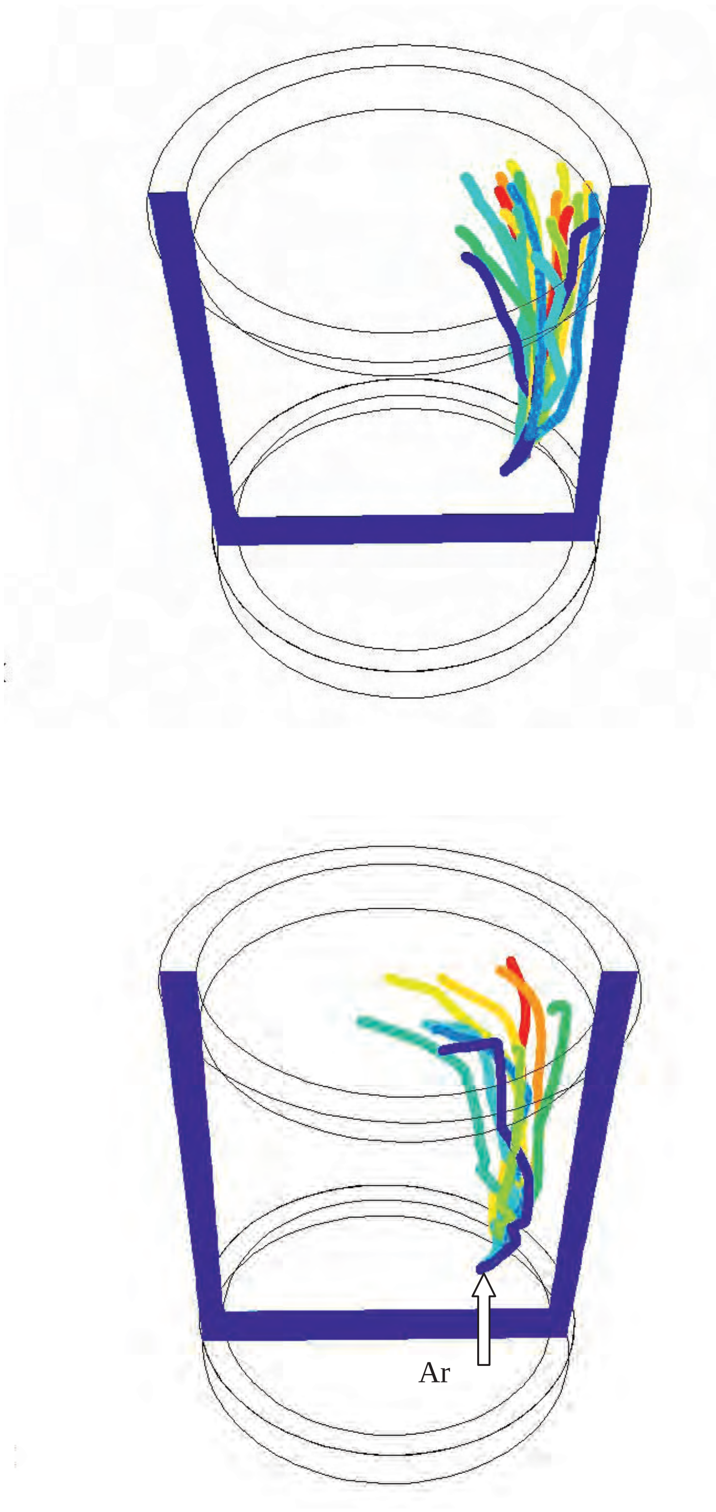

a) gas flow rate: 3 STP m³/h

b) gas flow rate:
27 STD m³/h

Figure S8 **Typical tracks of gas bubbles in the 170 t ladle with different gas flow rates**

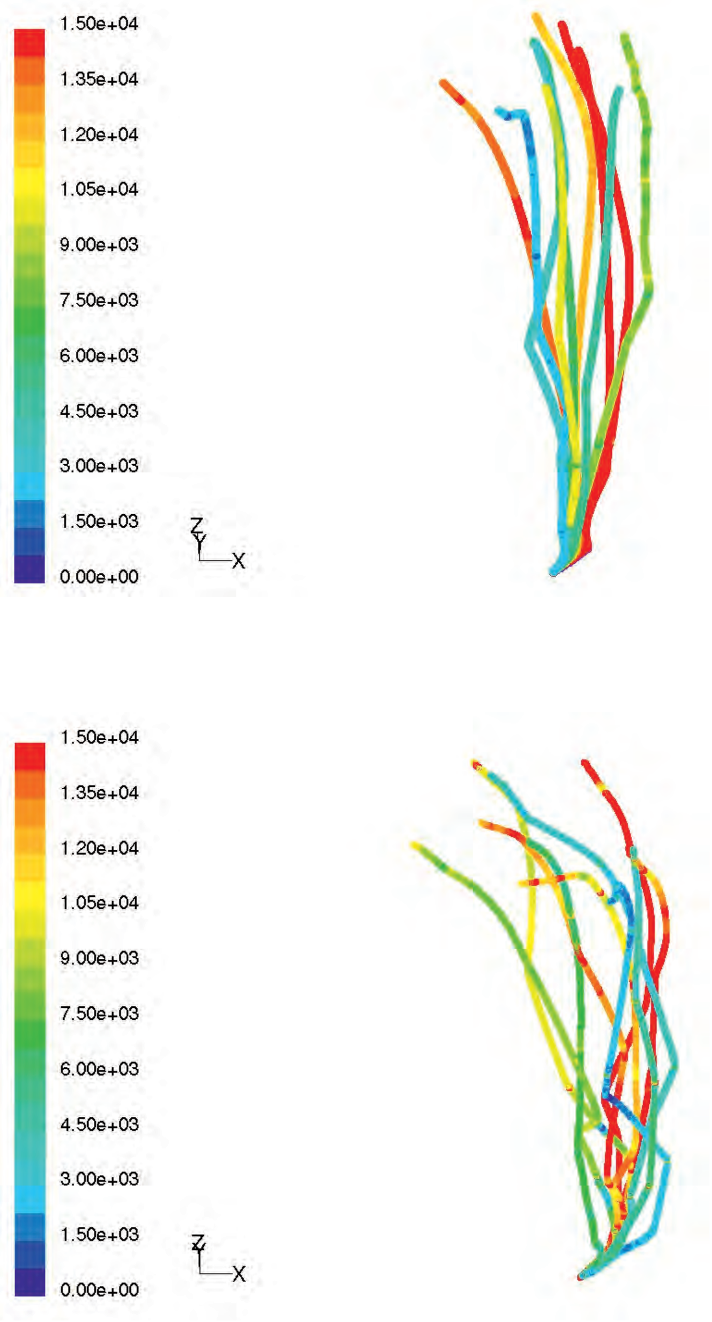

a) gas flow rate:
3 STD m³/h

b) gas flow rate:
27 STD m³/h

Figure S9 **Reynolds numbers of gas bubbles in the 170 t ladle with different gas flow rates**

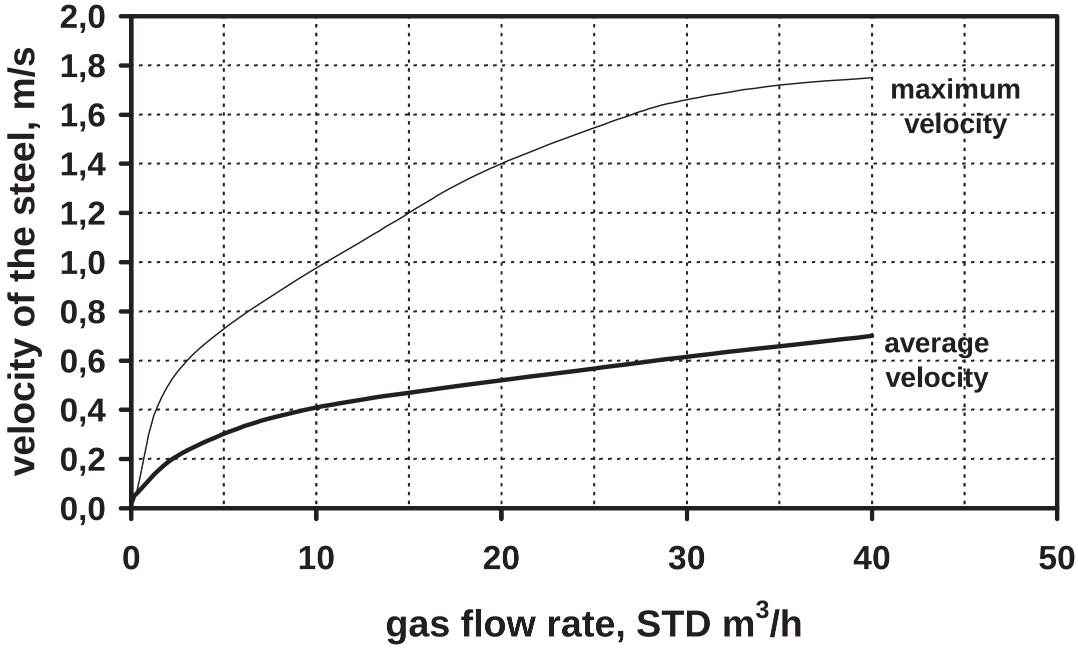

Figure S10

Influence of gas flow rate on the velocity of the steel

References

[sag1] Nobou Sano, Wei-Kao Lu and Riboud Paul V, 1997, Advanced physical chemistry for process metallurgy, Academic Press, San Diego, ISBN: 0-12-618920.

[sag2] Davidson Lars, 2001, An introduction to turbulence models, Chalmers University

[sag3] FLUENT 6 User's guide, 2002.

[sag4] Welty James, Wicks Charles and Wilson Robert, 1984, Fundamentals of Momentum, Heat and Mass Transfer, 3rd edition, John Wiley & Sons, Inc, USA, ISBN:0-471-87497-3.

[sag5] Oeters Franz, Metallurgy of steelmaking, 1994, Verlag Stahleisen mbH, Düsseldorf, 1994

8.2 Installation of a video camera at SIDNEOR for open-eye observation

The first step to fulfill image analysis is to install a digital camera in LF. But this was not an easy task in Sidenor Basauri LF. The main problem to install a camera in Sidenor Basauri's LF was that it was not designed to be watched, it was designed to avoid too much oxidation. For that reason the roof is almost touching the ladle and offers no open space between them. Over the roof, there is the working platform in such a way that it is impossible to see the ladle directly from working platform. Another difficulty is the roof itself, it is formed mostly by water cooled tubes and making a new hole there would require a complete redesign of the roof. Figure sid 10 shows a drawing of the roof, the lines are parallel or perpendicular to ladle sides, so any possible hole will have to be either perpendicular or in front of liquid steel/slag layer. Taking in count all this considerations it was stated the impossibility to locate a camera outside the ladle and far from the roof because there is no visual angle to observe the "open eye". On the other side, inside the roof, heat, dust and smoke conditions are too aggressive. In consequence four possible sites were studied to situate the image acquisition system. All of them are shown in figure sid 10.

1. The first location were the holes over the roof (number 1 in figure sid 10). One of the holes is used to automatic alloy addition and it is connected to addition tube, so it is not available for image analysis. The other two are the hole used for wire feeding and the hole used to get samples and take temperature measurements during the heat, both sampling and temperature measurement are automatic. They are similar in size and visual angles are not very different from one to the other. Nevertheless, both holes had several disadvantages: they are over the stirring plug, so optimal angle would be to place the camera just over one of them. But it was not possible because of the lack of space to sampling or wire feeding.. In consequence, incidence angles out of vertical positions were considered. However, it is difficult to get the right optical angle from there and the lack of space for the camera was a problem too, since working platform, electrodes, alloy additions tube, wire feeding tube and sampling device give not much chance to place anything there.

2. The second place was and small hole in one of the sides of the roof. It is there because ladle arms jut out a bit from the ladle and roof design is adapted to that. There are two equivalent positions for that but only one is available to visual observation. (Number 2 in figure sid 10). It had the advantage of the position, it is opposite to the stirring plug and so visual angles are easier to get. The three main problems of this site were: the small size of the hole (and it is not always the same because it is not really a hole, it is a gap); the risk of physical damage when the roof is placed over the ladle; and that this location is difficult to reach, so it would be very difficult to make any maintenance work.

3. The third possibility was a gate that was originally designed in the roof side (number 3 in figure sid 10). It was deactivated at LF 2when project began and did not exist in LF 1. The greatest problem was to make the gate run again properly with the maintenance work required. On the contrary, this location offered some potential advantages: As the gate was quite big the camera could be situated at some distance to avoid physical and thermal damage and it would not be very difficult to wash or make some maintenance; There would be space to place any necessary housing .

4. The last idea would be studied in case the other three would be rejected. It consisted of transporting the image inside the ladle outside, by means of optical fiber or similar. The location could be any of the precedent ones.

So the lateral gate in LF2 was regarded as the more suitable position among the four camera possible locations considered. To make it useful, the gate had to be activated. To fulfill that aim a considerable slag layer was eliminated, pneumatic and electrical components of the gate were repaired and finally the gate opened and closed properly. The gate was opened and closed several times during two months, to check for possible maintenance problems. The main problem encountered was that pneumatic hoses for gate operation suffered leaks due to slag splashing. When the leak has too great size the pneumatic closing of the gate stops to work correctly. Slag splashing occurs mainly when ladle car goes to vacuum degassing station from ladle furnace, during ladle furnace operation or vacuum degassing it is sufficiently protected. Up to that moment three problems arose related with the camera observation:

- The camera was not useful during heating due to the smoke.
- The electrodes must be up to watch the whole slag/steel surface, otherwise they obstruct the image.

Considering that those difficulties may be faced too, camera suppliers were contacted to buy and locate the camera as soon as possible. Following the specifications for the cameras learned from the BFI, and taking in count the temperatures in that site a camera and a housing were looked for. These are the main characteristics of the chosen devices:

- Camera: Retiga 1300; Housing: NxW Water cooled Stainless Steel housing from Videotec company; ONXAB Air barrier from Videotec company; Motored Zoom Lens; Toughened glass (350ºC Resistant); A computer for Camera Controlling; Camera Controlling and data acquisition Software

When all components were in Sidenor, the housing was installed in ladle roof near the gate. For that purpose a tube was welded to roof structure. It was the base for a pole mount adaptor and there was put the bracket which sustains the housing itself. Figure sid 11 show the whole system mounted in the roof including water supply for housing cooling and air supply for avoiding dust sticking in the front crystal of the housing. After housing installation the camera was not immediately installed until housing resistance and cooling capabilities were tested..

However several problems aroused after camera installation.

- As mentioned before, the gate for the camera opened and closed by a pneumatic system and due to slag splashing the air hoses suffered leaks that impede full gate closing. At first stages of the gate opening operation those hoses were changed to permit full gate open and closing, but this maintenance work could not be done always as soon as required and the gate slightly opened did not cause any trouble to the roof. But regrettably it represented a great problem for the housing, mainly for the front glass of the housing. In little time even with the gate only slightly opened a thick solid slag layer covered the front crystal impeding any visual observation through it. Slag splashing was greater than expected and in little time closed completely the front part of the housing as showed in Figure sid 12. This dramatic harm of front glass was more disappointing because it occurred in a short time and by the erosion of broken glass pieces it may be deduced that even first slag drops were enough to break the glass or at least to obstruct seriously the visibility. In spite of that the air flux created by housings air barrier worked quite well even after thick slag was sited in the housing front part; the air current was quite reliable but clearly not able to stop slag drops coming from the ladle. Different approaches were tried but finally this problem was solved welding a protective steel sheet in the inner part of the gate. This sheet is a good protection against slag splashing and does not need repairing or maintenance because as it gets a thick layer of slag quite fast and it is welded to the refrigerated gate.

- Another problem related with the camera was the connection with the PC. Retiga cameras connection to the PC is firewire and for this kind of connection it is not possible to get any desired length wires. Wire distance form the camera to the PC in Ladle Furnace cabin was slightly more than 20 m. Sidenor opted to install a new (not so standard) 10m firewire wires and with three of them united by repeaters. This configuration worked correctly as long as the repeaters were supplied with electrical power to maintain connection quality.

- A different situation occurred when, due to a mechanical failure in the ladle car, the ladle stopped for a long period (some minutes) just under camera equipment. This is a strange circumstance because this kind of failure does not occur more than 2-3 times a year a not necessarily in that site; but that time, as a consequence, electrical and signal wires were destroyed, however the camera itself did not suffer any harm because of the housing and the roof itself protection. After that, wires and connections were substituted and were have double protection against heat and it is expected it will be sufficient protections next time.

- Another important problem happened when lateral gate opened completely and did not close at all. This case is significantly different form not closing completely because apart from slag splashing the housing is receiving direct arc radiation too. The 3rd electrode is quite near to the housing. So, is this case, the lens glass itself resulted very seriously damaged with arc radiation (Figure sid 12). After short time slag splashing covered the front glass of the housing and protected the rest of the equipment. Hopefully the camera itself did not suffer important damages. A new lens was bought, an emergency protection sheet has been manufactured and two improvements in the gate have been developed in order to avoid any future failure of this kind, anyhow if this problem happened again it would be very damaging too.

- To get the appropriate orientation for the camera was not an easy task too. Positioning operation with full ladle was not safe and without ladle was impossible to check and housing movements were clumsy in the small space available.

Those difficulties led to several delays in the project development and impeded early beginning of image analysis related tasks. Anyway, useful images were got and image analysis was performed upon them as explained in the report. Some image acquisition was performed too in the ladle_introduction_to_the_car position. However, required maintenance work was considered too high to maintain this configuration as an on-line image acquisition system. An important conclusion from this work is that getting a reliable image acquisition system is highly depending on the ladle roof configuration and roof designs may be very helpful or very distorting for this purpose. In Sidenor case the three main general design difficulties have been: a closed roof combined with electrode heating and small free board in the ladle that produces more slag splashing.

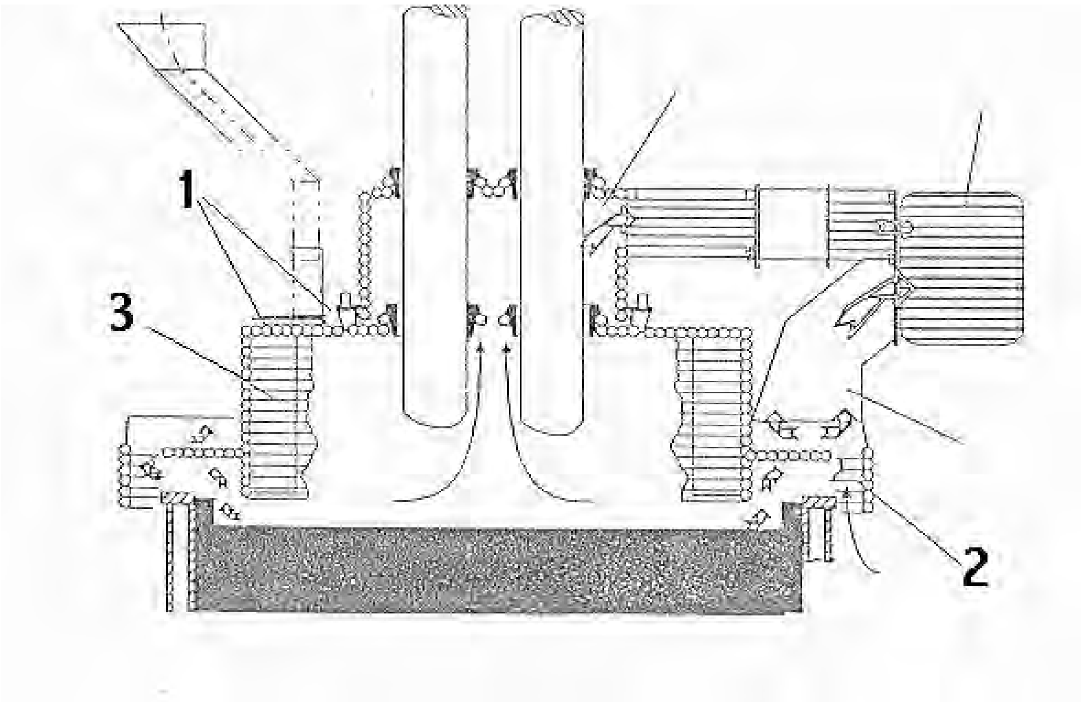

Figure sid 10 Schematic drawing of the roof in LF 2.

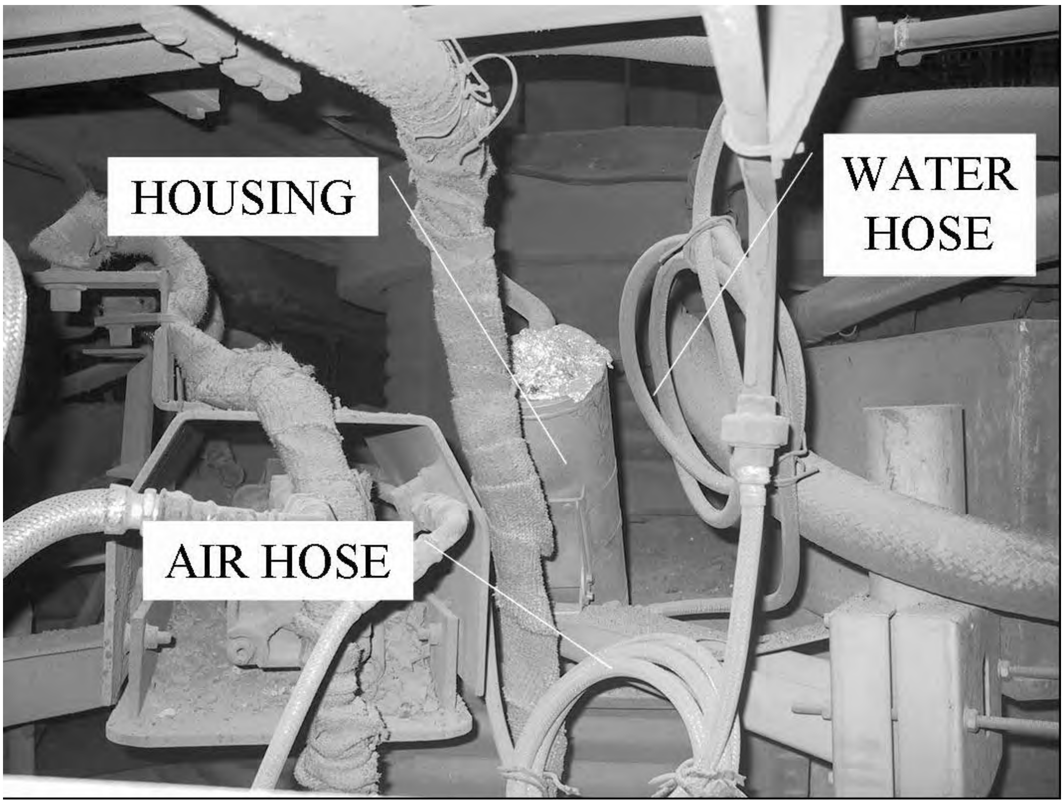

Figure sid 11 Housing mounting system on LF roof.

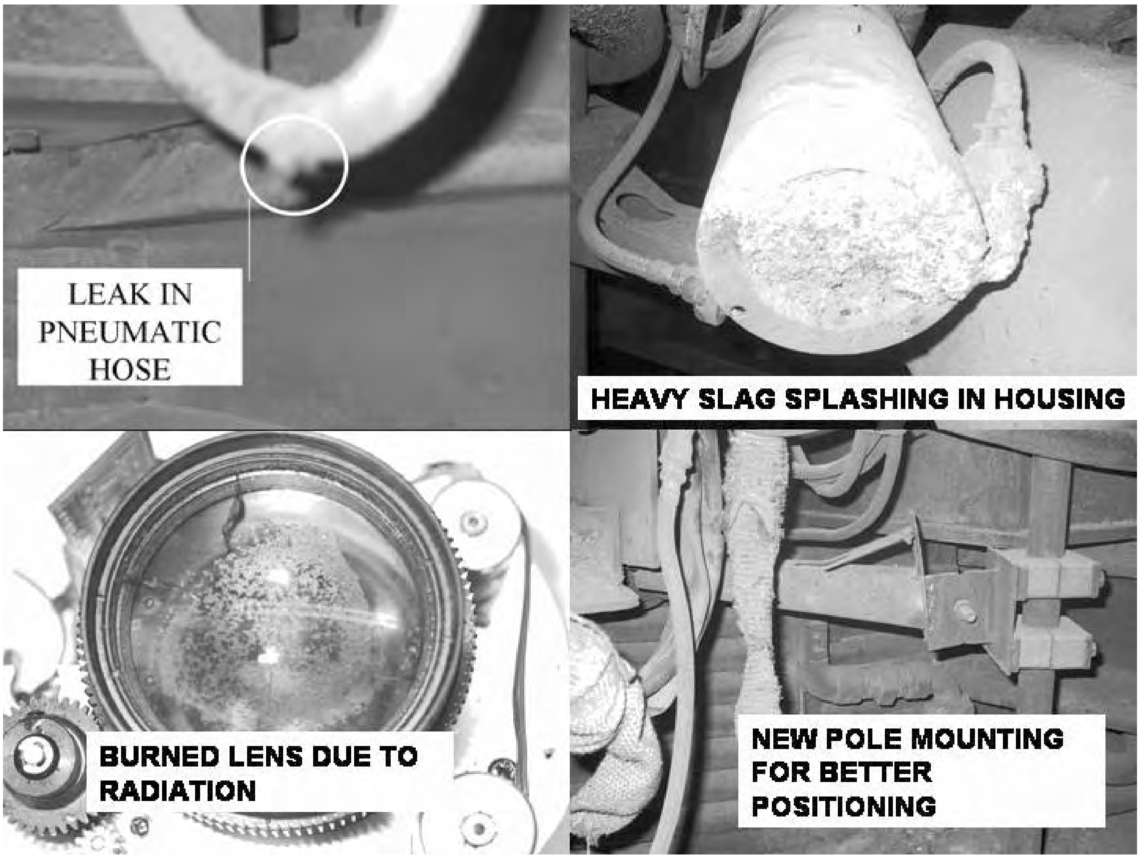

Figure sid 12 Several problems occurred with image acquisition system.

European Commission

EUR 22988 — Development of advanced methods for the control of ladle stirring process

M. Burty, C. Pussé, D. Y. Sheng, C. Dannert, H. Köchner, L. F. Sancho, J. Díaz,, P. Valentin, C. Bruch, A. Arteaga

Luxembourg: Office for Official Publications of the European Communities

2007 — 139 pp. — 21 × 29.7 cm

Technical steel research series

ISBN 978-92-79-07293-2

ISSN 1018-5593

Price (excluding VAT) in Luxembourg: EUR 20